AD-A171 587 INELASTIC GAS-SURFACE SCATTERING II RESULTS(U) CORNELL UNIV ITHACA NY LAB OF ATOMIC AND SOLID STATE PHYSICS M D STILES ET AL. 25 AUG 86 TR-27 N00014-82-K-0576 1/2

UNCLASSIFIED F/G 20/10 NL

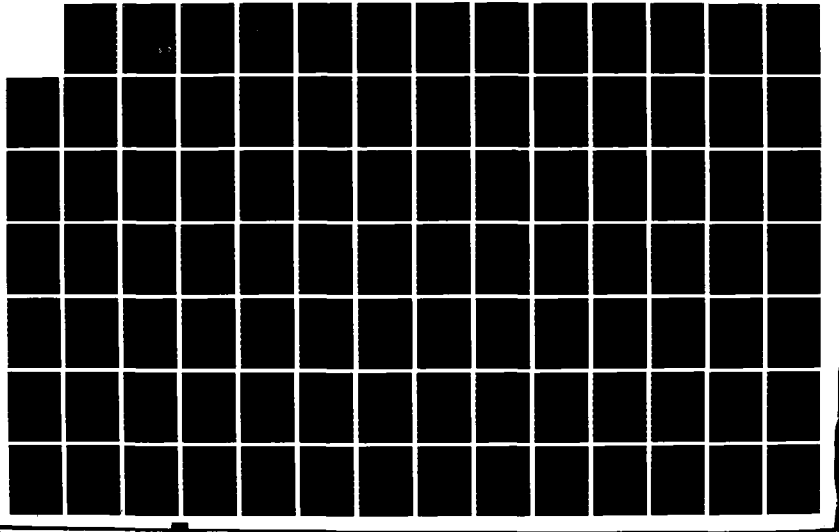

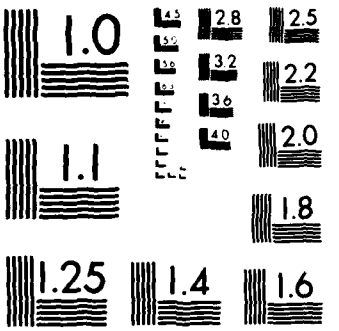

MICROCOPY RESOLUTION TEST CHART

(12)

OFFICE OF NAVAL RESEARCH

Contract N00014-82-K-0576

TECHNICAL REPORT NO. 27

INELASTIC GAS-SURFACE SCATTERING: II RESULTS

by

Mark D. Stiles and John W. Wilkins

Prepared for Publication in

Physical Review B

LASSP
Cornell University
Ithaca, New York 14853

August 25, 1986

SECURITY CLASSIFICATION OF THIS PAGE (When Data Entered)

REPORT DOCUMENTATION PAGE		READ INSTRUCTIONS BEFORE COMPLETING FORM
1. REPORT NUMBER 27	2. GOVT ACCESSION NO.	3. RECIPIENT'S CATALOG NUMBER
4. TITLE (and Subtitle) INELASTIC GAS-SURFACE SCATTERING: II RESULTS		5. TYPE OF REPORT & PERIOD COVERED Technical Report
		6. PERFORMING ORG. REPORT NUMBER
7. AUTHOR(s) Mark D. Stiles and John W. Wilkins		8. CONTRACT OR GRANT NUMBER(s) N00014-82-K-0576
9. PERFORMING ORGANIZATION NAME AND ADDRESS Laboratory of Atomic and Solid State Physics Cornell University Ithaca, NY 14850		10. PROGRAM ELEMENT, PROJECT, TASK AREA & WORK UNIT NUMBERS
11. CONTROLLING OFFICE NAME AND ADDRESS Office of Naval Research 800 Quincy St. Arlington, VA		12. REPORT DATE August, 1986 13. NUMBER OF PAGES 115
14. MONITORING AGENCY NAME & ADDRESS(if different from Controlling Office)		15. SECURITY CLASS. (of this report) unclassified 15a. DECLASSIFICATION/DOWNGRADING SCHEDULE

16. DISTRIBUTION STATEMENT (of this Report)

This document has been approved for public release and sale; its distributions unlimited.

17. DISTRIBUTION STATEMENT (of the abstract entered in Block 20, if different from Report)

18. SUPPLEMENTARY NOTES

Prepared for Publication in Phys. Rev. B

19. KEY WORDS (Continue on reverse side if necessary and identify by block number)

20. ABSTRACT (Continue on reverse side if necessary and identify by block number)

Helium and molecular hydrogen scattering from copper is calculated to examine general features of scattering for these systems, especially the quantum mechnics of the scattering process, both for the motion of the particle and the excciations of the lattice. These calculations use an interaction potential chosen to simplifiy the numerical calculation while eetaining the essential physics of the interaciton. The scattering calculations show that these approximations quantitatively reproduce experimental results. Based on theis success we show how the scattering probabilities depend on details of the system like the well depth and the steepness of the potential

DD FORM 1 JAN 73 1473 EDITION OF 1 NOV 65 IS OBSOLETE
S/N 0102-014-6601

SECURITY CLASSIFICATION OF THIS PAGE (When Data Entered)

as well as the assumptions made to simplify the interaction potential. H_2 and D_2 inelastic scattering and trapping probablilities show strong enhancement by selecti adsorption resonances and overall changes in scatteirng intensities due to other more subtle effects of the rotational degrees of freedom. Temperature-dependent HD scattering probabilities show the effect of inelastic scattering on rotationally inelastic scattering and selective adsorption resonances.

Inelastic Gas-Surface Scattering: II Results

Mark D. Stiles and John W. Wilkins

Laboratory of Atomic and Solid State Physics

Clark Hall, Cornell University, Ithaca NY 14853

ABSTRACT: Helium and molecular hydrogen scattering from copper is calculated to examine general features of scattering for these systems, especially the quantum mechanics of the scattering process, both for the motion of the particle and the excitations of the lattice. These calculations use an interaction potential chosen to simplify the numerical calculation while retaining the essential physics of the interaction. He scattering calculations show that these approximations quantitatively reproduce experimental results. Based on this success we show how the scattering probabilities depend on details of the system like the well depth and the steepness of the potential as well as the assumptions made to simplify the interaction potential. H_2 and D_2 inelastic scattering and trapping probabilities show strong enhancement by selective adsorption resonances and overall changes in scattering intensities due to other more subtle effects of the rotational degrees of freedom. Temperature-dependent HD scattering probabilities show the effect of inelastic scattering on rotationally inelastic scattering and selective adsorption resonances.

I. INTRODUCTION

A recent review of the gas-surface scattering field[1] summarizes the wide variety of systems studied using thermal energy atomic and molecular beams. In this paper we will concentrate on low-mass scattering particles, in particular helium and various isotopes of molecular hydrogen, and on inelastic scattering and the effect of inelastic scattering on elastic scattering in these systems. Although this program omits a considerable amount a work (such as heavier atomic and molecular scattering, chemical processes, and electronic interactions) it none the less covers a very significant amount of work that has been done on these systems.

The specific calculations we report are for He, H_2, D_2, and HD scattering from flat copper surfaces (such as (111) and (100)). We view these systems as prototypical, allowing generalization of our results to other systems. In the introduction of this paper we discuss experiments and previous theoretical treatments for these systems. The second section details the the specific potentials, phonon spectra and integration techniques used in these calculations. The results of the calculations are presented and discussed in the third section, and this work is summarized in the final section.

A. Experiments

1. *Elastic Helium Scattering* The elastic scattering of helium is sufficiently strong that well defined diffraction peaks can be observed. The intensities of the diffraction peaks are sensitive to the detailed structure of the surface and with some analysis can be used as a probe of the short-ranged structure of the surface much in the same way as x-ray and neutron scattering are used to determine the structure of solids. A typical example of a structural study using helium scattering is for the copper (110) surface[2]; a recent review[3] and a book[4] summarize the use of helium scattering to study surface structures.

To accurately interpret diffraction intensities in terms of a surface potential it is necessary to

extrapolate the experimental diffraction intensities to these intensities that would be measured if the the atom were scattering from a static surface. The temperature dependence of the diffraction intensities, which is one of the main interests of this thesis, is more complicated than the Debye-Waller factor for x-ray or neutron scattering; in particular the temperature dependence of the elastic scattering intensity from a copper[5,6,7] or nickel[8] surface is more complicated than is predicted by a typical bulk scattering analysis.

Another important complication of atom or molecule scattering – missing from the usual bulk structure probes and associated with an attractive potential – is *selective adsorption resonances* in the scattering intensities. These resonances occur when the scattering particle makes a virtual transition, either rotational or diffractive, into a bound state, and they strongly affect the scattering probabilities for resonant scattering energies. Since resonances are often prominent scattering features and are strongly tied to the bound state energies of the potential they are very useful for determining the potential for the scattering particle outside of the surface. One of the main emphases of this paper is the effect of these resonances on inelastic scattering and vice versa.

2. *Inelastic Helium Scattering* Time-of-flight measurements can be made with sufficient energy resolution and angular resolution of the final states so as to determine both the change in energy and the change in parallel momentum due to the scattering from the surface. For inelastically scattered helium atoms the energy and momentum have been transferred to phonon modes, so that just as neutron scattering can be used to measure bulk phonon dispersion curves so can helium scattering be used to measure the surface and surface-projected phonon modes. The most prominent surface phonon is the Rayleigh phonon which is a low energy mode pulled off the bottom of the bulk transverse phonon branch. The dispersion of the Rayleigh mode has been measured for metal[9,10,11,12,13] surfaces using inelastic helium scattering.

Under appropriate scattering conditions the intensity of the peaks associated with Rayleigh phonon modes, or bulk projected modes for that matter, will show a large enhancement due to

selective adsorption resonances.[14,15,16,17] If either the initial state or the appropriate final is state is a resonant state the inelastic scattering will be enhanced because the helium atom spends a long time near the surface. We discuss selective adsorption resonance enhancement of inelastic scattering at greater length in section III.

3. *Molecular-Hydrogen Scattering* Molecular-hydrogen scattering can be very similar to helium scattering provided the surfaces have a sufficiently large barrier to chemisorption that it does not occur. For both homoisotopic hydrogen molecules, H_2 and D_2, diffraction[18,19,20,21,22] can be used to determine the hydrogen-surface potential in a manner similar to that used in helium scattering. While molecular hydrogen has rotational degrees of freedom, the translational-rotational coupling is very weak because the charge density of the molecule is very close to spherical. In spite of the weak coupling the rotational degrees of freedom do exhibit themselves in rotationally mediated selective adsorption resonances[23,24] which occur when the molecule makes a virtual rotational transition into a bound state. These resonances can be used to determine the potential[24] and the translational-rotational coupling[25] in much the same way as diffractionally mediated selective adsorption resonances can.

4. *Rotationally Inelastic Scattering* The stronger translational-rotational coupling for HD leads to considerable differences between its scattering and that of H_2, D_2, and He. The most prominent difference is the large rotational excitation probabilities seen for scattering from many surface [25,26,27,28,29]. Since the rotational diffraction is strong for HD scattering, the temperature dependence (even for a flat surface) of the elastic and rotationally inelastic scattering is more complicated[23,27] than it is for helium or other isotopes of molecular hydrogen. In section III we discuss the temperature dependence of the HD scattering intensities and relate it to the temperature dependence of diffraction intensities.

5. *Sticking and Desorption* More complicated processes involve helium and molecular hydrogen

sticking onto or desorbing from either physisorption and chemisorption surfaces. H_2 has been observed to be freely rotating in electron energy loss experiments on flat metal surfaces such as Cu (100)[30] and Ag (111)[31]. The sticking probability for molecular hydrogen was measured in molecular beam scattering experiments[32] and found to depend on the angular momentum state of the incident molecule. On surfaces for which the dissociative sticking probability is appreciable, such as Pt(111)[26,27] or W(110)[33], it is still possible to observe selective adsorption resonances in the elastic and rotationally inelastic scattering probabilities. In section III we discuss the relevance of the calculations done in this paper to these processes.

B. Theory

Theories for these systems can be separated into several general categories. Since classical calculations are not valid for these systems the simplest way to include the necessary quantum mechanics semi-classically. Another approximation is to treat the potential as infinitely steep allowing the boundary conditions to determine the scattering probabilities. Finally, exact quantum mechanical calculations can be carried out for scattering from a periodic static surface and can be used a starting points for approximate calculations of the inelastic scattering probabilities.

Semiclassical methods are motivated by a desire for a calculational technique that has the simplicity of a classical calculation but includes just enough of the quantum mechanics that it is able to describe the quantum mechanical effects that are seen experimentally. Typically these methods are built around classical calculations and try to include quantum effects near the classical path. Two such methods that have been applied to the surface scattering problem are the classical S-matrix approach[34,35,36,37,38] and the wavepacket approach.[39,40,41,42,43]

Another approach for calculating scattering probabilities involves approximating the surface as a corrugated infinite barrier with the boundary conditions that the particle does not penetrate the surface. This hard wall approach can be generalized to treat inelastic scattering by allowing

the potential barrier to move, then averaging over the thermal fluctuations and using the boundary conditions to determine the scattering probabilities.[44,45,46,47,48,49]

For all systems, especially those that exhibit strong diffraction, the scattering probabilities can be calculated exactly using a coupled channels approach.[50,51,52,53,54,55,56,57] In this method part of the motion, usually the motion parallel to the surface or the motion of the orientation of the molecule, is expanded in terms of basis functions giving a coupled set of one-dimensional integrals for the remaining degree of freedom. Integrating these equations numerically and solving for the amplitudes of all the channels gives the diffraction probabilities. The number of included channels can be systematically expanded until the results do not change. This method runs surprisingly fast and has been applied successfully to a wide variety of helium and molecular hydrogen scattering problems.

Most calculations of inelastic scattering probabilities are related to the distorted-wave-Born approximation. There are four basic approaches: 1) distorted-wave-Born approximations based on including only the z-dependent potential in the zeroth order Hamiltonian,[58,59,60,10,54,61,62,63,64] 2) distorted wave Born approximations based on potentials that include the corrugation or translational-rotational coupling in the zeroth order Hamiltonian,[65,66,67] 3) extended coupled channels calculations that are exact calculations on a simplified Hamiltonian, for which the possible final states are restricted in some way,[68,69,70,71,72,73,74] and 4) methods related to the last, but leaving out intermediate steps, *i.e.*, calculating the elastic scattering probability using a self-energy.[75]

In this paper we calculate scattering probabilities for helium and molecular hydrogen using the formal methods developed in its companion paper[74] (hereafter referred to as I) which fall into the third category discussed in the previous paragraph. Together with the approximations we make for the interaction potential we use these methods to calculate many aspects of the scattering problem which we in turn use to make general statements for atom-surface scattering in the low mass limit.

II. DETAILS OF THE CALCULATIONS

Given the formalism developed in I it is necessary to make some additional choices to perform calculations. Specifically we need a potential, a phonon spectrum, and a procedure for solving the appropriate Schrödinger equations. In this section we will discuss the choices made; we have striven to consider simple models with no adjustable parameters so that our assumptions can be tested directly against experiment.

A. The Potential

The potential is usually described as due to two contributions, an attractive and a repulsive, which are calculated independently of each other. Far away from the surface the atom is attracted to the surface by a van der Waals attraction that falls off with the inverse cube of the distance from the surface. The other contribution is a repulsive potential due to the atomic electrons overlapping the surface electrons; since the helium atom is a closed shell system it costs energy to rearrange those electrons and the Pauli exclusion principle leads to a repulsive interaction. The repulsive potential is roughly proportional to the charge density of the surface.

For the calculations presented in this paper we use potentials calculated in the manner described above.[76] In Fig. (2.1) we show the potentials for He, H_2, and HD in the bottom panel all interacting with a copper surface. In Table 2.1 we give the parameters for each of the potentials. The helium potential consists of a repulsive part given by

$$V_r(z) = V_0 e^{-\alpha z}, \tag{2.1}$$

and an attractive part given by

$$V_a(z) = -f(z - z_{vw})\frac{C_{vw}}{(z - z_{vw})^3}; \qquad f(x) = 1 - (2(k_c x)^2 + 2k_c x + 1)e^{-2k_c x}. \tag{2.2}$$

The function $f(x)$ is a cut-off function that removes the divergence of the usual van der Waals dependence as $z \to z_{vw}$ and in the process softens the attractive potential inside the well minimum.

This function is chosen because of its simple form; the constant, k_c, is chosen to give the best comparison with the observed bound states when used in conjunction with a repulsive potential. We will call the attractive and repulsive parts together the exponential-van der Waals potential. For helium on copper this potential with a well depth of 5.66 meV supports five bound states.

Although a hydrogen molecule is very similar to a helium atom in terms of its charge distribution, the difference has marked effects on the potential. The hydrogen molecule is more polarizable than helium; in addition both its charge density[77] and its polarizability are asymmetric with respect to its orientation.[78] The increased polarizability of the molecule results in a potential that is more attractive at large distances and has a deeper potential well.[79,80] The orientational dependence of the polarizability leads to an attractive potential that tends to orient the molecular axis perpendicular to the surface plane. The asymmetric charge distribution gives an orientational dependence to the repulsive potential opposite of the attractive potential, tending to align the molecular axis parallel to the surface plane. These two anisotropies have opposite effects, and near the well minimum there is little orientational dependence. These two anisotropic contributions can be described by expanding the potential in Legendre polynomials

$$V(z,\theta) = V_r(z)\left[1 + \lambda_r P_2(\cos\theta)\right] + V_a(z)\left[1 + \lambda_a P_2(\cos\theta)\right], \tag{2.3}$$

where θ is the angle of orientation of the molecular axis with respect to the surface normal. Since H_2 has reflection symmetry only even terms enter the expansion in terms of Legendre polynomials, and since the orientational dependence is weak only the second term contributes. The orientational dependence of the potential is shown in the second panel of Fig. 2.1.

For the HD molecule the potential is slightly more complicated because the molecule no longer has reflection symmetry. While the potential for the hydrogen molecule is naturally defined with respect to its center of mass, it is due to the electron cloud around the nuclei. For the H_2 molecule the center of mass coincides with the centroid of the electron cloud. However, for the HD molecule this is no longer the case so the potential has to be converted to center of mass coordinates. Since the electronic structure of the HD and H_2 molecules are the same the HD potential can be written

in terms of the H_2 potential by

$$V_{\rm HD}(z,\theta) = V_{\rm H_2}(z + \delta\cos\theta, \theta), \tag{2.4}$$

where δ is the offset of the center of mass with respect to the centroid of the electron cloud. This potential can be reexpanded in terms of Legendre polynomials and is plotted in the bottom panel of Fig. 2.1. Since the deuterium atom is closer to the center of mass in the HD molecule the potential tends to orient the deuterium end closer to the surface when the molecule is close to the surface and further away when it is far from the surface. This is reflected in the sign of the $P_1(\cos\theta)$ term in the potential in Fig. 2.1.

For comparison we also calculate scattering probabilities using a variety of Morse potentials. Morse potentials are potentials with a simple form requiring the minimum number of input parameters that reproduces the general shape of the surface potential

$$V_M(z) = D(e^{-2\alpha z} - 2e^{-\alpha z}). \tag{2.5}$$

The well depth, D, and the range parameter, α, are the two input parameters which for this calculation are chosen to match the well depth and range parameter of the exponential-van der Waals potential. The Morse potential and the exponential-van der Waals potentials are plotted together for comparison in Fig. 2.2. The Morse potential reproduces most of the features of the exponential-der Waals potential except the highest lying bound states; the discrepancy is caused by the incorrect asymptotic behavior.

B. The Interaction Potential

Even less is known about the interaction potential than about the static potential. If pair potentials, *i.e.*, potentials that only depend on the distance between the scattering atom and each lattice atom were a good description of the static potential constructing the interaction potential would be straight forward. But pair potentials often do not work well even for classical calculations[81] giving

corrugations that are much too strong when applied to helium-surface potentials. Here we try to construct the most reasonable, but yet simple, model for the interaction potential. In addition to the flat surface approximation for smooth surfaces as discussed in I (see Eqs. (5.7,5.10)) we make a local height approximation. The local height, $h(\mathbf{R},\{n_i\})$ where $\{n_i\}$ is the occupation of the normal modes of the surface, shifts the origin of the potential by an amount that depends on the positions of the surface atoms in the immediate vicinity, this function will be discussed further below. While in general the interaction potential depends on the properties of each phonon in a complicated manner; in the local height approximation we assume that phonons shift the potential rigidly in the z-direction by an amount that differs from point to point in the surface plane. The periodicity of the shift is given by the parallel wavevector of the phonon and the amplitude of shift depends on the amplitude of the mode projected on the surface layer and the wavevector of the phonon. Then we expand the potential

$$V(z,\mathbf{R},\{n_i\}) = V[z - h(\mathbf{R},\{n_i\})], \tag{2.6}$$

in a Taylor series in the local height which, being typically much smaller than the characteristic length scales, allows us to truncate the expansion after the second term

$$V(z,\mathbf{R},\{n_i\}) = V(z) - V'(z)h(\mathbf{R},\{n_i\}). \tag{2.7}$$

The first term is the *static surface potential* and the second is a term linear in the phonon coordinates that will cause phonon transitions in the scattering process.

There are three aspects of the local-height approximation that need to be discussed: 1) over what range of z is this likely to be a good approximation, 2) should the derivative of the static surface potential or the derivative of the repulsive part of the potential be used in the second term of Eq. (2.7) and 3) what is the form of the local height function. *The range of z.* The dependence on the distance parallel to the surface that we will use is short ranged so only adjacent atoms affect the potential at each position. The local height approximation definitely breaks down far away from the surface because there the potential depends on a larger number of surface atoms. It also

breaks down very close to the top layer of atoms, but the helium atoms do not penetrate that far. However, near the classical turning point where the inelastic scattering is important, it should be a reasonable approximation because the local height will be dominated by the closest surface atom and the form of the cut-off function is chosen to match best in that region.

The distance dependence of the interaction potential. Many calculations of inelastic scattering assume that only the repulsive part of the potential couples to the phonons, *i.e.,* replacing V' by V'_r in the second term of Eq. (2.7). We think it is a better approximation to use the full potential. Typically the attractive part of the potential, far from the surface, is due to a large number of surface atoms so that when one atom moves it does not affect the potential, whereas the repulsive potential is local and dominated by the surface atoms closest to the scattering particle. In the region near the surface where the inelastic scattering takes place, however, breaking the potential into an attractive part and a repulsive part is somewhat artificial as the attractive part of the potential is also dominated by the closest surface atoms.

This choice of the interaction potential is shown in Fig. 2.3 for a simple model of the gas-surface potential. The potential is assumed to be a sum of a Morse potential from each layer in the solid. For this model the interaction potential is better approximated by the derivative of the full static surface potential rather than the derivative of the repulsive part of the same potential. In the next section we will show that the choice of the interaction potential has a very strong effect on both the strength of the inelastic scattering and on the dependence of the inelastic scattering on the well depth of the potential.

The form of the local height function. The local height function depends on lattice coordinates in a way related to one calculated[82] by assuming the potential is proportional to the charge density and the charge density is a sum of atomic charge densities. In this approximation only the first surface layer contributes to charge density near the turning point and hence to the repulsive part of the interaction potential, and as can be inferred from Fig. 2.3 the attractive potential is also dominated by the top layer close to the surface where the inelastic scattering takes place. We

model this by writing the local height function as a sum over each lattice site of the displacement of that site times a gaussian of the difference of the position in the plane of the surface between the particle and each lattice site.

$$h(\mathbf{R},\{n_i\}) = \sum_{i \text{ in surface}} u_{zi} \frac{e^{-Q_c^2(\mathbf{R}-\mathbf{R}_i)^2/2}}{\sum_{j \text{ in surface}} e^{-Q_c^2(\mathbf{R}-\mathbf{R}_j)^2/2}}. \tag{2.8}$$

The denominator in Eq. (2.8) normalizes the shift so that if the whole top surface layer makes a uniform shift the origin of the potential will shift by the same amount.

Since the classical turning point for the helium atom is very far from the surface the charge density at this point depends on the positions of more than just the closest atom. Said in another way, the displacement of a surface atom has a non-negligible effect on the local height above its neighbors. This dependence gives a value for the interaction potential phonon parallel wavevector cut-off $Q_c = .39\ a_0^{-1}$ that is smaller than the surface reciprocal lattice vector by more than a factor of two. This cut-off is primarily determined by the decay length of the surface density near the classical turning point and by the distance from the center of the displaced surface atom to the classical turning point and can be well approximated by considering just a single surface atom.[82] The validity of this approximation depends on how well the sum of atomic charge densities approximates the actual charge density in the asymptotic region of the surface. This treatment will overestimate rather than underestimate the coupling to large wavevector phonons if healing effects, where the surface charge rearranges to smooth out any perturbations, are important for the charge density away from the surface.

This cut-off explains[82] why it is much easier to observe zone boundary phonons for helium scattering from LiF[83] than it is for helium scattering from flat metal surfaces.[11,12] The atoms in the ionic solid, consistent with the surface being more strongly corrugated than these metal surfaces, are effectively smaller than those in the metals and do not cut-off the high wavevector phonons as efficiently.

When we make the flat surface approximation in which no point on the surface is different from

any other, the sums over lattice sites become integrals and give

$$h(\mathbf{R},\{n_i\}) = \int d^2R'\; u_z(\mathbf{R}')\; e^{-Q_c^2(\mathbf{R}-\mathbf{R}')^2/2}\; \frac{Q_c^2}{(2\pi)}. \tag{2.9}$$

We use the values of Q_c that have been calculated for helium scattering from copper.[82] In the calculation the important quantity is the Fourier transform of $h(\mathbf{R})$, $H(\mathbf{Q})$ which acts as a cutoff for high wavenumber phonons. Physically this cutoff reduces the effect on the change in the local height for phonons for which the near neighbor atoms are out of phase from each other. In the following section we will discuss the effect that this cut-off has both on the mean square displacement of the surface (Fig. 2.4) and on the inelastic scattering by changing the effective weighted phonon density as a function of the change in energy of the scattering particle (Fig. 2.5).

C. The Phonon Spectra

The final physical information about the system that is required is the phonon spectrum, or rather the phonon density of states projected onto the vertical displacements of the top surface layer weighted by the amplitude of the vibration. This quantity could be calculated for a force constant model using either a transfer matrix technique or a slab calculation.[84] These calculations would give accurate detailed information about the phonon density of states which would be necessary for calculations of specific inelastic scattering probabilities, but since the calculations in this paper deal mainly with the effect of inelastic scattering on elastic scattering, which depends only weakly on the details of the phonon spectrum, they would require more effort than appropriate.

The model we use is a semi-infinite isotropic elastic continuum model,[85,86] for which the appropriate density of states can be written down analytically. The primary defects of this model are that it has infinite extent in both frequency and wavevector and that the sound velocities are constant independent of the wavevector. Besides its analytic solution the main advantage of this model is that Rayleigh phonons are naturally introduced. This is important because the Rayleigh phonon modes are responsible for roughly one half of the mean square displacement of the surface.

Rayleigh modes are phonon modes that are localized to the surface and are the lowest frequency phonon modes at each wavevector.

The first problem with this model – its continuum nature – can be remedied by artificially introducing cut-offs into the spectrum; we choose to do this by cutting off the frequency at the Debye frequency and (since the surface is structureless) by cutting off the wavevectors with a circular surface Brillouin zone that has the same area as the actual surface Brillouin zone. Finally we choose the longitudinal and transverse sound velocities fixing the Rayleigh sound velocity in the model used. We choose these by averaging the principle axes sound velocities at the Γ point weighted by the occurrence of those axes. This choice, which insures that the model is most accurate for small wavenumbers, is appropriate because the high wavenumber phonons are cut-off as discussed in the previous section (see Eq. (2.8)). The choices for the phonon parameters are given in Table 2.1.

Figure 2.4 shows the mean square displacement of the surface as a function of temperature; it also shows the effect of the high wavevector cut-off discussed in Eq. (2.8) in the mean square effective height of the surface as a function of temperature for two choices of the cutoff parameter. The choice of cut-off used in the calculations in this paper drastically reduces the mean square effective height of the surface from the means square displacement of the surface. This reduction decreases the inelastic scattering from what it would be if the interaction potential did not decrease the coupling to high wavevector phonons.

Figure 2.5 shows the weighted density of phonon states as a function of the energy change in the motion normal to the surface due to each phonon

$$C(\Delta E_z) = \frac{1}{N}\sum_{\lambda,\sigma} n_{\lambda\sigma}|M_\lambda|^2(2\pi)\delta\left(\sigma\omega_\lambda - \left(\Delta E_z - \frac{(\mathrm{K}_i - \sigma\mathrm{Q}_\lambda)^2}{2m} + \frac{K_i^2}{2m}\right)\right). \tag{2.10}$$

M_λ is defined in Eq. (5.13) of I and is a measure of the amplitude of the phonon projected onto the surface layer; λ indexes the normal modes of the semi-infinite lattice and $\sigma = \pm$ indexes creation and destruction events. The integral of this density times the matrix element of the particle scattering states gives the inelastic scattering probability. Since the high parallel wavevector cut-off has a

larger effect on high energy phonons than it does on low energy phonons, the inclusion of the cut-off reduces the probability for high energy transfer inelastic scattering events. It also reduces the asymmetry between the energy loss and energy gain inelastic scattering probabilities.

Most of the calculations in this paper are for atoms scattering from surfaces at normal incidence because the calculation of the phonon density of states, $C(\Delta E_z)$, is simplified by the azimuthal symmetry of the phonon phase space. If we were treating corrugated surfaces the angle of incidence would strongly affect the diffraction probabilities, but for the flat surface approximation that we use the parallel momentum (due to the off-normal incidence) only affects the inelastic scattering through the phonon density of states. This effect is examined in Fig. 2.6 which shows the phonon density of states as a function of the normal energy change for a series of incident parallel momenta. If the phonon spectra were not cut off by the interaction potential the effect on the inelastic scattering probabilities would be large, but for the cut-off used in these calculations the effect is almost negligible (as seen in the bottom panel). For this potential the motion of the helium atom parallel to the surface only has a very small effect on the scattering probabilities.

We think that this model for the phonons contains all of the important features for calculating scattering probabilities, particular those that do not depend strongly on the details of the phonon spectrum. But for detailed comparison with inelastic scattering time-of-flight spectra a more detailed calculation would be required.

D. The Integration Techniques

To carry out these calculations numerically we have to discretize the differential equations and integrals in a manner that is both accurate and as simple as possible. We have to solve Schrödinger's equation on a discrete spatial mesh, using a prescription for correctly treating the boundary conditions, and using a discrete energy mesh for the possible final states.

1. Real space integration. There are very sophisticated and accurate methods for solving coupled channels equations for diffraction probabilities.[50,51,52,53,54,55,56,57] We use the simplest predictor method because more accurate methods which use the Numerov integration method or stabilization techniques require matrix inversions along the integration path which drastically increase the computation time. In addition we use a uniform spatial mesh rather than one that changes depending on the potential and the kinetic energy both for simplicity and because all the integrations of the inelastic wavefunctions must be done on the same spatial mesh as the elastic wavefunction. In spite of its simplicity we find that this method works quite well for calculating scattering probabilities.

The method is based on discretizing the differential equations for the scattering wavefunctions, Eqs. (5.30,5.31) of I on a uniform mesh with spacing Δz; the kinetic energy becomes the finite difference expression

$$-\frac{1}{2m}\frac{\Psi_{N+1}+\Psi_{N-1}-2\Psi_N}{(\Delta z)^2}. \tag{2.11}$$

where the Ψ's are square matrices whose rows are the different angular momentum channels (or for a more general problem the diffractive channels as well), and whose columns are form independent solutions with different boundary conditions. The subscript denotes the spatial point at which the wavefunctions are evaluated. Solving for the values of the wavefunctions at the $N+1$ spatial point in terms of the wavefunction and potential at the N and $N-1$ points gives the simple predictor method we use to solve the coupled Schrödinger equations.

$$\Psi_{N+1} = 2\Psi_N - \Psi_{N-1} - 2m(\Delta z)^2\left[\left(E - V(z_N)\right)\Psi_N - V_{int}(z_N)\Psi_N^{inhom}\right]. \tag{2.12}$$

The last term is the coupling to the inelastic wavefunctions for the elastic wavefunction or the coupling to the elastic wavefunction for the inelastic wavefunctions. Both V and V_{int} are matrices that include the translational-rotational coupling in the off-diagonal matrix elements.

This method has errors associated with it that are proportional to $(\Delta z)^2$, while the related Numerov method has errors proportional to $(\Delta z)^4$; however the Numerov method requires a matrix

inversion at each step of the integration. We have found that when the methods agree, which requires a smaller step size for the simple predictor method, that the simpler method usually is faster than the more complicated. When some of the angular momentum channels are strongly not allowed, *i.e.*, the kinetic energy in these channels is large and negative at positive infinity, the Ψ matrices can become singular. Typically stabilization methods are used to remedy this singularity; these methods involve diagonalizing the solution by multiplying both the solution and the solution at the previous point by the inverse of the solution at several points during the integration. To reconstruct the wavefunction from a stabilized integration (and not just the scattering probabilities as is usually desired) requires a significant increase in the number of matrix multiplications which might cause the same numerical instabilities that the method is trying to rectify. Using extended precision computations also removes the numerical instabilities and depending on the computer being used increases the computation time only by a factor slightly more than two.

2. *Boundary conditions* To solve Schrödinger's equation we choose boundary conditions at points far enough into the surface that the solutions can be approximated by decaying exponentials and at points far enough from the surface that the solution can be described in the WKB approximation. For energies close to zero this requires a very large distance from the surface. The differential equations are integrated from both ends toward the middle where both the solutions and their derivatives are matched to choose the solution with the correct boundary conditions at both ends. The boundary conditions on the final solution are that all of the channels decay into the surface, all the not allowed channels decay away from the surface, and all allowed channels behave like outgoing plane waves away from the surface except for the incident channel (present for the elastic, but not the inelastic wavefunctions) which behaves like a unit amplitude incoming plane wave with some additional outgoing component. Without the elastic wavefunction on the right hand side of Eq. (2.12) the solution for the inelastic wavefunctions with these boundary conditions will be identically zero. To guarantee a unique solution for a set of angular momentum channels it is necessary to integrate the same number of possible solutions as their are channels included

in the integration. The bound state energies are the energies for which it is possible to match the wavefunctions that have been integrated from both directions since there is no possible incoming channel.

In general we have found that the solution is not very sensitive to the boundary conditions in the surface because all channels have such a large negative kinetic energy that the component of the solution with the wrong boundary conditions, *i.e.*, the part that blows up into the surface, is strongly damped upon integration toward positive infinity. On the other hand the solution is very sensitive to the boundary conditions in the vacuum region away from the surface if the kinetic energy in any channel is close to zero, either positive or negative. To correctly calculate the wavefunctions under these conditions it is necessary to extend the integration far enough into space that it is possible to use a WKB approximation to start the integration. We do this by turning off the translational-rotational coupling and extending the integration for each channel as far as is necessary to remove the numerical singularities that would result otherwise for that channel. It is important to use the second WKB approximation, *i.e.*, the approximation that includes the square root of the local momentum

$$\sqrt{\frac{k_i}{k(z)}} \exp\left(i \int_{\infty}^{z} dz'\, k(z')\right), \tag{2.13}$$

where the local WKB wavevector $k(z)$ is defined as $k^2(z) = k^2 + 2mV(z)$. If the square root prefactor is omitted the inelastic scattering probability will diverge in the limit that the incident energy goes to zero. For channels in which the kinetic energy far from the surface is negative the same expression can be used for the boundary conditions by simply replacing the wavevector by the imaginary wavevector that gives solutions that decay away from the surface.

9. Energy integration For problems with narrow selective adsorption resonances it is non-trivial to find an energy mesh that both includes enough detail at the resonances and does not waste time by having a denser than necessary energy mesh away from the resonances. To find a mesh that satisfies these two criteria we calculate the T-matrix for scattering from a static surface as a function

of energy and record a mesh point every time the T-matrix has changed by a certain amount. Since the phase of the T-matrix changes by two pi through each resonance, this concentrates mesh points at the resonances. It is usually necessary to add several points by hand because there are often insufficient mesh points on the wings of the resonances. We then use this mesh in all the subsequent calculations of inelastic scattering probabilities. Using this mesh is made simple by the availability of an analytic expression for the phonon density of states; for densities of states based on slab calculations it would be necessary to interpolate between the calculated normal modes.

There are special energy grid points at the bound state energies of the potential. As is discussed in I trapping is treated by including a small imaginary part in the energy of the scattering particle. This imaginary part has to be chosen small enough that it does not affect the positive energy states, in particular it must be smaller than the energy width of the narrowest resonance. The bound state energies have to be found more precisely than this small imaginary part in the energy to get correct results for the trapping probability. A simple binary is used to find the bound state energies of the difference equation to an accuracy better than the small imaginary part; this accuracy, however, is not relevant for either the physical system or the differential equation that is being approximated by the difference equation.

III. RESULTS

This section, which is divided into three subsections, gives the details of our calculations of elastic and inelastic scattering probabilities. The first subsection gives the results for helium scattering from copper with the emphasis on the effect of inelastic scattering on elastic scattering and the effect of the shape of the surface potential on the various scattering probabilities. The second subsection emphasizes the trapping process and the the resonant enhancement of both inelastic scattering and trapping of H_2 and D_2 on surfaces. Finally the third subsection, which gives the results for HD scattering, presents the effect of inelastic scattering on both diffractive scattering

and selective adsorption resonances.

We choose to calculate the scattering probabilities for copper surfaces for several reasons, most importantly that all of these scattering particles have been scattered from Cu(100) or Cu(111). Additional considerations were that the surface be flat (low diffraction intensities), the phonons are not too soft (so the inelastic scattering does not get so large as to invalidate the approximations), models for the potentials exist in the literature, and no important electronic processes (*e.g.*, dissociation of molecular hydrogen) be important during the scattering process. For all of these reasons copper (100) and (111) are ideal surfaces to test these calculational techniques and examine the consequences.

A. Helium Scattering

We consider helium scattering not only for its own interest but also because it is not complicated by rotational degrees of freedom like molecular hydrogen. When we investigate hydrogen scattering we will have isolated the effects due to the rotational degrees of freedom from the effects that are independent of them. Since the main experimental interest in helium scattering is as a probe of the surface structure we concentrate our study on how elastic scattering probabilities depend on experimental conditions, such as the surface temperature and the incident energy. Toward this same end we examine the sensitivity of the elastic scattering probability to details of the potential besides the corrugation. Finally we discuss the difficulties involved in developing simple approximations that attempt to account for the effects of inelastic scattering on elastic scattering, in particular the use of optical potentials.

1. General results. Not surprisingly, the experimental fact that the elastic scattering probability falls off both with increasing surface temperature and with increasing incident energy is seen in these calculations. Beyond this behavior the important questions to be addressed are: 1) what is the most correct way to describe the elastic scattering probability, 2) how is the scattering behavior

related to interesting properties of the surface, and 3) how, if at all, is this behavior to be simply approximated.

We investigate five models for the elastic scattering probability, three related to the distorted wave Born approximation, and two related to the descriptions of diffraction intensities in x-ray and neutron scattering. Of the first three methods two are based on a one phonon approximation and are described in I and the last is an attempt to extend these approximations into the multi-phonon regime (this is discussed later in this section). The first of the last two methods (both discussed in this section) involves taking the Debye-Waller expression for the temperature dependence of neutron scattering intensities and applying it to surface scattering problems, and the second attempts to correct for some of the physics left out of this approach by including the effect of the attractive potential in an approximate manner. These methods are compared in Figs. 3.1-2, which show the scattering probability as a function of surface temperature and incident energy respectively.

The first method we explore is the distorted wave Born series. The first term in the Born series is the scattering from the static surface; for an uncorrugated system with no translational-rotational coupling this is always unity. The first correction due to the inelastic scattering to this first term can be shown to be equal to the negative of the total first-order inelastic-scattering probability, *i.e.,* the lowest order expression for the effect of inelastic scattering on elastic scattering is just one minus the total first-order inelastic-scattering probability calculated in the distorted wave Born approximation (DWBA)

$$P_{el}^{DWBA} \simeq 1 - P_{inel}^{DWBA}. \tag{3.1}$$

This result is only valid when the inelastic scattering probability is small compared to one; which is often not the case for situations of experimental interest. When the distorted wave Born approximation for the inelastic scattering probability becomes greater than one (which is allowable in this approximation) Eq. (3.1) produces a negative elastic scattering probability.

A related approach for calculating the elastic scattering probability which we do not consider is to calculate the T-matrix to lowest order and then square it giving a result that is the same as

the distorted wave Born series result in the weak scattering limit and is positive definite for all scattering strengths.[59,58] However, like the approximation discussed above, this approximation is also not constrained to be less than one, and furthermore it includes some fourth order contributions to the elastic scattering probability but omits others that are the same size.

The second method we consider, which is also a one phonon approximation, is the self-consistent one-phonon approximation developed in I. Essentially it involves making the one-phonon approximation in the self-energy of the scattering particle rather than in the scattering probability. Even though this approximation constrains the elastic scattering to lie between zero and one it is still a one phonon approximation and does not have a significantly larger range of validity than the Born series. It is more useful for calculating the temperature dependence of diffraction and rotational diffraction intensities especially near selective adsorption resonances.

To extend these distorted wave Born approximation methods into the multi-phonon regime we use a method we call the exponentiated inelastic scattering model. As its name suggests it involves exponentiating the first-order inelastic-scattering probability to predict the elastic scattering

$$P_{el}^{EI} = \exp\left(-P_{inel}^{DWBA}\right). \tag{3.2}$$

In the weak scattering limit the expanded exponential is identical to the distorted wave Born approximation result and the probability is bounded between zero and one. Even though we feel this method is the best available extension of the one phonon results to the multi-phonon regime we regard it as ad hoc. Two possible ways to argue that this is a reasonable approximation might be 1) that it is the result of a cumulant expansion[60] and 2) that the probability for a n-phonon-change scattering event is assumed to be a Poisson distribution.[36] Unfortunately, (1) the other terms in the cumulant expansion have not been checked to see how important they are, (2) multi-phonon terms have only been calculated under very restrictive approximations[49,87] so that the form of multi-phonon scattering probabilities is still an open question.

Figure 3.1 is a Debye-Waller plot, in which the elastic scattering probability is plotted on a logarithmic scale against the surface temperature. It is called a Debye-Waller plot because similar

plots of neutron scattering intensities give straight lines for temperatures larger than the Debye temperature of the surface. Figure 3.2 shows the elastic scattering probability also plotted on a logarithmic scale, but as a function of the incident energy. The scale on the right hand side of both plots gives the negative of the natural logarithm of the elastic scattering probability; for the exponentiated inelastic scattering model this is equal to the distorted-wave Born-approximation result for the inelastic-scattering problem which can be used as a gauge of when the scattering is in the one phonon and and when it is in the multiphonon regime.

Both plots show that all three methods agree well in the one phonon regime where the inelastic scattering is small compared to one, but disagree in the multiphonon regime. The distorted-wave Born results diverges on this type of plot when the inelastic scattering probability becomes greater than one. In addition to a curvature in each curve at low temperatures due to the zero point motion of the surface there is unphysical curvature at high temperatures in the distorted-wave Born series results due to the divergence caused by the increasing inelastic scattering outside the one phonon regime. Even though the elastic scattering probability in the self-consistent one phonon approximation is bounded between zero and one so that its logarithm does not diverge, there is still downward curvature outside the one phonon regime (where the distorted-wave Born-approximation results are not small compared to one, which occurs at high temperatures in this plot) that seems unphysical because of its resemblance to the curvature seen in the distorted wave Born approximation results. In other words it is not possible to attach any significance to the downward curvature that is present outside of the one-phonon regime because the approximation is not valid there; in addition, the downward curvature bears a strong resemblance to the definitely unphysical result seen in the distorted-wave Born-approximation results. This curvature is necessarily absent from the exponentiated inelastic scattering model because the distorted wave Born approximation inelastic scattering probability is proportional to the temperature for temperatures larger than the surface Debye temperature. Since none of these models are valid in the multi-phonon regime, none of them can reliably predict that the logarithm of the elastic scattering probability should be pro-

portional to the temperature in this limit or whether there would be less or more elastic scattering than is predicted in this regime.

The other two methods shown in these two figures are related to the Debye-Waller factor; which for scattering from a surface gives the temperature dependence of the specular (specular scattering refers to the particles that scatter elastically without diffracting, for a flat surface specular and elastic scattering are the same) scattering probability as

$$P_{el}^{DW} = \exp\left(-8mE_z\left\langle u_z(\mathrm{R})^2\right\rangle_{th}\right), \tag{3.3}$$

where E_z is the energy in the motion normal to the surface. For diffraction there are also contributions from the motion of the particle and the phonons in the plane of the surface, but these are much less important, both in general and especially for the flat surfaces we are considering. There is no reason to expect that this expression should describe surface scattering (see Appendix B). Ignoring the complications due to the strength of the scattering, *i.e.,* weak for neutrons and strong for helium, the potential for an atom scattering from a surface is much different than it is for neutron scattering from a solid. In particular: the potential is soft as opposed to delta function-like, there is an attractive part to the potential, and the potential cannot be described by pair potentials so that the effective amplitude of high wavevector phonons is reduced more than that of the low wavevector phonons.

This result Eq. (3.3) can be modified in several ways to approximately include some of the physics that is different in surface scattering situations. One way, illustrated in Figs. 3.1,3.2, is to use the mean-square effective height of the surface rather than the mean-square displacement

$$P_{el}^{DW} = \exp\left(-8mE_z\left\langle h(\mathrm{R})^2\right\rangle_{th}\right). \tag{3.4}$$

Since the mean square displacement is more than twice as large as the mean square effective height, if we were to use the former in place of the latter the elastic scattering probability would be much smaller and further from the perturbation theory based results in the weak inelastic scattering limit.

Surprisingly it is possible to account for most of the changes in scattering probabilities for systems with different attractive potentials by shifting the incident normal energy by the change in the well depth. Applying this shift in the Debye-Waller factor leads to

$$P_{el}^{BCDW} = \exp\left(-8m(E_z + D)\left\langle h(\mathbf{R})^2\right\rangle_{th}\right), \tag{3.5}$$

where D is the well depth. This is known as the Beeby-corrected Debye-Waller factor;[44] in Figs. 3.1,3.2 it is seen to move the elastic scattering probability even further from the perturbation based results. This increased deviation could be compensated for by including the effects of the softness of the surface potential because that correction would increase the elastic scattering probability from the Debye-Waller result. In the next section of this chapter we study the effect of a steeper potential would have on the elastic scattering probability. We find that it reaches a hard wall limit in which the elastic scattering probability is very close to the Beeby-corrected Debye-Waller result implying that the differences are due to the softness of the potential. Unfortunately we know of no simple way to account for the softness of the potential in a Debye-Waller-like analysis; a correction that would have to depend not only on the range parameter of the potential but also on the well depth and on the scattering energy. This dependence can be seen in Fig. 3.2 in the non-linearity of the inelastic scattering probability as a function of the incident energy.

In these comparisons of the Debye-Waller factors (see also the discussion of the range parameter dependence of the scattering probabilities in the next section) to the distorted wave Born approximation based methods, we are biased in favor of there being agreement by the use of the exponentiated inelastic scattering model. This bias results from the assumption in the exponentiated inelastic scattering model that the elastic scattering probability is equal to the exponential of some weighted measure of the mean square displacement of the surface, specifically the first order distorted wave Born approximation for the inelastic scattering. It may seem bizarre to view the distorted wave Born approximation as a weighted average of the phonon density of states but it is essentially that. Taking that point of view the exponentiated inelastic scattering model is very similar to the Debye-Waller factor derived for neutron scattering, and when the differences between

the two ways of averaging the phonons are taken into account the methods become identical; the important differences, which are due to the form of the interaction potential, are the attractive potential, the large phonon wavevector cut-off, and the softness of the potential. However, we have no reliable way of testing the validity of the exponentiated inelastic scattering model or ruling out that higher order contributions do not have a more complicated temperature dependence.

Figure 3.3 compares elastic scattering probabilities, calculated using the exponentiated inelastic scattering model, with experimentally measured ones.[5,6] The agreement is surprisingly good for a calculation with no adjustable parameters; although it is better for the 63 meV results than it is for the 21 meV results which are closer to the one-phonon regime in which this calculation is more reliable.

The assumptions about the potential that have the largest effect on the scattering probability are 1) the range parameter of the repulsive potential, 2) the choice of using the derivative of the full potential or of the repulsive potential in the interaction potential, and 3) the choice of the form and values for the dependence of the interaction potential on the phonon parallel wavevector. The dependence of the elastic scattering probability on the first two choices is discussed in the following section. Of these two, the second is the more important for these systems because the inelastic scattering probability used in the exponent for the elastic scattering would be roughly twice as large. The effect of the third assumption is illustrated in Fig. 2.4 which compares the mean-square displacement of the surface with the mean-square effective height of the surface. The inelastic scattering probability is roughly proportional to the mean-square effective height; if the parallel wavevector cut-off were not included in the interaction potential the inelastic scattering would be approximately twice as large. This difference highlights the difficulty in extracting information about the scattering system from the experimental temperature dependence, here the mean square effective height that would be extracted from these calculated curves is not simply related to the mean square displacement of the surface atoms.

2. Dependence on potential parameters. Using a Morse potential, which allows easy variation of the potential parameters, this calculation can be used to test the sensitivity of the elastic scattering probability to the choice of the potential. Calculations[59,58] using a one-dimensional model and the distorted wave Born series have found similar results to these calculations. We use the exponentiated inelastic scattering model because it is the simplest and because the behavior should not differ from the other two perturbation-based approaches in the regime where the three can be trusted. Figure 3.4 shows the elastic scattering probability for the exponential-van der Waals potential and a Morse potential chosen to have the same well depth and the same range parameter for the repulsive part of the potential.

We attribute the slight difference between the two results to the difference between the attractive potentials in the region of the classical turning point; the difference between the potentials can be seen in Fig. 2.2. As we show in section III.C, the inelastic scattering primarily takes place near the classical turning point and not in the region where the potential is dominated by the attractive potential. At the classical turning point the Morse potential is steeper than the exponential-van der Waals potential so the inelastic scattering is stronger and hence the elastic scattering is weaker for the Morse potential than it is for the other. That a steeper potential gives weaker elastic scattering is born out by studying the elastic scattering probability as a function of the range parameter.

Figure 3.4 also shows the elastic scattering probability for several other Morse potentials in which the range parameter varies by a factor of sixteen. As expected a steeper potential produces stronger inelastic scattering, although the variation is much more dramatic as the range parameter is decreased. The results for the two steepest potentials lie on top of each other indicating that the potential has reached a hard wall limit. The differences between the results for the physical potential and the results for the potentials in the hard wall limit are very close to the differences between the physical potential and the Beeby-corrected Debye-Waller factor results in Fig. 3.2. For these systems, helium and molecular hydrogen on copper, the potential is close to but not in the hard wall limit.

In the previous section we mentioned that the effect of the attractive potential can be accounted for to a large extent by adding the well depth to the energy in the motion normal to the surface; this is examined in Fig. 3.5 by varying the well depth of the Morse potential by a factor of eight. Adding the well depth does not completely correct for the effects of the attractive potential because the Morse and exponential-van der Waals potentials that have the same well depths but different forms of the attractive potential do not have identical scattering probabilities (as seen in Fig. 3.4). The difference is due to the slope at the classical turning point depending on the form of the attractive potential even for potentials that give the same well depth. If the idea behind the Beeby-correction is correct the curves in this figure should be shifted with respect to each other along the energy axis by an amount equal to the difference between the well depths. Using the inset at the top of the figure as a guide this is seen to be correct for this choice of range parameter and these various well depths.

In contrast to the results given in Fig. 3.5, Fig. 3.6 shows the same calculation repeated using just the repulsive part of the static surface potential in the coupling to the phonons rather than the full potential. For this model of the interaction potential the inelastic scattering is stronger by at least a factor of two than it is for the other model using the same static surface potential. The attractive potential is also much more effective at increasing the inelastic scattering than it is for the other model because it allows the helium atom to get into a region of much stronger inelastic coupling. The Beeby correction underestimates the effect of the attractive potential for this model of the interaction potential. By comparing He and D_2 scattering from several flat surfaces it should be possible to distinguish between models for the interaction potential because, except for the presence of weak rotationally mediated selective adsorption resonances, the most important difference between the two systems is the strength of the attractive potential. The surfaces should be flat because the increased attraction for the deuterium molecule can also increase the effective corrugation that the molecule experiences.

Figure 3.7 shows the dependence of the elastic scattering probability on the mass of the scat-

tering particle for two different well depths, that for helium and one four times the helium well depth which happens to be quite close to the molecular hydrogen well depth. Over the range spanned by these plots the inelastic scattering is proportional to the mass as is predicted by the Debye-Waller and related treatments. The distorted wave Born approximation integrated over all final momenta, depends on the mass through an overall factor of mass and the mass dependence of the wavefunctions. The mass dependence of the incident wavevector at constant incident energy is canceled by a similar factor from the integration over the final states. That the inelastic scattering probability scales with the mass implies that the matrix element of the scattering states is only very weakly dependent on the mass.

To summarize the dependencies we have found: 1) the potentials we use for helium and hydrogen scattering are almost but not quite in the hard wall limit with respect to the variation of the range parameter, 2) for the model of the interaction potential we are using, the effect of the attractive potential can be accounted for by adding the well depth to the incident energy in the motion normal to the surface (but not if we were to use the repulsive potential inelastic coupling), and 3) the inelastic scattering, which is the exponent in the exponentiated inelastic scattering model, is proportional to the mass of the scattering particle. Previously, in section III.C, we showed that 4) the inelastic scattering is roughly proportional to the effective mean-square effective height based on the form of the phonon-wavevector dependence of the interaction potential.

3. Optical Potentials. It would be desirable to develop an approximation scheme that could be used to calculate elastic scattering probabilities more simply than is done in this calculation. Above we concluded that Debye-Waller factors can be used a phenomenological fitting factors but need drastic modification to be used to predict scattering probabilities. Another possible approach is to use an optical potential, a potential with an imaginary part that causes flux to be absorbed from the incident wavefunction. We have not been able to find a model that can reproduce the desired features; to illustrate why we have calculated the self-energy for the self-consistent one-phonon

approximation (see Eq. (4.12) of I). The self-energy is equivalent to a non-local energy dependent optical potential because the zero-phonon-change amplitude discussed in I satisfies

$$\left[H_{part} - E_{\mathbf{k}} - i\eta\right] \psi^{(+)}_{0ph}(\mathbf{r},\mathbf{k}) = \int d^3r' \; \Sigma(\mathbf{r},\mathbf{r}',E_{\mathbf{k}})\psi^{(+)}_{0ph}(\mathbf{r},\mathbf{k}), \tag{3.6}$$

where Σ is the self-energy calculated in the one-phonon approximation. Using the assumptions for the form of the interaction potential discussed in I the self-energy reduces to

$$\Sigma(z,z',E_z) = \int \frac{d\Delta E_z)}{(2\pi)} \, V'(z) G^r_1(z,z',E_z - \Delta E_z - i\eta) V'(z'). \tag{3.7}$$

The Green function can be calculated for small but finite value of the imaginary piece, η, by using its spectral form.

Figure 3.8 shows the imaginary part of the self-energy for three different energies as a function of the two spatial arguments for a surface temperature of 240 K. The main point of this figure is that it is very difficult to approximate this function in any manner that retains the important physics. The difficulty arises because this self-energy is strongly energy-dependent, non-local, and non-separable as well as being temperature dependent. The energy dependence of the elastic scattering probability results from the energy dependence not only in the incident scattering state, but it also from energy dependence of the final scattering states near the incident energy. This dependence on the final states complicates any optical potential treatment because the strength of the optical potential depends on the incident energy.

The non-local and non-separable aspects of an optical potential will drastically slow any numerical calculation. If the self-energy were approximately local, *i.e.*, proportional to a delta function of the difference of the two spatial arguments, it would be possible to treat the optical potential as though it only had one spatial argument, which would allow calculating scattering probabilities in a way that would not be much more complicated than the calculation for a static surface. On the other hand, if the self-energy dependence were separable, the calculation of the scattering probabilities would involve an extra spatial integration over the second spatial argument, but that integration could be done independently of the other spatial argument allowing a simple self-consistent solution

of just a single differential equation. The temperature dependence of the self-energy would be well approximated as proportional to the mean-square effective height of the surface.

B. H_2 and D_2 Scattering and Trapping

Molecular hydrogen scattering differs from helium scattering because 1) the mass is different (except for D_2), 2) the potential well is deeper because the attractive potential is stronger, and 3) the molecule has rotational degrees of freedom. The effects of changing the mass and the well depth are among the the topics discussed in the previous section helium scattering probabilities. The rotational degrees of freedom affect molecular hydrogen scattering in two ways, 1) the molecule can make rotational transitions, both real transitions and virtual rotational transitions into bound states of the surface potential, and 2) the potential of the molecule depends on its rotational state (even if no rotational transitions occur). For H_2 and D_2 the effects of the rotational degrees of freedom, which are discussed in this section, are much less important than they are for the much more asymmetric HD molecule, which is discussed in the next section.

Selective adsorption resonances. Although the rotational effects are more prominent for HD scattering they can still be seen for H_2 and D_2 in Fig. 3.9 which shows the inelastic scattering probability for different incident angular momentum states. The large peaks are due to the selective-adsorption resonance enhancement of the inelastic scattering. A rotationally mediated selective adsorption resonance occurs when a molecule makes a virtual rotational transition into a bound state of the gas-surface potential and spends a long time in this rotationally excited state before it leaves the surface. (See Appendix A for a more complete description of selective adsorption resonances.) Typically selective adsorption resonances are seen in a scattering experiment through diffraction (or rotational diffraction) intensities; at the resonances there are large rearrangements of the scattering intensities between various elastic and rotationally inelastic scattering channels (allowed zero-phonon-change final states). For low incident energies in the systems studied here

specular scattering is the only possible zero-phonon-change final state, *i.e.*, no rotational transitions can occur and no rearrangement can take place. However, selective adsorption resonances still have experimental consequences because they enhance inelastic scattering which in turn changes the elastic scattering probability.

Since the particle spends a long time in the region of the potential minimum the probability for inelastic scattering is increased giving the peaks seen in Fig. 3.9. For these symmetric hydrogen molecules the translational-rotational coupling is very weak so that the resonances are narrow, *i.e.*, once a molecule makes a transition into a rotationally trapped state it remains there for a long time before it makes a transition out of the trapped state (ignoring inelastic scattering).

At this point it is useful to define several terms used in this discussion of selective adsorption resonances, particularly with respect to the widths of the resonances as a function of energy (all widths refer to functions of energy in this chapter). The term static surface refers to the surface with all of the lattice displacements fixed to zero, and should not be confused with a zero temperature surface for which the lattice atoms move with their zero point motion. If we hypothetically scatter molecules from a static surface there is no inelastic scattering and the selective adsorption resonances have a width that is determined by the translational-rotational coupling; we call this width the elastic width and its inverse the elastic lifetime

$$\Gamma_{el} = \tau_{el}^{-1}. \tag{3.8}$$

For particles that scatter from a surface that is free to move, even if it is zero temperature, the width of the selective adsorption resonances increases due to the inelastic scattering. The width of a resonance is given by the sum of the elastic width and the inelastic width

$$\Gamma = \Gamma_{el} + \Gamma_{inel} = \frac{1}{\tau} = \frac{1}{\tau_{el}} + \frac{1}{\tau_{inel}}. \tag{3.9}$$

In the distorted wave Born approximation the resonances are not broadened by the inelastic scattering so the width of the resonant enhancement of the inelastic scattering is given by the elastic scattering width. The self-consistent one-phonon approximation allows the inelastic scattering to

affect the elastic scattering in a way that allows the resonances to broaden inelastically. Most of the resonances we discuss have inelastic widths that are greater than their elastic widths when calculated in the self-consistent one-phonon approximation.

The narrow H_2 and D_2 resonances produce enhancements of the inelastic scattering probability that are so large that the distorted-wave Born approximation used to calculate the scattering probabilities is not valid at the resonances. Unfortunately calculations using the self-consistent one-phonon approximation are difficult because the peak heights are so large that an iterative solution does not converge even when the background values of the inelastic scattering probability are in the one-phonon regime. Nonetheless the results of the self-consistent calculation applied to HD scattering can be used to qualitatively understand what happens to H_2 and D_2 scattering near selective adsorption resonances when inelastic scattering is important. Both HD resonances and H_2 and D_2 resonances for which the inelastic width is much larger than the elastic width should behave similarly to each other because the processes that contribute to the inelastic width are similar.

The resonant enhancements, although extremely large, are narrow enough that their contribution to the inelastic scattering is comparable to the background when both the resonant contribution and the background are integrated over a typical experimental resolution of 0.5 meV. For instance, the H_2 resonance near 33 meV has a width of about 4×10^{-3} meV and a weight integrated over energy of 0.7 meV while the background at that energy integrated over 0.5 meV has a value of 0.2 meV. If inelastic scattering did not affect the resonance widths the resonances would show up as suppressions of the elastic scattering probability. However the peak value of the inelastic scattering at the 33 meV resonance is 56 which is an unacceptable value for a scattering probability. Since the peaks are so large they broaden considerably to the point where the widths of the peaks are dominated by the inelastic lifetime as opposed to the elastic lifetime that determines the widths of the peaks as seen in Fig. 3.9. The broadened peaks will have a much smaller effect compared to the background inelastic scattering as is seen below in the temperature dependence of the HD

resonances. The inelastic lifetimes of the HD selective adsorption resonances which should be comparable to the inelastic lifetimes of the H_2 and D_2 resonances are much shorter than the elastic lifetimes of the H_2 and D_2 resonances.

The resonances are different for H_2 and D_2 because the mass and hence the moment of inertia is larger for the latter. The larger D_2 mass yields more bound states in the gas-surface potential, and further the bound states are closer together in a given energy range. The mass also increases the background value of the inelastic scattering probability by roughly a factor of two as was discussed in the previous section of this thesis and hence the height of the resonances is also increased by a factor of two over what it would be if the other aspects of the resonance were unaffected by the difference in the mass. Since the moment of inertia is also larger by a factor of two for D_2 compared to H_2 the rotational energy splitting is smaller and the resonances occur at lower energies than they do for H_2.

Rotational state dependencies of the potential. In addition to the difference in the selective adsorption resonances the inelastic scattering probabilities in Fig. 3.9 depend on the rotational state of the molecule due to the fact that the potential depends on the orientation of the molecule. Since the potential depends on the configuration of the system, expanding the state in terms of a set of functions that describe part of the system, like spherical harmonics describing the orientational state of the molecule, leads to a potential that depends on the expansion function, *i.e.*, in this case the angular momentum state of the molecule, that describes the state of the system. For example, the rotational energy splittings for these molecules are large enough relative to the other energies in the problem that it is appropriate to use a quantum mechanical description of the molecules in which the molecules are in a particular rotational state rather than being oriented in a particular direction. These rotational states are given by the spherical harmonics of the angles that describe the orientation of the molecule. The dependence of the gas-surface potential on the orientation of

the molecule can be expanded in Legendre polynomials

$$V_0(z,\theta) = \sum_{l''} V_{l''}(z) P_{l''}(cos\theta). \tag{3.10}$$

Since we use an angular momentum state description of the scattering molecule it is convenient to take the spherical harmonic matrix elements of this potential (Eq. 3.10)

$$V_{ll'}(z) = \sum_{l''} V_{l''}(z) \int d\Omega \; Y^*_{lm}(\theta,\phi) P_{l''}(cos\theta) Y_{l'm}(\theta,\phi). \tag{3.11}$$

The diagonal parts of this description of the potential govern the motion of a particle in a particular angular momentum state and the off-diagonal parts govern the coupling between different angular momentum states. The diagonal parts of this description of the potential are shown in Fig. 3.10 for several different rotational states.

Figure 3.10 illustrates the potentials that lead to the differences in the inelastic scattering probability seen in Fig. 3.9 for the incident angular momentum states $l = 0$ and $l = 1$ both $m = 0$ and $m = 1$. These potentials cause the differences in the background value of the inelastic scattering probability because the slope of the potential in the neighborhood of the classical turning point is sufficiently different for the each rotational state, *e.g.*, the $l = 1, m = 0$ angular momentum state has the least steep potential and the weakest inelastic scattering. In the inset of the figure the potentials have indistinguishable slopes, but since the $l = 1, m = 0$ potential reaches a given value further into the surface and the potentials have the same value at the potential minimum, the slope averaged over the extent of the first peak in the wavefunction of the scattering particle is smaller for a molecule in this rotational state. In spite of the differences in the potentials for the molecules with different azimuthal quantum numbers the D_2 selective adsorption resonances occur at very close to the same energy for both $l = 1, m = 0$ and $l = 1, m = 1$ because the potentials for the rotationally excited molecules with the same azimuthal quantum numbers are very close to each other in the well region where the bound state wavefunctions are large, *i.e.*, the $l = 3, m = 0$ and $l = 3, m = 1$ potentials.

These differences in the inelastic scattering probabilities lead naturally to the discussion of the dependence of the sticking probability on the rotational state of the molecule, a topic of current

experimental interest. The interest in this problem is due to the observation in electron energy loss and work function change measurements that there were different proportions of para-hydrogen and ortho-hydrogen measured on the surface for the same exposure of each gas.[30] Subsequent molecular beam measurements of the sticking probability have born out this observation in a surprising way; there are peaks in the sticking probability when the total energy of the incident molecule is equal to a rotational excitation.[32] The results of this experiment are difficult to understand in terms of the assumptions we make in these calculations, particularly difficult are the peaks that occur when the total energy of the particle is equal to a rotational transition energy.

Our earlier calculations for the trapping probability[67] showed that the rotational dependence of the sticking probability was not due to selective-adsorption resonance-enhanced trapping because the resonances were extremely narrow and had a very small weight. In that calculation we used a form for the potential[77] that had a much weaker orientational dependence than found in subsequent calculations.[79] We used different phonon cut-offs, a larger value of ω_D and Q_c, than we currently believe to be the most appropriate. Our potential choice lead us underestimate the differences due to the rotational degrees of freedom and our choice of cut-offs lead to an overestimation of the effects of the selective adsorption resonances because it allowed resonances with higher energies to contribute to the trapping probability.

Figure 3.11 shows the results of a calculation for the probability for trapping onto a zero temperature copper surface as a function of incident energy. The calculation was done for the molecules normally incident on the surface and then the energy was scaled by $(\cos 60°)^{-2}$ to convert from the normal energy to the total energy for an angle of incidence of 60°, the experimental angle of incidence. We showed in section III.C that using the energy in motion normal to the surface is sufficient to account for almost all of the effect of off-normal incidence on the inelastic scattering probabilities. The curves for ortho-hydrogen and para-deuterium (both odd angular momentum species) have been averaged over the possible values of the azimuthal quantum number. For the values of the parameters used in this calculation there are no resonances that contribute to one-

phonon trapping for H_2 and the ones that contribute for ortho-deuterium are extremely weak. There are differences of about ten percent between the even and odd angular momentum species of both H_2 and D_2 due to the differences in the potential discussed with respect to Fig. 3.10. These ten percent differences are probably below experimental resolution because the populations of para- and ortho-hydrogen in the two different gas mixtures are not that well known. The H_2 trapping probability is roughly twice that of D_2 at low energies, but at higher energies they are almost the same. The low-energy ratio of the experimentally measured deuterium sticking probability is larger than that of hydrogen by a factor of two, but the ratio increases at higher energies rather than decreases. This increase in the ratio is understandable because multi-phonon contributions (relative to the one-phonon contributions) to the trapping are more important for deuterium, since its mass is greater, than they are for hydrogen.

It is not appropriate to directly compare the measured sticking probabilities to the calculated trapping probabilities because a calculation of sticking probabilities should use the trapping probabilities as inputs in a kinetic calculation.[88] We envision that sticking is a several step process; the initial trapping step is describable within the methods described in this thesis and then the trapped particle becomes incoherent with respect to its incident conditions as it undergoes a series of inelastic transitions that bring the particle into equilibrium with the surface. The kinetic calculation that describes this incoherent thermalization process would have to include the motion parallel to the surface as well as the motion normal to the surface since the energy in motion parallel to the surface is typically larger than the well depth in this experiment. As we discussed in section III.C of this thesis the phonons that cause large parallel wavevector transfer are cut off in the interaction potential which means that many phonon transitions are necessary to remove the energy in motion normal to the surface. This combined trapping and kinetic calculation is likely to preserve some of the features of the trapping calculation such as the factor of two difference between the D_2 and the H_2 results. It is also likely to depend more strongly on the energy in motion parallel to the surface than the trapping calculation because that energy has to be transferred to the surface

before the particle is considered stuck to the surface. This may explain why the experimental sticking probability depends on the total energy of the scattering particle rather than the energy in motion normal to the surface like the trapping probability does. The total energy dependence of the sticking probability is consistent with the sticking process starting with a trapping event.

It is hard to imagine how the calculations discussed in this thesis for flat surfaces can explain the observed peaks in the sticking probability that occur when the total energy of the scattering particle is equal to a rotational transition in the molecule. The selective adsorption resonances are too weak and occur when the energy in motion normal to the surface is equal to a bound state energy plus a rotational transition. A possible explanation is that the sticking, *i.e.*, conversion from being trapped to being stuck, is dominated by the presence of defects on the surface. Even if defect densities are very low most trapped particles encounter at least one defect while they are on the surface since their wavefunctions are very spread out and they are moving relatively fast. Defects break the translational invariance parallel to the surface and hence couple the parallel momentum more strongly to the motion normal to the surface. The coupling to rotations at defects may be strong enough at defects that sticking is enhanced when the energy of the particle on the surface is close to a rotational transition energy.

C. HD Scattering

The asymmetry of the HD molecules has two important consequences for the dependence of the scattering probabilities on the rotational degrees of freedom, 1) since the nuclei are distinguishable odd angular momentum transitions are allowed and 2) since the center of mass is offset from the centroid of the electron cloud the translational-rotational coupling is much stronger than it is for H_2 or D_2. The increased coupling to rotations gives much stronger rotationally inelastic scattering and much broader selective adsorption resonances. These resonances are broad enough that they can be treated within the self-consistent one-phonon approximation developed earlier in

this thesis which allows a quantitative calculation of resonant scattering for these systems leading to a qualitative understanding of the effect of inelastic scattering on selective adsorption resonances in other systems.

Static surface scattering. Figure 3.12 gives the scattering probability for HD scattering from a static (lattice atoms fixed) copper surface. The top panel shows the elastic, or $l = 0$, scattering probability which is unity for all energies below 11 meV because there are no other accessible outgoing states. Above 11 meV the molecules can scatter from the surface into either the $l = 0$ state or the rotationally inelastic $l = 1$ state which is shown in the middle panel of the figure. The translational-rotational coupling is strong enough that most of the molecules scatter into the rotationally excited state. At the selective adsorption resonances the scattering probabilities change rapidly as a function of energy with the elastic scattering probability approaching unity and the rotationally inelastic scattering probability approaching zero. This rapid change in the scattering probabilities is due to the constructive and destructive interference between the directly scattering flux and the flux that has coupled back out of the rotationally trapped state. The bottom panel shows the occupation of the rotationally trapped states that lead to the selective adsorption resonances; below 11 meV the figure shows the probability density in the $l = 1$ state, and above 11 meV it shows the probability density in the $l = 2$ state. The probability density is calculated by integrating the amplitude squared in that angular momentum channel of the scattering state over all z.

The roughly Lorentzian peaks in the probability density are better measures of the resonance widths than the Fano-like elastic scattering lineshapes because the shape of the latter obscures its width

$$P_{el}(E_z) \approx P_{background} \frac{((E_z - E_r) - q)^2}{(E_z - E_r)^2 + \Gamma^2}, \tag{3.12}$$

where Γ is the width of the resonance and q is a parameter that measures the asymmetry of the lineshape. Because the lineshapes are Fano-like there is structure in the resonance lineshapes that

extend over a larger range of energy than the width of the resonance. This Fano-like shape with a peak and dip in both channels is not a general expression for a selective adsorption resonance lineshape; resonances can consist of isolated peaks or dips or even more complicated shapes.[89,90,91,92] This shapes does, however, happen to describe these lineshapes quite well over a small energy range that is nonetheless large compared to the width of the resonance.

The low energy resonances are much broader than the higher energy ones. The resonance widths depend on the matrix element of the off-diagonal parts of the potential (see Eq. (3.11)) with the bound states, and the density of continuum states at the resonance energy. The overlap of the bound states with the off-diagonal parts of the potential, the largest part of which is due to the $l'' = 1$ term in the potential (Eq. 3.10), is roughly equal to the derivative of the diagonal part of the potential times the offest of the center of mass. Starting from the lowest bound state which is centered near the well minimum where the derivative of the potential is small, the subsequent bound states penetrate further into the surface but also have more and more of their amplitude centered far from the surface. Due to these conflicting trends the matrix element tends to be largest for the second and third bound states from the bottom (for these potentials). The density of states is larger the closer the rotationally deexcited state is to the vacuum since the density of states in one dimension (due to the flat surface approximation the parallel degrees of freedom decouple completely in this aspect of the problem) is inversely proportional to the square root of the kinetic energy of the scattering particle, $E^{-\frac{1}{2}}$. For resonances at energies high enough that there are several final states the width depends on contributions from all possible final states but the largest contribution is from the lowest energy rotational deexcitation because the matrix element is larger (that term in the coupling potential is largest) and the density of states is largest for the rotational deexcitation that is closest to the vacuum.

Finite temperature surface scattering. Molecules can also scatter inelastically off a *dynamic* surface by exciting or absorbing a phonon. Inelastic scattering strongly affects the scattering

resonances in Fig. 3.12, as is seen in Figs. 3.13 where scattering probabilities, calculated using the self-consistent one-phonon approximation discussed in I, are plotted as a function of incident energy for a series of surface temperatures. In these plots the resonances below 11 meV become observable in the elastic scattering probability due to the enhanced inelastic scattering for molecules scattering under resonance conditions. The higher energy resonances are all considerably broadened and damped by the inelastic scattering.

The apparent size of each low energy resonance increases, with respect to the background, as a function of temperature. This somewhat surprising result – the resonances become easier to observe as the inelastic scattering increases – is due to two reasons. First, the resonances are observable only because the inelastic scattering provides additional channels for the particle flux besides the elastic channel. The enhanced inelastic scattering at the selective adsorption resonances in turn decreases the amount of elastic scattering; this decrease in elastic scattering at the resonances allows the observation of those resonances that were unobservable for scattering from a static surface. Second, the rotational lifetimes of the resonances are larger than the inelastic lifetimes for all the temperatures shown in this plot. These resonances are also very broad because they are both low in energy which couples them to a large density of continuum states and have a large matrix element with the translational-rotational coupling potential. Since the inelastic coupling is strongest between states with the same angular momentum the inelastic lifetime of the resonances does not depend as strongly on the energy of the resonances as the rotational lifetime does because the matrix elements and the densities of states for those states are independent of the rotational state. In fact, the inelastic lifetime of a resonance is dominated by coupling to the other bound states with the same angular momentum as is shown below in Fig. 3.17. The inelastic lifetime of the resonance is affected by which bound state is resonant in much the same way the the elastic lifetime is; it is the matrix element of the bound state wavefunction with the derivative of the diagonal part of the potential (the inelastic interaction potential is proportional to the derivative of the static surface potential) that is important. For example, high lying bound states have longer

inelastic lifetimes than lower lying ones.

The higher energy resonances have a much longer rotational lifetimes (narrower widths) than the lower energy states so that the inelastic scattering affects the lineshapes more strongly. The effect of inelastic scattering on one of the higher energy resonances is shown in fig. 3.12b; which shows the resonances broadening and becoming less distinct as the surface temperature (and hence inelastic scattering) increases. Using the width at half maximum of the approximately Lorentzian trapped state density as a measure of the inverse lifetime or width of the resonance gives a change in width of roughly a factor of two between the zero temperature and the 280 K surface and another factor of two between the static surface width and the zero temperature width. For the resonance near 25 meV for example, the static surface width is 0.08 meV, the 0 K width is 0.15 meV and the 280 K width is 0.25 meV. As is discussed with respect to Eq. (3.9) the inverse of the static surface width gives the elastic lifetime of the resonance, and the inverse of the difference between the full width and the static surface width gives the inelastic lifetime of the resonance.

Since the inelastic width is determined by scattering to other states with the same angular momentum, the inelastic widths for the H_2 and D_2 resonances are likely to be very close to the inelastic widths found for the HD resonances that are due to bound states with roughly the same energy. Since these inelastic HD widths are much larger than the elastic widths found for the H_2 and D_2 resonances (the para-hydrogen resonances around 25 meV has a width of .003 meV while that zero temperature inelastic width for HD at the same energy is .07 meV), the total widths of the H_2 and D_2 resonances will be dominated by inelastic scattering rather than the translational-rotational coupling.

Calculations of scattering probabilities are most often done for scattering from a static surface, particularly if a series of potentials are to be evaluated as to which best matches the experimental data. To make this comparison it is necessary to take experimental data which is measured at a finite surface temperature and convert it into data that would be measured for scattering from a static surface. Toward this end we use scattering probabilities calculated in the self-consistent one-phonon

approximation as experimental data and try to evaluate the best way to convert finite temperature data to static surface scattering probabilities. Figures 3.14a,b show the elastic and rotationally inelastic scattering probabilities plotted on a logarithmic scale as a function of temperature for fixed energies. The analysis used to interpret these results can be generalized to the interpretation of diffraction intentities for helium scattering used as a structural probe.

Since the high temperature limit of the mean-square displacement and the mean-square effective height extrapolate to zero at zero temperature rather than to their zero temperature values, *i.e.*, the extrapolation eliminates both thermal and zero-point-motion effects, it is not unreasonable to expect that the same type of extrapolation would work for elastic and rotationally inelastic scattering probabilities. If an analysis like some type of Debye-Waller factor or exponentiated inelastic scattering model describes the effect of inelastic scattering on elastic scattering then the extrapolation of the logarithm of the scattering probability exactly gives the static surface scattering probabilities because in the high temperature limit the argument of the exponential of these models is proportional to the temperature. We do not, however, expect such an extrapolation to work for resonant scattering conditions because these methods do not account for the effect of inelastic scattering on the resonance widths.

Figure 3.14a shows the scattering probability for three energies below 11 meV; the static surface scattering probabilities for each of these is unity. None of these scattering probabilities extrapolate back to this value which is not surprising since the resonances below 11 meV all overlap (see Fig. 3.12). As was discussed above these resonances are not broadened very much by inelastic scattering for these temperatures so the extrapolation is within ten percent of the correct value. The closer the energy is to the center of a resonance the further from unity the extrapolated value of the scattering probability is. Since the resonances above 11 meV are much narrower than those below and do not overlap, both the elastic and the rotationally inelastic scattering probabilities, shown in Fig. 3.14b, extrapolate back to the static surface scattering values for non-resonant energies. Again, the resonant scattering probabilities do not extrapolate to the static surface values and

because inelastic scattering plays a much more important effect on the widths of these resonances the extrapolations miss by a much greater amount than those for the lower energy resonances. The extrapolation as a function of energy is given in Fig. 3.15 and is compared with the static surface scattering probabilities.

Related to the extrapolation question is whether it is possible to use a Beeby-corrected Debye-Waller factor to extrapolate scattering probabilities back to a static surface value. The advantage of this type of extrapolation is that it can be done with data taken at a single temperature, whereas the previously discussed method required data at several temperatures. A Beeby-corrected Debye-Waller analysis of diffraction intensities predicts a temperature dependence given by

$$P_{el}^{BCDW} = \exp\left[-2m\left((E_z + D)^{1/2} + (E_z + D - E_{rot})^{1/2}\right)^2 \left\langle h(\mathrm{R})^2 \right\rangle_{th}\right], \qquad (3.13)$$

where E_{rot} is the change in the rotational energy during the scattering process. The temperature dependence is in the mean square effective height of the surface, $\langle h(\mathrm{R})^2 \rangle_{th}$. A simple Debye-Waller analysis predicts the same general form for the temperature dependence without the addition of the well depth to the incident energy. The extrapolations of the high temperature scattering probabilities using a Beeby-corrected Debye-Waller, also shown in Fig. 3.15, do not work as well as the extrapolations using calculated scattering probabilities for several temperatures. In fact they predict an incorrect overall energy dependence for the rotationally inelastic scattering probability.

All the difficulties encountered using a Beeby-corrected Debye-Waller for analyzing temperature dependent helium scattering from a flat surface, discussed earlier in this chapter, also persist for analyzing scattering in systems that allow rotationally inelastic scattering. For these systems there is the additional question of whether inelastic scattering leads to rearrangement of scattering intensity between different rotational channels. To answer this question we compare in Fig. 3.15 the ratio of the rotationally inelastic scattering and the elastic scattering for the static surface scattering probabilities to the same ratios for the extrapolated scattering probabilities and the Beeby-corrected Debye-Waller predictions for the static surface scattering probabilities. The agreement between the static surface values and the extrapolated values indicates that out of resonance rearrangement is

temperature independent. The disagreement between the static surface values and the Beeby-corrected Debye-Waller values indicates that this later method incorrectly describes the differences in the elastic and rotationally inelastic scattering due to the loss in energy in motion normal to the surface.

Much can be learned about the scattering process by examining the probability and flux densities as a function of distance from the surface as shown in Fig. 3.16. Comparing the $l = 2$ probability density of the resonantly and non-resonantly scattering molecules shows the large build-up in the rotationally trapped state for the resonantly scattering molecule. It should be kept in mind that these probabilities are plotted for scattering from an 80 K surface so that the probability density in the rotationally trapped state has been significantly reduced by inelastic scattering from its static surface value. The difference between this probability density and the static surface value (roughly a factor of four) indicates why the distorted wave Born breaks down at selective adsorption resonances. Because the amplitude in the rotationally trapped state is significantly decreased by the inelastic scattering a calculation that ignores this effect (the inelastic contribution to the width or lifetime of the resonance) will overcount the inelastic scattering due to the selective adsorption resonance. This feature can also be seen in the bottom panels of figures 4.13 which show the integrated probability density in the rotationally trapped states for a series of temperatures.

While both the probability density and the flux density show that the molecule does not penetrate into the surface the probability density can be difficult to interpret because the plane waves have unit normalization rather than flux normalization and there are interference effects between incoming and outgoing waves in the incident channel. The flux density provides a more straightforward interpretation of the dynamics of the scattering process because it shows directly where the scattering between the various channels occurs. The spatial location of the flux changes between the various channels shows that for non-resonantly scattering molecules most of the rotationally inelastic and inelastic scattering takes place very close to the classical turning point. This fact justifies our use of the local height approximation which is valid just where it needs to be valid to

correctly describe the inelastic scattering – near the classical turning point. This narrow spatial region in which the scattering takes place is due to the molecular wavefunctions decaying rapidly into the surface and the potential decaying rapidly away from the surface.

For resonantly scattering molecules there is rearrangement of flux between channels much further from the surface because the large build up of probability in the rotationally trapped state, seen in the $l = 2$ probability density, compensates for the weakness of the interaction potential at those distances. This rearrangement is probably not calculated quantitatively correct because the local height approximation is not as valid that far from the surface.

It is also possible to compute the distribution of the inelastic (one-phonon-change) flux far from the surface over the possible final states which is shown in Fig. 3.17 for both resonantly and non-resonantly scattering molecules. Here the distributions are plotted as a function of the change in energy in motion normal to the surface and are integrated over possible parallel momenta. For the flat surface potential model that we use in these calculations the full distribution over final states separates into a product of a factor that depends just on the change in the energy in motion normal to the surface and a factor that depends on both the change in that energy and the change in parallel momentum but not on any details of the state of the scattering molecule (only on the phonon density of states). This separability means that the integral over all parallel momenta of the final state distribution still contains all the information about the scattering from the point of view of the molecule.

The most prominent features in Fig. 3.17 are the strongly enhanced resonant final states for the resonant initial state. The enhancement of the final state resonances for the non-resonant initial state is much weaker than it is for the resonant initial state. These two features are due to the form of the interaction potential that couples the zero-phonon-change states with the one-phonon-change states; since the interaction potential is the derivative of the static surface potential it couples states with the same angular momentum much more strongly than it does states with different angular momenta. This form also explains why the trapping probability is not as strongly enhanced by

resonant scattering as inelastic scattering to other continuum states is, because the bound states tend to be predominantly lower angular momentum states than the resonantly trapped state. The trapping probability into each bound state can be seen as vertical bars in the left part of each figure.

Even though the self-consistent one-phonon approximation qualitatively describes the correct behavior of resonances coupled to inelastic scattering this figure shows why it should not be trusted quantitatively. The problem is that inelastic scattering out of the resonant final states is not included in the approximation. The method would work quantitatively correctly if the resonant final states (or any small set of states) were not as strongly enhanced as they are. When the background value of the inelastic scattering probability is small the effect on the elastic scattering of multi-phonon-change processes will be small; when the inelastic scattering probability for resonant states is large and the resonant final states are strongly enhanced the approximation breaks down. We tried to remedy this breakdown by including an optical potential in the Schrödinger equation for the one-phonon-change amplitudes, but, as might be expected given our inability to find an optical potential that could treat the effect of one-phonon-change inelastic scattering on the zero-phonon-change amplitude, we were unable to gets this approximation to work.

There are also several features in this figure that seem generally applicable. 1) The phase difference between different angular momentum channels causes interference effects that change the lineshape of the final state resonances. 2) A related effect is that when there a more than one possible angular momenta final states the coupling seems to be strongest to the final state that is most strongly scattered to in the static surface scattering problem. 3) There is a decrease in the final state flux near the incident energy indicating that the matrix elements for coupling to small energy transfers is small because for finite temperatures the phonon matrix element is largest for small energy transfers.

The self-consistent one-phonon approximation is useful for understanding the interaction between elastic scattering effects and inelastic scattering but since it is a one-phonon approximation it

will not work quantitatively in situations, like at selective adsorption resonances, that are inherently multi-phonon scattering dominated.

IV. SUMMARY

This paper considers helium and molecular hydrogen scattering from flat copper surfaces as prototypical light atomic or molecular-physisorptive scattering systems. Our interest is both to quantitatively interpret experimental results for He, H_2, HD, and D_2 scattering from flat copper surfaces and to generalize these results to understand qualitatively related systems. The conclusions will concern: A) the development of a model for the interaction potential between the scattering particle and the normal modes of the surface displacements (phonon scattering) that includes the essential physics but is simple enough to allow computation, as is discussed in the second section, and B) the calculated scattering and trapping probabilities for helium and molecular hydrogen scattering from copper.

It is useful to compare and contrast helium-surface scattering with neutron-bulk scattering. The masses and typical scattering energies are similar for both systems and the quantum mechanical time scales are such that a stationary state scattering treatment is valid. The experimentally observed quantum mechanical effects both with respect to the scattering particle and the lattice confirm that it is necessary to treat both the scattering particle and the lattice quantum mechanically as a stationary state perturbative approach does. The most important difference is that the cross section for neutron scattering is very small and the cross section for atomic and molecular scattering is so large that the particles do not penetrate the surface. These large cross sections make it necessary to use a distorted wave approach for atomic and molecular scattering while the usual Born approximation suffices for neutron scattering. Within a distorted wave approach part of the surface is treated exactly and the rest is treated as a perturbation. The inelastic scattering probabilities are not so strong as to invalidate such a perturbative approximation.

In a previous paper, I, we develop a method for calculating thermally averaged scattering probabilities without having to explicitly thermally average them. This method greatly simplifies a calculation because the calculation only has to be done for average lattice states rather than an ensemble of lattice states. Using this method for thermal averaging we developed a self-consistent one-phonon approximation that allows us to calculate the effect of inelastic scattering on elastic scattering features such as diffraction intensities and selective adsorption resonances. If there are no extremely narrow features in the scattering probabilities as a function of energy this method can be solved iteratively, significantly speeding up the numerical calculation.

A. Model assumptions

To carry out numerical calculations it is necessary to have a model for the potential of the interacting system that includes coupling between the scattering particle and the thermal motion of the substrate atoms. In constructing such a potential we made a series of assumptions that include the essential physics necessary for understanding the scattering process but allow simple computation of the scattering rates. These assumptions are described as the flat surface approximation and the effective height approximation. The flat surface approximation allows us to decouple the motion of the scattering parallel to the surface from its motion normal to the surface. The effective height approximation models the interaction between the scattering particle and the normal modes of the surface in a separable manner with the dependence on the phonon's parallel wavevector given by a gaussian that cuts off high wavevector phonons, the dependence on the particle's position in the plane of the surface by plane waves of the phonon wavevector, and the dependence on the particle's position normal to the surface by the derivative of the static surface potential, including the attractive part of the potential. These assumptions about the form of the interaction potential allow it to be modeled without parameters that are not available in the published literature.

The second section includes a discussion of the parameters that we have chosen for the sub-

sequent calculations in the third section of the paper. These parameters consist of those for the helium and hydrogen potentials near a copper surface, the density and the sound velocities for the surface which determine the correlation functions for the surface displacements in the isotropic elastic continuum model for the surface, and the cut-off parameter in the interaction potential.

B. Results

The main result discussed in the third section of this paper is that these methods and approximations produce scattering probabilities that compare quantitatively with those measured experimentally for He scattering from Cu(100). In particular we compare calculations and measurements of the elastic scattering probability as a function of surface temperature for a series of different incident energies and angles. Since the experiment is done for conditions outside the one-phonon regime it was necessary to use an ad hoc extension of the distorted wave Born approximation into the multi-phonon regime. But this extension does retain much of the important physics omitted from simpler treatments of the thermal attenuation of the elastic scattering probability.

Guided by the agreement between our calculation and the measured of scattering probabilities we were able to use these methods and approximations to show that simple methods of calculating scattering probabilities miss some of the essential physics of the scattering process even though they describe surprisingly many aspects of it correctly. The Beeby-corrected Debye-Waller factor correctly accounts for the mass dependence, the effect of the attractive potential (only if the attractive potential should be included in the interaction potential), and the proportionality of the logarithm of the elastic scattering probability to the surface temperature in the high temperature limit for a system with no diffraction. It fails quantitatively because it does not correctly account for the softness of the potential and the temperature dependence of diffraction probabilities. These conclusions were based on the sensitivity of scattering probabilities to variations in parameters describing the system. In particular we found that when we varied the well depth that it was possible

to account for the stronger attractive potential by adding the well depth to the incident energy; when we varied the steepness of the potential that the inelastic scattering decreased in a way that is not accounted for in a Debye-Waller type analysis, and when we varied the mass of the incident particle the logarithm of the elastic scattering probability was proportional to the mass. We also found that the attractive potential could not be accounted for by simply shifting the normal energy if only the repulsive part of the static surface potential was included in the interaction potential.

The self-consistent one-phonon approximation can be rewritten so that the effect of the inelastic scattering on the elastic scattering is described by an optical potential in the equation for the elastic scattering wavefunction. We found that this optical potential is energy dependent, non-local, and non-separable. Because of these complications we were unable to find simple models to that could be used to calculate elastic, diffractive, and/or rotationally inelastic scattering probabilities with any reliability.

H_2 and D_2 selective adsorption resonances on a static copper surface are very narrow because the molecule is almost spherically symmetric and the nuclei are distinguishable (distinguishability means that only even angular momentum transitions are allowed). Inelastic scattering considerably broadens the resonances based on the behavior of similar HD scattering resonances. We do not calculate the broadened resonances for H_2 and D_2 because the inelastic width is so much larger than the elastic width that our iterative calculation will not converge. While the H_2 and D_2 inelastic widths are comparable to those for HD resonances the HD elastic resonance widths are so much larger than those for H_2 and D_2 that the iterative solution for HD converges rapidly. When resonances broaden their net effect on the scattering probabilities is significantly decreased. The rotational degrees of freedom also affect the dynamics of the scattering process in a subtle way by changing the effective potential that the molecule moves in when the molecule is described in terms of its angular momentum state rather than its orientation.

We were able to reproduce some of the features of the experimentally measured H_2 and D_2 sticking probabilities, but are unable to compare directly because we calculate trapping proba-

bilities that are only indirectly related to the measured experimentally sticking probabilities.

For HD the rotationally inelastic scattering is strong enough and the selective adsorption resonances are broad enough that we were able to study the temperature dependence of these quantities in the one-phonon inelastic scattering limit. Toward this end we calculated the scattering probabilities for HD scattering from copper as a function of energy and surface temperature.

The scattering probabilities as a function of energy at a series of temperatures show the effect of inelastic scattering on selective adsorption resonances and vice versa. Selective adsorption resonances enhance inelastic scattering because the molecule has a large amplitude near the surface in the rotationally excited state. Inelastic scattering in turn affects resonances in two important ways, it allows the observation of resonances that are obscured by there being only one open channel in the static surface scattering case, and it broadens and reduces the observability of other narrower resonances. We find that at room temperature the inelastic width is larger than the elastic width of many of the selective adsorption resonances. These large widths imply that for the narrow H_2 and D_2 resonances that the total widths of the resonances will be dominated by the inelastic widths and will be very similar to the widths of HD resonances at similar energies.

The scattering probabilities as a function of temperature show how well scattering probabilities measured for a finite temperature surface extrapolate back to the values that would be measured for scattering from a static surface for which there is no inelastic scattering. The extrapolation of theoretically calculated scattering probabilities for which we know all the details of the inelastic scattering process can determine how well various extrapolation schemes work with no adjustable parameters. In the high temperature limit the rotationally inelastic and the elastic scattering probabilities can be extrapolated back to the static surface scattering probabilities, but not in the way predicted by various Debye-Waller factors. Since the differences between diffraction from a weakly corrugated surface and rotationally inelastic scattering are not as great as they might seem these results can be generalized to imply that care must be used when extrapolating helium scattering probabilities when helium scattering is used as a probe of surface structure.

The probability and flux densities as a function of position normal to the surface and the flux distribution over final states allow us to evaluate the approximations we have made in this theoretical treatment. The spatial location of the changes in the flux densities almost all occur near the classical turning point justifying the assumption behind the effective height approximation; that is that the detailed shape of the interaction potential is only important near the classical turning point. Unfortunately the final state flux densities show that for resonant incident states the enhancement of the inelastic scattering is strongest into final state resonances which means that for resonant states the one-phonon approximation breaks down.

ACKNOWLEDGEMENTS

This work was supported by the Office of Naval Research. We would like to thank Mats Persson and Cyrus Umrigar for nemerous discussions and direct assistance with aspects of this calculation. We would also like to thank both Horia Metiu for his hospitality during our stay in Santa Barbara and the Institute for Theoretical Physics where some of this manuscript was prepared.

APPENDIX A SELECTIVE ADSORPTION RESONANCES

Diffraction intensities for light atoms and molecules scattering from surfaces are strongly affected by selective adsorption resonances. Rotationally mediated selective adsorption resonances, a principal topic of this paper, arise from the translational-rotational coupling in the surface potential for molecules, while the more common diffractionally mediated selective adsorption resonances are caused by the corrugation of the surface. These resonances, arising from the discrete bound state structure of the surface potential, are typically seen in the diffraction intensities as rapid changes in the scattering intensities as a function of the incident conditions, *i.e.,* the incident energy or

the incident angle. Because the scattering resonances are sensitive to the bound state energies, the resonance energies and their shape provide information about the surface potential.

Two useful ways to think about selective adsorption resonances are that 1) they evolve from positive energy bound states as the coupling terms in the potential are increased from zero and 2) that they are due to virtual transitions into bound states of the surface potential during a scattering process. Both of these are equivalent ways of thinking about the general problem of coupling a discrete state into a continuum of states often called Feshbach resonances or Fano resonances in other fields of Physics.

1) Positive energy bound states. This discussion of rotationally mediated selective adsorption resonances is, with only a few changes, equally valid for diffractionally mediated resonances. The top panel of Fig. A1 shows the potential for an HD molecule outside of a flat copper surface expanded in terms of Legendre polynomials of the orientation. It also shows the bound states of the angularly averaged potential, which is the $l = 0$ term in the expansion of the potential in terms of spherical harmonics. Temporarily setting the coupling terms, the higher order terms in the expansion of the potential, to zero allows the eigenfunctions of the molecule to be written as product states

$$\psi(z, \mathrm{R}, \theta, \phi) = \psi(z, k_z) Y_{lm}(\theta, \phi) e^{i\mathrm{K}\cdot\mathrm{R}}, \qquad (A1)$$

where k_z labels the z-dependent part of the state by its momentum far from the surface (both incoming and outgoing), K is the momentum parallel to the surface, and l and m describe the rotational state of the molecule. The energy of this state is given by a sum of the energies in each degree of freedom

$$E = \frac{k_z^2}{2m} + \frac{l(l+1)}{2I} + \frac{K^2}{2m}. \qquad (A2)$$

Note that the z-dependent part of the state could also be a bound state in which case the label k_z would be replaced by n and the energy in this part of the wavefunction would be $E_n < 0$.

Since the motion parallel to the surface is not coupled by potential in Fig. A1 (see Eq. 2.3)

to the rest of the motion it will not effect these other degrees of freedom. If the surface were corrugated, on the other hand, the parallel motion would be coupled to the perpendicular motion and the corrugation would lead to resonances in the same way that the translational-rotational coupling does. As the possible rotational transitions of the molecule are discrete, so is the motion parallel to the surface for this problem is essentially discrete since the periodic surface potential allows the parallel wavevector to change only by a reciprocal lattice vector (ignoring any inelastic scattering).

The expansion of the state in terms of spherical harmonics leads to the concept of channels, each channel being associated with an angular momentum state. In a description in terms of channels the particle has an amplitude to be at a position in each angular momentum state, rather than an amplitude to be at a position with each orientation. A continous degree of freedom, orientation, has been exchanged for a discrete set of channels, angular momentum. This exchange is very useful for molecular hydrogen scattering because the rotational energy splittings are so large that only a few angular momentum channels are important for a given problem.

For all positive energies there will be an energy eigenstate for each rotational state with an energy lower than the total energy of the state. Two possible complete sets of states for the molecule are the incoming and outgoing scattering states indexed by the total energy, the rotational state in the asymptotic incoming or outgoing channel, and the parallel momentum (which we are ignoring for the present). To be complete each set of states also has to include all of the bound states of the potential.

If a molecule is in a bound state of the angularly averaged potential and in its rotational ground state it will have negative total energy; on the other hand, if it is in a bound state and in a rotationally excited state it can have positive total energy. In this latter case, even though the total energy of the molecule is positive, the molecule will stay bound to the surface as long as there is no coupling between the rotations and the z-translations.

When the coupling terms in the full potential are included the the eigenfunctions are no longer

pure angular momentum states

$$\psi(z, \mathbf{R}, \theta, \phi) = \sum_{l,m} \psi_{l,m}(z, k_z) Y_{lm}(\theta, \phi) e^{i\mathbf{K}\cdot\mathbf{R}}. \qquad (A3)$$

The negative energy bound states of the potential without the coupling will remain bound states, but their energy will shift due to the coupling. Positive energy bound states will become resonances and molecules in these states will no longer be bound to the surface. In the limit that these coupling terms are weak the energies of these positive energy bound states

$$E_r = E_n + \frac{l(l+1)}{2I} > 0, \qquad (A4)$$

are the selective adsorption resonance energies.

Each positive energy bound states is degenerate with states that are unbound since the unbound states form a continuum; when the translations and rotations are coupled by the potential the discrete positive energy state will couple with the continuum states, cease to be a discrete state and become a selective adsorption resonance. Although the coupling will not lead to a change in the energy of the continuum states, there will be drastic changes in the phase shifts associated with all of the continuum states with energies within some characteristic width of the resonance energy, and there will be a large amplitude in the bound angular momentum channel (or rather trapped channel, since this state has a finite lifetime) near the surface for those states. The bottom panel of Fig. 4.12 shows the amplitude squared *integrated over all z of the resonant rotational channel* as a function of the energy of the eigenstate. The large peaks below 11 meV are due to the $l = 1$ state being resonant with the bound states of the potential, and those are above 11 meV are due to the $l = 2$ state being resonant. The effect of the resonances on the elastic scattering can be seen in the top panels of the same figure. At the resonance there is the usual signature of a resonance, a rapid change in the scattering probabilities as a function of the incident energy. There are no rapid changes for the resonances below 11 meV because there is only one possible final state and the scattering probability into it must be exactly unity.

2) Virtual transitions. Now consider a scattering experiment for the system described by the potential in the top panel of Fig. A1. If there is no translational-rotational coupling a molecule incident on the surface in its rotational ground state will scatter and stay in its ground state. On the other hand, if there is some translational-rotational coupling and the energy is higher than the first rotationally excited state, the molecule can scatter either into the rotational ground state or into the rotationally excited state. Molecules with incident energies above 11 meV can leave the surface in either the $l = 0$ or the $l = 1$ angular momentum state because those channels have positive kinetic energy far from the surface and all other channels have negative kinetic energy. In the top panels of Fig. 4.12 the probability to leave the surface in each rotational state is plotted as a function on incident energy. For most of the incident energies above 11 meV most of the molecules leave the surface rotationally excited.

The bottom panel of Fig. A1 shows the HD-surface potential, its bound states, and the asymptotic kinetic energy of the HD molecule in all the relevant rotational states for a particular incident energy. The asymptotic kinetic energy, which is equal to the total energy minus the energy of the rotational state of the channel, is the kinetic energy that the molecule has far from the surface in that rotational state. As the incident energy of the molecule changes the asymptotic kinetic energies move up and down together. Even though a molecule can not leave the surface in a rotational state with a negative asymptotic kinetic energy, if that energy is above the well minimum the molecule can have a large probability to be in that rotational state close to the surface. This is particularly true if the asymptotic kinetic energy is equal to a bound state energy.

As the energy of the molecule is increased the asymptotic kinetic energy of the $l = 2$ rotational channel eventually becomes close to each of the bound state energies (of the angle averaged potential). When this condition is met the molecule, which is scattering in a selective adsorption resonance, can make a virtual rotational transition into this bound state and tumble on the surface for a long time before it eventually leaves. A measure of the time spent in the trapped channel near the surface is the probability density in the rotationally excited state as seen in the bottom

panel of Fig. 4.12. The dramatic effect of the resonances on the scattering probabilities as can be seen in the top panel of of the same figure.

Selective adsorption resonances affect the elastic, diffractive, and rotationally inelastic scattering probabilities in two ways; first the relative scattering probabilities get scrambled between these channels as discussed above, and second inelastic scattering probabilities are enhanced at selective adsorption resonances as is discussed in chapter IV of this paper. This enhancement is due to the large amplitude in the trapped state for particles that scatter resonantly from the surface. Since the scattering probabilities must all sum to one an increase in the inelastic scattering will lead to a decrease in the elastic scattering probabilities (here elastic includes rotationally inelastic) and an increase in resonance width. The interplay between resonances and inelastic scattering is one of the main subjects of this paper.

APPENDIX B GENERAL DIFFRACTIVE SCATTERING

To understand gas-surface scattering it is useful to compare the quantum mechanics of atom scattering with that of neutron and x-ray scattering.[93] Because these three processes have many similarities the temptation to overextend the similarities exists, particularly with respect to the temperature dependence of the diffraction intensities. Since these three techniques all involve measuring diffraction intensities, the wavelength of the scattering particle is comparable to the lattice spacing. As a consequence, the wavepacket of a particle with well defined energy is spread out over very many lattice sites and can not be thought of as localized. The diffraction intensities each technique measures are temperature dependent but for a variety of reasons the temperature dependence of the atom scattering intensities is more complicated than the simple dependence of the other two techniques. Table 1.2 summarizes the following discussion comparing these experimental techniques.

Neutrons, on one extreme, scatter primarily from nuclei so the scattering intensities are de-

termined completely by the interference between the lattice sites and there is no complicating dependence on the structure of the scatterer. (Neutrons also scatter from the magnetic moments of the atoms in the solid but this is a weak effect and not part of this discussion. We will assume that the nuclei are all singlets. We will also ignore electronic excitations that might occur in these scattering processes.) X-rays scatter from the electrons in the solid; since the interaction is weak they scatter most strongly from the parts of the solid where the electron density is largest, *i.e.*, the core electrons. The x-ray scattering intensities depend not only on the interference between the scattering from different unit cells but also on the details of the atomic charge densities since these densities vary on length scales that are comparable to the x-ray wavelength. On the other extreme, thermal energy helium atoms are strongly scattered by the valence electrons. This strong scattering has several consequences; the first and most important is that helium does not penetrate the surface. A second consequence is that the diffraction intensities are strongly affected by the details of the charge density of the surface atoms. Our ability to calculate valence charge densities is not nearly as refined as it is for core electrons, so it is more difficult to connect the helium-surface potential with the surface structure than it is to connect x-ray scattering intensities with bulk structures.

Neutrons and helium atoms in diffraction experiments have energy resolutions (usually some small fraction of the incident energy) that are smaller than typical phonon energies and are therefore able to resolve energy losses. The uncertainty principle and the energy resolution being low compared to the relevant energies in the problem means that the time for which the particle interacts with the solid is long compared to all but the slowest phonon oscillation periods. Since the interaction times are long the phonons are a dynamic perturbation of the scattering particle and that the elastic and inelastic scattering probabilities can be calculated using a scattering state calculation in which phonons cause energy-conserving transitions between different states of the particle.

In diffraction experiments x-ray energies are much larger than the phonon energies in the solid;

in most cases the energy uncertainties are also greater than the phonon energies. When the energy resolution is much greater than the phonon energies it is impossible to resolve energy losses in the experiment. This lack of resolution is equivalent to the time the x-ray spends interacting with the lattice being shorter than all of the phonon oscillation periods so that the x-ray essentially scatters from a static lattice that is slightly disordered due to the phonons. This important difference between x-ray scattering, on one hand, for which there is effectively no inelastic scattering and neutron and helium atom scattering, on the other hand, for which there is arises from the large difference in energy of the diffracting particles, (*i.e.,* x-rays in the 20 keV range and neutrons and helium atoms in the 50 meV range).

Both x-ray and neutron scattering are weak; this allows the scattering to be treated in the Born approximation. Both diffraction and inelastic scattering are weak and can be treated as first order perturbations. Thus the thermal attenuation of elastic scattering is the reduction of the diffraction peaks due to decreased amplitude of the Fourier expansion of the potential caused by the thermal disorder. Since the temperature does not change the strength of the perturbing potential, the weakening of the diffractive part of the potential is equivalent to an increase in the strength of the inelastic scattering potential. Since this is a first order approximation the forward scattering is unaffected by the temperature. In the case of neutron scattering the loss in diffraction intensity as the temperature increases is due to real inelastic scattering; there is no diffuse elastic neutron scattering from a perfect crystal (assuming the nuclear spins are either singlets or perfectly ordered). This would also be the case for x-ray scattering if the energy resolution were the same absolute magnitude as it is for neutrons, but given the poorer resolution the drain on diffraction intensities can be thought of as due to either thermal disorder or unresolved inelastic scattering.

Neutron scattering intensities are given by the product of the interaction strength with the structure factor which is a property of the lattice and independent of any properties of the neutrons. The structure factor, which depends on both the energy change and the change in the wavevector of the scattering process, is a sum of two parts, one part that describes diffraction and is non-zero

only for scattering events in which the energy is unchanged and the wavevector changes only by a reciprocal lattice vector. The other part describes inelastic scattering and is non-zero for processes that conserve total energy and total momentum, *i.e.*, the change in the energy and momentum of the particle must be the opposite of the change in energy and momentum of the lattice. Because the potential is very anharmonic this second part contains all possible first order multi-phonon contributions for which the temperature dependence is given by the occupation factors of the relevant modes. Since the total strength of the potential is independent of temperature both parts are multiplied by the temperature-dependent Debye-Waller factor, which keeps the integral over frequency and wavevector of the structure factor constant. Thus the Debye-Waller factor gives the temperature dependence of the diffraction intensities and represents the intensity lost to inelastic scattering. This simple form for the Debye-Waller factor depends on the scattering potential consisting of an array of delta function scatterers and on the inelastic scattering being weak. If the inelastic scattering were strong enough that it was a significant drain on the forward scattering probability the temperature dependence of the diffraction peaks would be modified by higher order corrections that are not important for weak scattering.

For x-ray scattering the situation is more complicated. Since the energy transfer is not resolved the structure factor must be integrated over all frequencies. Although the scattering potential still consists of independent scatterers, the scatterers are not delta-function-like, each has structure on the same length scale as the wavelength of the x-ray. The Fourier transform of this structure, called the form factor, modifies the scattering intensity. Because the scatterers are independent, the temperature dependence of the diffraction intensities is still given by the Debye-Waller factor as it is for neutron scattering.

In contrast to x-rays or neutrons helium is very strongly scattered by the solid; the forward scattering probability is zero, *i.e.*, the atom does not penetrate into the solid. This strong scattering greatly complicates the theoretical treatment of helium scattering as compared with these other processes. A Born approximation treatment of the scattering is impossible; it is necessary to use

a distorted wave Born approach which accounts for a large part of the scattering exactly and then treats the rest as a perturbation. This requires calculating the transition matrix elements between states that are eigenfunctions of the part of the Hamiltonian that is solved exactly, hence distorted waves. There are several choices for what is included in the zeroth order Hamiltonian (this is the part that gets solved exactly); the simplest involves using the lateral average of the thermal average of the full potential. In this case both diffraction and inelastic scattering are treated as perturbations. If the diffraction is too strong to treat perturbatively it is necessary to include the full thermal average of the potential in the zeroth order Hamiltonian. If, in addition, the inelastic scattering is too strong to be treated in first order perturbation theory the scattering probabilities become too difficult to calculate without drastic approximations.

The strength of the helium-surface potential complicates the calculation of the scattering probabilities in several ways. One such complication in treating helium atom scattering is that the diffractive and inelastic scattering probabilities depend not only on the strengths of the corresponding potentials but also on the details of the zeroth order Hamiltonian. This complication results from breaking the scattering potential into two parts, one being included with the kinetic energy and the uncoupled lattice Hamiltonian in the zeroth order Hamiltonian, and the other being the coupling to inelastic scattering. The temperature dependent Debye-Waller-like factors modify the diffractive and inelastic parts of the potential in a complicated manner, but since there are similar factors that come into the zeroth order Hamiltonian it is impossible to say without a detailed calculation what the effect of these factors will be. In addition the effects that lead to a Debye-Waller factor for the temperature dependence of neutron scattering are much different; the potential is not periodic in all three directions and the scattering potentials are soft rather than delta function-like so that anharmonic contributions are less important. Further, the surface atom displacements do not affect the potential in a pair-wise additive manner so that the inelastic scattering does not depend on the atomic correlation functions in a straightforward manner. This effect is primarily due to the large overlap of the surface atomic charge densities in the regions

of density from which the helium scatters. Finally the inelastic scattering is typically not weak enough to be treated in first order and the effect of inelastic scattering on elastic and diffractive scattering depends on of order higher terms.

It is useful to summarize the important concepts treating for thermal energy helium scattering. 1) A helium atom scattering from a surface is a very spread out object and should not be thought of as localized. 2) in contradistinction with neutron scattering the scattering is strong; this necessitates a distorted wave treatment of the scattering probabilities. 3) Even within a distorted wave treatment the the diffractive and inelastic scattering probabilities are often too large to treat in a first order calculation. 4) The effects that give Debye-Waller factor temperature dependence for neutron diffraction probabilities are completely different because of the soft scattering potentials, the necessity of a distorted wave approach, the non-pairwise additivity of the contributions to the potential of each surface atom displacement, and the large inelastic scattering probabilities. 5) The interaction time for a helium atom scattering from a surface is long rather than short; it is given not by the time which a classical particle would spend near the surface as it scattered, which is typically on the order of phonon oscillation periods, but by the time which the wavepacket interacts with the surface.

A final conceptual point to consider is whether it is more useful to approach the inelastic scattering from an adiabatic or a diabatic point of view. Adiabatic or diabatic refers to different descriptions of the phonons that couple the different helium atom states; an adiabatic description uses phonons that depend on the instantaneous classical location of the helium atom, while a diabatic description is one that uses the unperturbed phonons that are the lattice eigenstates in the absence of the helium atom. The adiabatic description of the phonons is similar to the description of the electron states in a Born-Oppenheimer approximation in which the states depend on the classical location of the nuclei. Adiabatic states are defined using the normal modes of the classical lattice for a fixed position of the helium atom; so that to zeroth order the lattice adjusts instantaneously to the position of the helium atom. Transitions between different states are caused

by the breakdown of this instantaneous response in much the same way that electronic transitions are caused by the breakdown of the Born-Oppenheimer approximation for electronic states. For an adiabatic description of helium scattering the phonons play the role of the electrons, and the helium atom the role of the nuclei.

Most inelastic helium-surface scattering calculations use a diabatic approach. This is reasonable because initially the lattice is unaffected by the scattering particle and even when the particle is very close to the surface it only weakly perturbs it especially hydrogen and helium. An adiabatic calculation is much more difficult to carry out because the position dependence of the potential energy and of the phonons must be calculated from the Hamiltonian before a calculation similar to a diabatic calculation is performed. It also requires care since the mass ratio that validates a Born-Oppenheimer approximation is inverted, *i.e.*, the substrate atom to helium mass ratio is large whereas the electron to nuclei mass ratio is small. A consequence of the small mass of the helium atom and its weak interaction with the surface is that the helium atom tends to be very delocalized even when it is trapped on the surface. It may be necessary to use an adiabatic approach for heavier scattering particles when they trap or stick onto a surface because they effectively become defects in the lattice. To describe the dynamics of lattice defects it is important to account for the changes in the normal modes of the lattice for the results to converge.

REFERENCES

1. J. A. Barker and D. J. Auerbach, *Surf. Sci. Reports* **4**, 1 (1985).
2. A. Liebsch, J. Harris, B. Salanon, and J. Lapujoulade, *Surf. Sci.* **123**, 338 (1982).
3. T. Engel and K. H. Reider, in *Structural Studies of Surfaces with Atomic and Molecular Beam Diffraction, Springer Tracts in Modern Physics* **19**, 1 (1980).
4. *Dynamics of Gas-Surface Interaction,* ed. G. Benedek and U. Valbusa (Springer-Verlag, Berlin 1982)
5. J. Lapujoulade, Y. Lejay, and G. Armand, *Surf. Sci.* **95**, 107 (1980). [He/Cu]
6. J. Lapujoulade, J. Perreau, and A. Kara, *Surf. Sci.* **129**, 59 (1983). [He/Cu]

7. J. Pereau and J. Lapujoulade, *Surf. Sci.* **122**, 341 (1982). [He/Cu]

8. E. H. Conrad, D. S. Kaufman, L. R. Allen, R. M. Aten, and T. Engel, *J. Chem. Phys.* **83**, 5286 (1985). [He/Ni]

9. U. Harten, J. P. Toennies, and C. Wöll, *Faraday Discuss. Chem. Soc.* **80**, 9 (1985). [He/Ag]

10. V. Bortolani, A. Franchini, F. Nizzoli, G. Santoro, G. Benedek, V. Celli, and N. Garcia, *Solid State Commun.* **48**, 1045 (1983). [He/Ag]

11. B. F. Mason and B. R. Williams, *Phys. Rev. Lett.* **46**, 1138 (1981). [He/Cu]

12. R. B. Doak, U. Harten, and J. P. Toennies, *Phys. Rev. Lett.* **52**, 578 (1983). [He/Ag]

13. J. Lapujoulade and Y. Lejay, *J. Chem. Phys.* **63**, 1389 (1975). [He/Cu]

14. P. Cantini, S. Terreni, and C. Salvo, *Surf. Sci.* **109**, L491 (1981).

15. P. Cantini and R. Tatarek, *Surf. Sci.* **114**, 471 (1982). [He/Gr]

16. D. Evans, V. Celli, G. Benedek, J. P. Toennies, and R. B. Doak, *Phys. Rev. Lett.* **50**, 1854 (1984). [He/LiF]

17. G. Lillenkamp and J. P. Toennies *J. Chem. Phys.* **78**, 5210 (1983). [He/LiF]

18. G. Boato, P. Cantini, and R. Tatarek, *J. Phys.* F **6**, L237 (1976). [He,H_2/Ag]

19. M. Chiesa, L. Mattera, R. Musenich, and C. Salvo, *Surf. Sci.* **151**, L145 (1985). [H_2,D_2/Ag]

20. J. M. Horne, S. C. Yerkes, and D. R. Miller, *Surf. Sci* **93**, 47 (1980). [He,H_2/Ag]

21. J. Lapujoulade and J. Pereau, *Phys. Scr.* **T4**, 138 (1983). [H_2 /Cu]

22. L. Mattera, F. Rosatelli, C. Salvo, F. Tammasini, U. Valbusa, and G. Vidali, *Surf. Sci.* **93**, 515 (1980). [H_2,D_2/Gr]

23. C. F. Yu, K. B. Whaley, C. S. Hogg, and S. J. Sibener, *Phys. Rev. Lett.* **51**, 2210 (1983). [H_2/Ag]

24. C.-F. Yu, K. B. Whaley, C. S. Hogg, and S. J. Sibener, *J. Chem. Phys.* **83**, 4217 (1985). [H_2/Ag]

25. K. B. Whaley, C.-F. Yu, C. S. Hogg, J. C. Light, and S. J. Sibener, *J. Chem. Phys.* **83**, 4235 (1985). [HD/Ag]

26. J. P. Cowin, C. F. Yu, S. J. Sibener, C. S. Hogg, and L. Wharton, in *Many-body Phenomena at Surfaces,* edited by D. Langreth and H. Suhl (Academic, Orlando, 1984), p. 351. [HD/Ag]

27. J. P. Cowin, C.-F. Yu, and L. Wharton, *Surf. Sci.* **161**, 221 (1985). [HD/Pt]

28. C. F. Yu, C. S. Hogg, J. P. Cowin, K. B. Whaley, J. C. Light, and S. J. Sibener, *Isr. J. Chem.* **22**, 305 (1982). [HD/Ag]

29. J. P. Toennies, in *Proceedings of the* 6^{th} *General Conference of the European Physical Society,* (1984). [HD/Au]

30. S. Andersson and J. Harris, *Phys. Rev. B* **27**, 9 (1983). [H_2 /Cu]

31. Ph. Avouris, D. Schmeisser, and J. E. Demuth, *Phys. Rev. Lett.* **48**, 199 (1982). [H_2 /Ag]

32. S. Andersson, L.Wilzén, and J. Harris, *Phys. Rev. Lett.* **55**, 2591 (1985). [H_2 /Cu]

33. C. T. Rettner, L. A. DeLouise, J. P. Cowin, and D. J. Auerbach, *Faraday Discuss. Chem. Soc.* **80**, 9 (1985). [HD/W]

34. J. D. Doll, *J. Chem. Phys.* **61**, 954 (1974).

35. L. M. Hubbard and W. H. Miller, *J. Chem. Phys.* **80**, 5827 (1984).

36. H.-D. Meyer, *Surf. Sci.* **104**, 177 (1981).

37. R. I. Masel, R. P. Merrill, and W. H. Miller *Phys. Rev. B* **12**, 5545 (1975).

38. A. Nourtier, *Jour. Phys. (Paris)* **40**, 55 (1985).

39. G. Drolshagen and E. J. Heller, *J. Chem. Phys.* **79**, 2072 (1983).

40. G. Drolshagen and R. Vollmer, *Chem. Phys. Lett.* **122**, 333 (1985).

41. B. Jackson and H. Metiu, *J. Chem. Phys.* **83**, 1952 (1985).

42. B. Jackson and H. Metiu, (private communication)

43. S.-I. Sawada, R. Heather, B. Jackson, and H. Metiu, *J. Chem. Phys.* **83**, 3009 (1985).

44. J. L. Beeby, *J. Phys.* C **4**, L359 (1971).

45. N. Garcia, A. A. Maradudin, and V. Celli, *Phil. Mag.* A **45**, 287 (1982).

46. J. Lapujoulade, *Surf. Sci.* **134**, L529 (1983). [He/Cu]

47. A. C. Levi and H. Suhl, *Surf. Sci.* **88**, 221 (1979).

48. A. M. Marvin, V. Celli, and F. Tiogo, *Surf. Sci.* **154**, 121 (1985).

49. J. H. Weare, *J. Chem. Phys.* **61**, 2900 (1974).

50. R. Schinke, *Surf. Sci.* **127**, 283 (1983).

51. K. B. Whaley and J. C. Light, *J. Chem. Phys.* **81**, 1112 (1984).

52. A. Liebsch and J. Harris, *Surf. Sci.* **123**, 355 (1982).

53. L. L. Barnes, N. F. Lane, and C. C. Liu, *Phys. Rev.* A **137**, 388 (1965).

54. R. G. Gordon, *J. Chem. Phys.* **51**, 14 (1969).

55. A. Tuschida, *Surf. Sci.* **14**, 375 (1969).

56. H. Chow, *Surf. Sci.* **62**, 486 (1977).

57. R. B. Laughlin, *Phys. Rev. B* **25**, 2222 (1982).

58. G. Armand and J. R. Manson, *Phys. Rev. Lett.* **53**, 1112 (1984).

59. G. Armand and J. R. Manson, in *Dynamics on Surfaces* ed. by B. Pullman *et al.* (D. Reidel 1984)

60. W. Brenig, *Z. Phys.* B **36**, 81 (1979).

61. J. R. Manson and V. Celli, *Surf. Sci.* **24**, 495 (1971).

62. H.-D. Meyer and R. D. Levine, *Chem. Phys.* **85**, 189 (1984).

63. J. Stutzki and W. Brenig, *Z. Phys.* B **45**, 49 (1981).

64. M. Lagos, *Surf. Sci.* **65**, 124 (1977).

65. J. Böheim, *Surf. Sci.* **148**, 463 (1984).

66. D. Eichenauer and J. P. Toennies, in *Proceedings of the* 17^{th} *Jerusalem Symposium on Dynamics of Molecule-Surface Interactions,* edited by B. Pullman and J. Sortner (D. Reidel, Dordrecht, 1984).

67. M. D. Stiles and J. W. Wilkins, *Phys. Rev. Lett.* **54**, 595 (1985).

68. B. H. Choi and R. T. Poe, *J. Chem. Phys.* **83**, 1330 (1985).

69. B. H. Choi and R. T. Poe, *J. Chem. Phys.* **83**, 1344 (1985).

70. Y.-W. Lin and G. Wolken, *J. Chem. Phys.* **65**, 2634 (1976).

71. Y.-W. Lin and G. Wolken, *J. Chem. Phys.* **65**, 3729 (1976).

72. G. Wolken, *J. Chem. Phys.* **60**, 2210 (1974).

73. M. Lagos and L. Birstein, *Surf. Sci.* **52**, 391 (1975).

74. M. D. Stiles, J. W. Wilkins, and M. Persson, (to appear in *Phys. Rev.* B.) Hereafter referred to as I.

75. V. Celli and A. A. Maradudin, *Phys. Rev.* **B 31**, 825 (1985).

76. P. Nordlander and J. Harris, *J. Phys.* **C 17**, 1141 (1984).

77. J. Harris and A. Liebsch, *Physica Scripta* **14**, 14 (1983).

78. J. Harris and P. Feibelman, *Surf. Sci.* **155**, 1133 (1982).

79. P. Nordlander, C. Holmberg, and J. Harris, *Surf. Sci.* **152/153**, 702 (1985).

80. A. Liebsch and J. Harris, *Surf. Sci.* **130**, L349 (1983).

81. E. K. Grimmelmann, J. C. Tully, and E. Helfand, *J. Chem. Phys.* **74**, 5300 (1981).

82. V. Bortolani, A. Franchini, N. Garcia, F. Nizzoli, and G. Santoro, *Phys. Rev.* **B 28**, 7358 (1983).

83. G. Brusdeylins, R. B. Doak, and J. P. Toennies, *Phys. Rev. Lett.* **46**, 937 (1981). [He/LiF]

84. J. E. Black, T. S. Rahman, and D. L. Mills, *Phys. Rev. B* **27**, 4072 (1983).

85. A. A. Maradudin and D. L. Mills, *Ann. Phys.* **100**, 262 (1976).

86. A. A. Maradudin, in *Lattice Dynamics* , edited by M. Bulkanski (Flammarion, Paris, 1978),p.284

87. Z. W. Gortel, H. J. Kreuzer, and R. Teshima, *Phys. Rev.* **B 22**, 512 (1980).

88. W. Brenig, *Z. Phys.* **B 48**, 127 (1982).

89. V. Celli, A. M. Marvin, and G. Benedek, *Surf. Sci.* **148**, 54 (1984).

90. W. L. Nichols and J. H. Weare, *Phys. Rev. Lett.* **56**, 753 (1986).

91. K. L. Wolfe and J. H. Weare, *Phys. Rev. Lett.* **41**, 1663 (1978).

92. V. Celli in *Dynamics of Gas-Surface Interaction,* ed. G. Benedek and U. Valbusa (Springer-Verlag, Berlin 1982) p. 2

93. N. W. Ashcroft and N. D. Mermin, *Solid State Physics,* (Holt, Rinehart, and Winston, New York 1976) p. 790.

Table 2.1

The parameters used in these calculations. For these calculations it is necessary to specify both the potential energy of helium[76] or molecular hydrogen[79] near a copper surface and the phonons of the copper surface in the elastic continuum model.[85,86]

The Potentials

		He	H_2
Range Parameter	α	1.26 a_o^{-1}	1.21 a_o^{-1}
Repulsive potential constant	V_0	12.0 eV	5.21 eV
van der Waals constant	C_{VW}	1.52 eV/a_o^3	4.83 eV/a_o^3
Mirror plane	z_{VW}	.462 a_o	.563 a_o
van der Waals cutoff	k_c	1.0 a_o^{-1}	.4 a_o^{-1}
Well depth	D	5.66 meV	22.3 meV
Bound states	N_{BS}	5	7

The Phonons

Longitudinal sound velocity	c_l	4.3×10^3 m/sec
Transverse sound velocity	c_t	2.2×10^3 m/sec
Rayleigh sound velocity	c_R	2.1×10^3 m/sec
Debye frequency cutoff	ω_D	30 meV
Debye wavector	Q_D	.907 a_o^{-1}
Interaction Potential wavevector cutoff	Q_c	.39 a_o^{-1}

Table B1

A comparison of x-ray, neutron, and helium atom scattering. This table compares and contrasts the similarities and differences between these scattering systems that are important for understanding the thermal attenuation in each system.

	X−ray Scattering	Neutron Scattering	HeliumAtom Scattering
Scatterer	all electrons, (primarily core)	nuclei	valence electrons
Characteristic Wavevector of Perturbation	$\frac{1}{2}\ a_0^{-1}$	$\frac{1}{2}10^5\ a_0^{-1}$	$\frac{1}{5}\ a_0^{-1}$
Energy	10 − 50 keV	20 − 200 meV	20 − 200 meV
Time Scale of Perturbation	static	dynamic	dynamic
Strength of Perturbation	weak	weak	strong (for distorted wave treatment− weak or strong)
Theoretical Treatment	Born approximation	Born approximation	distorted wave Born approximation
Perturbing Potential(s)	$V(\mathbf{r},t_0)$	$V(\mathbf{r},t)$	$\langle V\rangle_{th} - \frac{1}{A}\int d^2R\ \langle V\rangle_{th}$ $V(\mathbf{r},t) - \frac{1}{A}\int d^2R\ \langle V\rangle_{th}$ $V(\mathbf{r},t) - \langle V\rangle_{th}$
Intensity	structure factor	structure factor	complicated
	$\int \frac{d\omega}{(2\pi)}\ f(\mathbf{k})S(\mathbf{k},\omega)$ no energy resolution, k − dependence from charge distribution in unit cell	$S(\mathbf{k},\omega)$	
Thermal Attenuation	Debye− Waller factor	Debye− Waller factor	complicated
	$e^{-\left\langle(\Delta\mathbf{k}\cdot\mathbf{u})^2\right\rangle_{th}}$	$e^{-\left\langle(\Delta\mathbf{k}\cdot\mathbf{u})^2\right\rangle_{th}}$	

FIGURE CAPTIONS

Figure 2.1 The potentials used for calculating the inelastic scattering probabilities. The top panel shows the helium-copper potential; the second panel, the H_2-copper potential, and the bottom panel, the HD-copper potential. The horizontal lines superimposed on each potential show the energy of each of the bound state of that potential (these are the bound states of the full orienationally dependent potential); the lines, starting and stoping at the classical turning points for those energies, give some idea of the spatial extent of the bound state wavefunctions. The well depth of the helium potential is roughly one fourth that of the hydrogen potentials leading to bound states wavefunctions that are further from the surface. The bound states, being further from the surface, do not couple as strongly to the inelastic scattering and so reduce the trapping probability for helium compared to hydrogen because the bound states. The two hydrogen potentials have been expanded in Legendre polynomials of the orientation of the molecular axis with respect to the surface normal; the solid curves are the $l = 0$, angle-averaged, terms in the expansion the dashed lines are the $l = 1$ terms, and the dotted lines are the $l = 2$ terms. Since the H_2 molecule has an axis of inversion symmetry, the $l = 1$ term in the potential vanishes identically. The orientational dependence of the HD molecule is much stronger because its center of mass is offset from the centroid of the electron cloud; since electronically the HD molecule is identical to the H_2 molecule the HD potential is just the H_2 potential adjusted for this offset of the center of mass.

Figure 2.2 A comparison of potential forms. The helium-copper potential used in this paper (the solid curve) differs only slightly from a Morse potential (the dotted curve) with the same well depth and range parameter the repulsive part of the actual potential. The largest difference is in the attractive part of the potential far from the surface which leads to very different bound states energies, but does not affect the inelastic scattering very strongly. The slight difference in the attractive potential near the back wall of the potential lead to the slight differences in the inelastic scattering probabilities seen in Fig. (4.4).

Figure 2.3 A Morse-potential model for the interaction potential. A Morse potential form of the gas-surface potential can be constructed from a Morse potential contribution from each layer in the solid; this construction is useful for determining how to model the interaction potential for other forms of the static gas-surface potential. The top panel shows the static surface potential (solid line) and the contribution to this potential from the top layer of the surface (dashed line). The difference between these two potentials shows that a large part of the attractive well is due to the subsurface layers even for a potential as short-ranged as a Morse potential. The parameters for the potential have been chosen so that the static surface Morse potential is the same as the one in Fig. (3.2). The bottom panel shows the derivative of the static surface potential (solid line), the derivative of the contribution from the top layer (dashed line), and the derivative of the repulsive part of the static surface potential (dotted line). The interaction potential for phonon modes in which the top surface layer rigidly shifts normal to the surface is given (in the low amplitude limit) by the derivative of the potential due to the top layer of the solid. This figure shows that this interaction potential is much better approximated by the derivative of the full static surface potential than by the derivative of the repulsive part of the static surface potential even though the subsurface layers make a large contribution to the attractive region of the potential. The static surface potential is a better approximation because the attractive part of the potential is more strongly dominated by the top layer contribution the closer the particle is to the surface. This conclusion that the derivative of the full static surface potential is a better approximation than the derivative of the repulsive potential, however, may depend on the parameters of the Morse potential. However, it also holds for Lennard-Jones potentials summed over all atoms in the substrate that give the small depth and curvature as this Morse potential.

Figure 2.4 The mean square displacement of the surface. This figure shows as a function of surface temperature the mean square displacement of the surface (top curve), and the mean square displacement of the effective height of the surface in the interaction potential for two choices of the cut-off wavevector. This cut-off is contained in the interaction potential as a factor that reduces

the contribution to inelastic scattering of high parallel wavevector phonons. At temperatures high compared to the Debye temperature all three curves are roughly proportional to the surface temperature and go to a finite value at zero temperature due to the zero-point motion of the surface. The mean square effective heights are lower than the mean square displacement because the contributions from high wavenumber phonons is reduced much in the same way that the inelastic scattering is reduced due to the same cut-off. The lowest curve is for the cut-off used in these calculations, and the middle curve is for the cut-off equal to the surface reciprocal lattice vector appropriate to these calculations.

Figure 2.5 The dependence of the phonon density of states on the change in energy in the inelastic scattering process for several surface temperatures. These three panels show for surface temperatures ranging from 0 K to 420 K in steps of 60 K, the density of phonons (weighted by their amplitude projected on the surface layer) as a function of the change in the normal energy of the scattering particle. Each of the three panels corresponds to one of the weightings of the density by the high parallel wavevector cut-off that are discussed in Fig. (2.4), *i.e.*, the top panel shows the energy density of all phonons and the two lower panels show the energy density of the phonons reduced by the large wavevector cut-off in the interaction potential for the same two values of the cut-off wavevector (as in Fig. 2.4). The effect of the large wavevector cut-off is to reduce the weight of phonons contributing to large normal energy changes without strongly affecting the low energy transfers because low frequency phonons necessarily have low parallel wavevectors. These plots show that the parallel wavevector cut-off in the interaction potential has a more complicated effect on the inelastic scattering than just reducing the effective mean square displacement of the surface because it also changes the distribution over final states, *i.e.*, it reduces the importance of high normal energy transfers. This will have a large effect on the sticking probabilities. The steps in these curves, which are most pronounced in the top panel are due to the Debye parallel wavevector cut-off of the Rayleigh phonons; this size of which indicates the importance of the Rayleigh phonon modes to the projected density of states.

Figure 2.6 The dependence of the phonon density of states on the chane in energy in the inelastic scattering process for different incident parallel momenta. Similarly to the last figure these three panels show the density of phonons (weighted by their amplitude projected on the surface layer) as a function of the change in the normal energy of the scattering particle, here for a series of incident parallel energies ranging from 0 meV to 52.5 meV in increments of 7.5 meV. For all the curves the surface temperature is 240 K. Each of the three panels corresponds to one of the weightings of the density by the high parallel wavevector cut-off that are discussed in in Fig. (2.4), *i.e.,* the top panel shows the energy density of all phonons and the two lower panels show the energy density of the phonons reduced by the large wavevector cut-off in the interaction potential for the same two values of the cut-off wavevector. These panels show the effect of off-normal incidence on the phonon density of states, which is the only way off-normal incidence affects the scattering probability in this approximation. With increasing parallel momentum, or energy, the density of phonons tends to peak more strongly at small energy transfers, but the effect is only important for the phonon density that is not weighted by the interaction potential phonon parallel wavevector cut-off. For the model of the interaction potential used in the calculations in this thesis (the bottom panel) the effect of off-normal incidence is small and can be neglected except in detailed calculations, provided the correct three-dimensional phonon density of states is used.

Figure 3.1 A comparison of different calculations of elastic scattering probabilities as a function of temperature. The results of three calculations based on the distorted wave Born approximation (solid curves) and two based on a Debye-Waller approach (dotted curves) are compared for calculations of the elastic scattering probability for helium scattering from copper at normal incidence. The three distorted wave based methods are: 1) the second-order distorted-wave Born approximation (solid triangles), 2) the self-consistent one-phonon approximation developed in this thesis (solid squares), and 3) the exponentiated-inelastic-scattering model (solid circles) discussed in this chapter. The axis on the left side of the figure gives the elastic scattering probability on a logarithmic scale, and the axis on the right hand side gives the natural logarithm of the elastic scattering

probability. For the exponentiated-inelastic-scattering model the (negative) natural logarithm of the elastic scattering probability is just the distorted wave Born approximation result for the total first-order inelastic-scattering probability. The total inelastic scattering can be used to gauge the temperatures for which the one-phonon approximation is valid because the first-order inelastic scattering probability should be small compared to one; this condition is not satisfied for most of the temperatures on this plot. The second-order distorted-wave Born approximation becomes negative when the the first-order Born approximation becomes greater than one; this change in sign leads to a divergence in this scattering probability seen in this figure at 220 K. The self-consistent one-phonon result is bounded between zero and one so that there are no divergences, but the curvature as a function of temperature has to be affected by the breakdown of the one-phonon approximation. In the high temperature limit the distorted-wave Born result for the inelastic scattering is proportional to the temperature so that in this same limit the exponentiated inelastic scattering model should give results that are linear on this plot. The other two results, both of which are proportional to the temperature in the high temperature limit are the Debye-Waller factor (open squares) and the Beeby-corrected Debye-Waller factor (open circle). Both of these quantities are calculated using the mean-square effective height of the surface rather than the mean square displacement because the former quantity is used in the distorted wave methods, this choice increases the log of the scattering probability by a factor of roughly two and a half.

Figure 3.2 A comparison of different calculations of elastic scattering probability as a function of energy. As in the previous figure the results of three calculations based on the distorted wave Born approximation (solid curves) and two based on a Debye-Waller approach (dotted curves) are compared for calculations of the elastic scattering probability for helium scattering from copper at normal incidence. The three distorted wave based methods are: 1) the second-order distorted wave Born approximation (solid triangles), 2) the self-consistent one-phonon approximation (solid squares), and 3) the exponentiated inelastic scattering model (solid circles). The other two results, which are both straight lines in this plot, are the Debye-Waller factor (open squares) and the

Beeby-corrected Debye-Waller factor (open circle). The axis on the left side of the figure gives the elastic scattering probability on a logarithmic scale, and the axis on the right hand side gives the negative natural logarithm of the elastic scattering probability. The second-order distorted wave Born and the self-consistent one-phonon results both show the curvature due to the breakdown of the one-phonon approximation. The exponentiated inelastic scattering results also has some curvature which is even more apparent in other systems (such as H_2). By construction the Beeby-corrected Debye-Waller factor extrapolates to unit elastic scattering probability at an energy equal the negative of the well depth, here $D = 5.656$ meV; somewhat unexpectedly the exponentiated inelastic scattering model also behaves this way if the low energy parts of the curve are used.

Figure 3.3 Comparison of calculated with experimental elastic scattering probabilities. The two panels show experimentally measured[6] (dotted curves and open symbols) and theoretically calculated (solid curves and full symbols) elastic scattering probabilities as a function of surface temperature for two incident energies, 63 meV in the top panel and 21 meV in the bottom, and several incident angles 71.6° (squares), 61.7° (circles), 51.9° (triangles), 39.0° (diamonds and crosses), and 19.0° (stars) in the upper panel and 73.5° (squares), 55.5° (circles), and 31.8° (triangles) in the lower panel. The agreement is surprisingly good for a comparison with no adjustable parameters and may be fortuitous given the uncertainty in some of the approximations made in this model. The probabilities have been calculated using the exponentiated inelastic scattering method (discussed in this section) with the additional assumptions about the form of the potential which includes the flat surface approximation (see I), the isotropic elastic continuum model for the phonon spectrum (section II.C), and the form of the interaction potential (section II.B). The assumptions about the interaction potential are the least understood; in particular 1) the use of the derivative of the full static potential in the interaction potential as we do here instead of the derivative of just the repulsive potential, and 2) both the form of the parallel wavevector dependence in the interaction potential which is gaussian in this model, and the choice of parameters used in it. Using the derivative of the repulsive potential will increase the inelastic scattering, or the exponent in

the exponentiated inelastic scattering model, by roughly a factor of four. Ignoring the wavevector cutoff in the interaction potential will increase the inelastic scattering probability by slightly more than a factor of two.

Figure 3.4 The range parameter dependence of the elastic scattering probability. The inelastic scattering probability in the distorted wave Born approximation (the right hand scale) and the elastic scattering probability in the exponentiated inelastic scattering model (same curves, but left hand scale) are shown as a function of incident energy for different models of the potential. The dotted line is calculated using the exponential-van der Waals potential used in the previous figures and the solid line closest to it is calculated using the Morse potential with the same well depth and range parameter in the repulsive part of the exponential-van der Waals potential; these two potentials are shown plotted in Fig. (2.2). This and the next four figures show how the inelastic scattering changes as a function of the potential that is used in its calculation. Here, the range parameter of the Morse potential is varied in the series: $\alpha = \alpha_o/4,\ \alpha_o/2,\ \alpha_o, 2\alpha_o,\ 4\alpha_o$, where $\alpha_o = .63\ a_o^{-1}$, and gives the curves from the uppermost to the lowest respectively. The well depth for these potentials is $D_o = 5.656$ meV. The curves for the two steepest potentials, $\alpha = 2\alpha_o$ and $\alpha = 4\alpha_o$ are coincident to within the accuracy of the calculation indicating that they are both in the hard wall limit. That the curve for $\alpha = \alpha_o$ does not agree with the two for the steeper potentials indicates that the physical potential is not in the hard wall limit. The difference between the results for the hardwall potential and the physical potential account for most of the differences between the Beeby-corrected Debye-Waller factor results and the results for the physical potential. As the value of the range parameter is decreased from the hard wall value the inelastic scattering probability depends more and more strongly on the value of the range parameter.

Figure 3.5 The well depth dependence of the elastic scattering probability. Similarly to the previous figure the elastic scattering probability, calculated using the exponentiated inelastic scattering model, is shown as a function of energy for a variety of potential well depths. For the curves from the top to bottom the well depths are $D = D_o/2$, $D = D_o$, $D = 2D_o$, and $D = 4D_o$,

where the the physical well depth is $D_o = 5.656$ meV. The ticks on the inset in the top right hand corner give the separation of the energies of the potential wells used in these calculations; the Beeby-corrected Debye-Waller approach gives elastic scattering probability curves separated by these amounts. Surprisingly this exponentiated inelastic scattering model gives the same result because the curves calculated using this approach are also separated by these amounts. The dotted curves are each of the calculated curves shifted horizonally by the well depth of the potential that was used to calculate them. This implies that it is a reasonably good approximation to treat the attractive well as effectively increasing the kinetic energy in the motion normal to the surface; this is not a rigorous result because the details of the potential form also change the separation but it is reasonable approximation. The next figure shows that this is not the case if only the repulsive part of the static potential is used in the interaction potential.

Figure 3.6 The well depth dependence using just repulsive potential coupling Like the previous figure this plot shows the elastic scattering probability for several potential well depths, but for these curves the interaction potential only included the derivative of the repulsive part of the potential rather than both the repulsive and attractive parts. The three well depths used here are form top to bottom $D = D_o/2$, $D = D_o$, and $D = 2D_o$; the curve for $D = 4D_o$ falls outside the range of this plot for all values of the energy. These curves show a much stronger dependence on the well depth than do those for which the derivative of the full static potential is used in the interaction potential. Clearly the attractive potential can not be modeled by adding the well depth to the incident energy in the motion normal to the surface.

Figure 3.7 The mass dependence of the elastic scattering probability The two panels in this figure show the dependence of the elastic scattering probability on the mass as a function of incident energy for potentials with two different well depths, $D = D_o$ in the top panel and $D = 4D_o$ in the bottom panel. The potential in the top panel has the well depth of the helium on copper potential and the one in the lower panel has roughly the same well depth as the molecular hydrogen on copper potential. The curves are labeled by the atom or molecule for which the mass has been

used to generate that curve. For the range of parameters spanned by the curves in this plot the inelastic scattering probability is proportional to the mass.

Figure 3.8 The self-energy for helium scattering from copper in the one-phonon approximation. The imaginary part of the non-local self-energy (see Eq. (3.7)) is plotted as a function of the first spatial argument with the second spatial argument taking the values $z' = 3.0, 3.2, \ldots, 4.6$ a_0 for three different energies (given in each panel). The static surface potential for helium scattering that is used in these plots is shown in Figs. (2.1,2) and the phonon density as a function of energy is shown in the bottom panel of Fig. (2.5) as the 240 K curve. To associate each curve in a panel with its second spatial argument find the curves for which the first peak (moving from left to right) occurs at the same position; the curve with the lowest peak height has the lowest value of the spatial argument. The first peak in the optical potential is near the classical turning point ($z = 3.6$ a_0 for $E_i = 24$ meV, $z = 3.45$ a_0 for $E_i = 36$ meV, and $z = 3.3$ a_0 for $E_i = 48$ meV). This peak height increases as the second spatial argument increases until it reaches a maximum. Then as the second argument increases further the peak shifts to the right and decreases, reaching the righmost part of the panel for the last value of the second spatial argument included. The self-energy goes to zero for large values of either spatial argument because the interaction potential vanishes and goes to zero for small (and negative) values of either spatial argument because there are no inelastic wavefunctions with energies near the incident energy that penetrate into the surface. This figure shows why it is difficult to make a simple approximation for the optical potential that can be used to calculate inelastic scattering probabilities as a function of temperature or energy. The difficulty is that this self-energy is strongly energy dependent, non-local, and non-separable. If the self-energy were energy independent all of these three panels would be identical. If it were local each panel would consist of a series of spatial delta functions of varying heights as a function of either spatial argument. If it were separable all of the curves would have the same shape but different amplitudes.

Figure 3.9 Molecular hydrogen inelastic scattering probabilities. The top panel (H_2) and the bottom panel (D_2) show the distorted wave Born approximation results for the inelastic scattering

probability for molecular hydrogen scattering from a zero temperature copper surface. The three curves - solid ($l = 0, m = 0$), dashed ($l = 1, m = 0$), and dotted ($l = 1, m = 1$) - are for different rotational states of the incident molecule. These three states are not coupled by the surface potential because the flat surface conserves the azimuthal quantum number and there is no nuclear spin coupling to convert ortho (odd l H_2 and even l D_2)into para (even l H_2 and odd l D_2) or vice versa. For the low incident energies the scattering is in the one-phonon regime except at selective adsorption resonances which are the sharp narrow peaks in the inelastic scattering probability. The inelastic scattering is strongly enhanced to th point where it is well outside the one-phonon regime, because the molecule spends a long time near the surface in the rotationally excited state. The difference between the curves in each panel are due to 1) the different rotational energy splittings for the odd and even angular momentum species leading to different selective adsorption resonance energies, and 2) the different spherical harmonic matrix elements of the potentials that are important for each species (see Fig. 3.10). The differences between H_2 and D_2 are due to the difference in the mass leading to 1) stronger inelastic scattering for D_2 , 2) lower rotational energy splitting so that the resonances occur at lower energies, and 3) more and more closely spaced bound states for D_2 .

Figure 3.10 Spherical harmonic matrix elements of the hydrogen-copper surface potential. The different curves in this figure are the diagonal parts of the matrix elements of the position and orientation dependent potential with respect to the orientational state of the molecule which is described by spherical harmonics. The curves are labeled by the rotational state in the inset in the upper right hand corner of the figure. These matrix elements, together with the off-diagonal matrix elements, determine the dynamics of the scattering process. The off-diagonal parts determine the coupling between different angular momentum states and the widths of the selective adsorption resonances. In the absence of coupling betwenn angular momentum states the diagonal parts of the potential describe the motion of the scattering molecule so that when the coupling is weak the inelastic scattering probabilities are primarily determined by the diagonal matrix element of

the potential with the incident angular momentum state. Even though the shapes and widths of the selective adsorption resonances are determined by the off-diagonal coupling the energies of the selective adsorption resonances are determined by the rotationally excited state diagonal matrix elements of the potential rather than the incident state matrix elements. The resonant part of these states should be thought of as a rotationally excited molecule moving in its effective potential which is determined by its angular momentum state. At the bottom of the figure are two insets to emphasize some of the features in Fig. 3.9; the left inset shows the potential near the classical turning of a 30 meV incident hydrogen molecule, the differences between the solid, dashed, and dashed-dotted curve lead to the differences in the background values of the inelastic scattering probability. Even though there are large differences in the inelastic scattering probabilities for the $l = 1, m = 0$ and $l = 1, m = 1$ states the selective adsorption resonances occur at energies that are very close to each other because the $l = 3, m = 0$ and $l = 3, m = 1$ potentials are very similar as is seen in the inset in the bottom left hand corner. Note that corrugation mediated selective adsorption resonances are likely to occur at perceptibly different energies for different rotational states because the potentials for the *incident* rotational state determine those resonance energies rather than the potentials for the rotationally excited species.

Figure 3.11 The trapping probability for molecular hydrogen scattering from copper. The top panel shows the trapping probability for H_2 and the bottom panel that for D_2 calculated in the distorted wave Born approximation for scattering from a zero degree copper surface for an incident angle of 60°. The calculation has been done for a normally incident molecules and then the incident energy adjusted to account for the off-normal incidence, since it was shown in Sec. II.B of this paper that using the normal energy rather than the total energy accounts for almost all of the effects of off-normal incidence. The solid curves are the trapping probability for the $l = 0$ incident rotational state molecules (para-hydrogen and ortho-deuterium) and the dotted curves are for the $l = 1$ rotational states averaged over the azimuthal quantum number. Because of the mass ratio the D_2 trapping coefficients are a factor of two larger than those for H_2 except the the highest

energies where they are about the same. There are no selective adsorption resonances for H_2 in this energy regime, and those for D_2 are weak; even if the resonances were not weak in a distorted wave Born approximation treatment, their effect on trapping would be reduced because all the inelastic scattering probabilities are enhanced, so that the enhancement of each is reduced in a self-consistent calculation. These trapping probabilities can not be directly compared to sticking coefficients, but should be used as inputs to a kinetic calculation of sticking probabilities.

Figure 3.12 HD scattering probabilities from a static copper surface. The elastic (top panel), and rotationally inelastic (middle panel) scattering probabilities for HD scattering from a static copper at normal incidence are plotted as a function of the incident energy. The bottom panel shows the density in the rotationally excited trapped state integrated over the position normal to the surface also as a function of the incident energy. This quantity, a measure of the time spent near the surface in this rotationally excited state, is strongly peaked at the selective adsorption resonances. As seen in the middle panel, no molecules with incident energies below 11 meV leave the surface rotationally excited. For these energies the $l = 1$ rotational state can be resonant with the bound states of the surface potential as seen from the broad overlapping peaks in the bottom panel, but the elastic scattering probability is not affected in this approximation. There is no effect because there is only one possible final state; they will be observable, however, when inelastic scattering is included in the calculation. Above 11 meV the molecule can scatter into either an $l = 0$ or an $l = 1$ state and leave the surface, and the $l = 2$ state can be resonant with the bound states giving selective adsorption resonances. Resonances for which there are more than one possible final state cause peaks in the elastic, $l = 0$, scattering probability and dips in the rotationally inelastic, $l = 1$, scattering probability as well as increased trapped state densities. Unlike the resonances for energies below 11 meV these resonances are much sharper and do not overlap each other.

Figure 3.13a The energy dependence of HD scattering from copper. The elastic (top panel), and rotationally inelastic (middle panel) scattering probabilities for HD scattering from copper at normal incidence are plotted as a function of the incident energy for a series of eight temperatures

between 0 K and 280 K in increments of 40 K. The bottom panel shows the density in the rotationally excited trapped state integrated over the position normal to the surface. The shapes and sizes of these peaks are strongly affected by the inelastic scattering as can be seen by comparing these curves to each other and to the static surface scattering probabilities shown in Fig. 3.12. The resonances for energies below 11 meV, which are the dips in the elastic scattering probability for scattering from a finite temperature surface but not apparent for scattering from a static surface, are only observable through the enhanced inelastic scattering caused by the resonances. They are not significantly broadened by the inelastic scattering as is shown by the temperature independence of the width of the trapped state density peaks. A consequence of this temperature independence is that the resonance enhancement of the inelastic scattering increases proportionally to the background inelastic scattering making the resonances are more pronounced at higher temperatures. The next figure shows a detail of these curves near one of the higher energy resonances.

Figure 3.13b A detail of the scattering probabilities near a selective adsorption resonance. The elastic scattering probability, $l = 0$, has a maximum and the rotationally inelastic scattering probability, $l = 1$, has a minimum due to a resonance. The maximum in the elastic scattering is strongly reduced by the inelastic scattering as the temperature increases (for a static surface the the amplitude of the peak becomes very close to unity), while the minimum in the rotationally inelastic scattering probability is less strongly affected. The trapped state probability is also strongly reduced by the inelastic scattering suggesting that the resonance lifetime is dominated by the inelastic scattering rather than the translational-rotational coupling. The peak in the trapped state density broadens as it decreases in height also indicating that the inelastic lifetime of the resonance is dominating its total lifetime. Details of the other resonances above 11 meV all look qualitatively the same as this figure; the main difference is that each resonance has different elastic and inelastic widths

Figure 3.14a Elastic scattering probabilities as a function of temperature for HD scattering from copper. The three solid lines show the elastic scattering probability as a function of energy for

incident energies below 11 meV, the energy below which there is no rotationally inelastic scattering, for HD scattering at normal incidence from copper. The dotted lines are the extrapolation to zero temperature of the high temperature parts of the solid lines. At zero temperature the extrapolated lines should give the static surface scattering probability if the extrapolation is to be useful for interpreting experimental data. Since elastic scattering is the only open channel the static surface scattering probability should be unity. The two top curves, which are for incident energies away from resonances, extrapolate back to about .95 while the bottom curve, which is for a resonant incident energy extrapolates back to .9, a ten percent error. This discrepancy between the static surface scattering probability and the extrapolation of the high temperature scattering probability is due to the overlap of the resonances below 11 meV; none of these energies is non-resonant. That the extrapolation works for incident energies far away from resonances is shown in the next figure.

Figure 3.14b Elastic and rotationally inelastic scattering probabilities as a function of temperature for HD scattering from copper. The elastic (solid lines) and rotationally inelastic (dashed lines) scattering probabilities are plotted as a function of temperature for one resonant (the middle two curves, 20.5 meV) and two non-resonant energies (the two top and two bottom curves, 17.7 meV and 22.7 meV). In addition the extrapolation of the high temperature part of each curve is shown in the dotted lines. For the non-resonant energies the scattering probabilities decrease with increasing temperature as expected and the high temperature curves extrapolate back close to the static surface values which are shown as solid squares, $l = 0$, and open squares, $l = 1$, on the left axis of the figure. However the resonant scattering probabilities behave differently; although the total scattering probability decreases with increasing temperature, the rotationally inelastic scattering probability increases with increasing temperature due to the inelastic scattering changing the shape and width of the resonance. The resonant scattering probabilities do not extrapolate back to the static surface values which are not shown on this plot since they would not appear to be associated with any of the curves; the $l = 0$ scattering probability for this energy is 0.998 and the $l = 1$ scattering probability is 0.002. The next figure compares these extrapolations with the

static surface scattering probabilities as a function of the incident energy.

Figure 3.15 A comparison of finite-temperature-extrapolation predictions for elastic and rotationally inelastic scattering probabilities. The self-consistent one-phonon approximation results are analyzed as experimental data in two ways: 1) the log of the high temperature scattering probabilities are extrapolated to zero temperature (dotted lines), and 2) the effects of inelastic scattering is accounted for by a Beeby-corrected Debye-Waller factor (dashed lines). These predictions are to be compared to the static surface scattering probability (solid lines). The top panel shows the elastic scattering probability and the middle panel shows the rotationally inelastic scattering probability. For non-resonant scattering there is good agreement between the extrapolated scattering probability and the static surface scattering probability as was illustrated in the previous figure. The Beeby corrected Debye-Waller factor does not do nearly so well, in particular it gets the energy dependence of the rotationally inelastic scattering probability wrong. If experimental data were analyzed in this way and then used to fit a static surface potential the resulting potential would be incorrect. If the Beeby-corrected Debye-Waller factor analyzed data was further corrected by requiring that the sum of the elastic and rotationally inelastic scattering probabilities be unity the predicted static surface scattering probabilities would be closer to the actual values but would still not be as close as the the extrapolated data would be with the same correction. This correction is illustrated in the bottom panel which shows the ratio of the rotationally inelastic scattering probability to the elastic scattering probability for the static surface scattering probability and each of the methods used to analyze the high temperature (calculated) data. While the agreement between the extrapolated predictions (dotted line) and the actual static surface results (solid line) is good for non-resonant scattering there is a roughly ten percent discrepancy between the Beeby-corrected Debye-Waller factor analyzed data (dashed line) and the static surface results.

Figure 3.16a Probability and flux densities for HD scattering from copper out of resonance. The top panel shows the probability density of the part of the wavefunction for which the phonons in the surface have not changed their state (the square of the zero-phonon-change amplitude) as

a function of position for each angular momentum state. The HD molecule with a non-resonant energy of 23 meV is incident normally on the copper surface at 80 K . The incident part of the molecular wavefunction (an $l = 0$ angular momentum state) beats against a much smaller amplitude outgoing wave in the same angular momentum state giving the oscillatory behavior in the solid curve. There is also an outgoing wave in the $l = 1$ angular momentum state, but none in the $l = 2$ because there is not enough energy in the incident particle to leave the surface in a state that highly rotationally excited. There is a slight average decrease in the probability in the potential well where the particle would be moving faster classically and a build up of probability just before the classical turning point. It is very hard to tell from this plot but there is a net flux toward the surface in this wavefunction because some flux has been lost to inelastic scattering. This is much clearer in the lower two panels showing the flux density in each angular momentum state as a function of position. Positive values of the flux are net fluxes toward the surface and negative values are fluxes away from the surface. The solid line, $l = 0$, shows the unit incident flux and the almost imperceptible outgoing flux in that angular momentum state, and the dashed line, $l = 1$, shows the flux away from the surface in the rotationally excited part of the zero-phonon-change state. Finally, the bottom panel shows the flux, which is all away from the surface, in each angular momentum state integrated over all of the one-phonon-change states. Whereas the amplitudes of these states can not be added together since the corresponding lattice states are orthogonal the flux densities can be. The distribution of flux between the different channels change very close to the classical turning point implying that all of the rotational and inelastic scattering takes place at this point. Adding all the zero-phonon-change fluxes and the one-phonon-change fluxes together will give a net flux toward the surface because there is flux lost to trapping in this model.

Figure 3.16b Probability and flux densities for resonant HD scattering from copper. This figure shows the same quantities as Fig. 3.16a, except that the incident energy is the resonant energy 20.5 meV. The resonance is immediately apparent in the large probability density seen in the $l = 2$ angular momentum state in the top panel. For this energy both the inelastic scattering

probability has increased as can be seen in the bottom panel and the elastic, $l = 0$ zero-phonon-change, scattering probability has increased as can be seen both in the increased amplitude of the oscillations in the $l = 0$ zero-phonon-change probability density and in the deviation of the $l = 0$ zero-phonon-change flux from one in the middle panel. The spatial location of the changes in the flux densities show that the rotational and the inelastic scattering no longer just take place near the classical turning point, but also further into the well where the build up in probability density in the rotationally excited trapped state is large and the derivative of the potential is still appreciable.

Figure 3.17 Final state scattering probabilities for HD scattering from copper. For the scattering conditions in the previous two plots, these two panels show the final state distribution as a function of the *final* energy in both motion normal to the surface and in rotational motion integrated over all final parallel momenta. The top panel shows these quantities for a non-resonant incident energy, 22 meV, and the bottom panel for a resonant incident energy, 20.5 meV. The solid curves are for molecules that leave the surface in the rotational ground state after scattering inelastically and the dotted line is for the molecules that leave the surface rotationally excited after scattering inelastically. The short vertical lines in the lower right part of each panel give the trapping probability in each bound state of the surface potential. The top panel shows that most of the particles that scatter inelastically with final energies greater than 11 meV also scatter into a rotationally excited, $l = 1$ state. For the non-resonant incident state, the enhancement of inelastic scattering by resonant final states is small, but for the resonant incident state the final state resonance enhancement is very large except for resonant states with energies close to the incident energy. The strong coupling between initial and final state resonance is due to the diagonal (in the angular momentum states of the scattering particle) elements of the interaction potential being much stronger than the off-diagonal elements so that the large amplitude in the rotationally trapped state couples most strongly to the part of each final state wavefunction with the same angular momentum.

Figure A1 Rotationally mediated selective adsorption resonances. A selective adsorption

resonance in a scattering probability results when a molecule can make a virtual transition to a rotationally excited trapped state. The top panel shows the HD-copper surface potential expanded in terms of Legengre polynomials of the orientation of the molecular axis relative to the surface normal (see inset). Also shown are the bound states of the angle averaged ($l = 0$) exponential-van der Waals potential. The next panel shows, superimposed on the potential, the asymptotic kinetic energy (due to motion normal to the surface) of the angular momentum channels of the HD molecule for a particular incident energy. As the total energy increases from zero the molecule can make virtual roational transitions into different bound states.

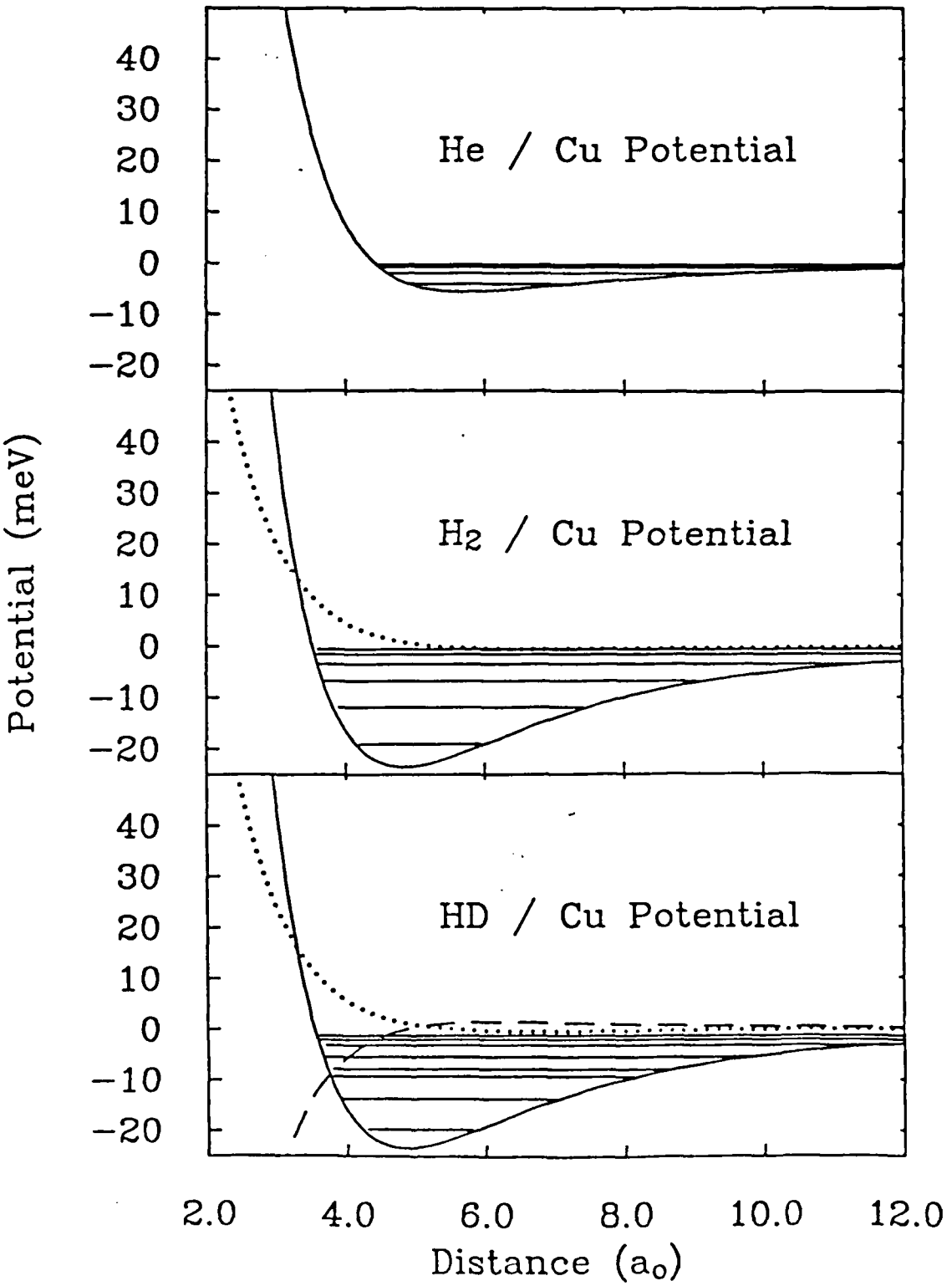
He / Cu Potential
H2 / Cu Potential
HD / Cu Potential
Potential (meV)
40
30
20
10
0
−10
−20
2.0
4.0
6.0
8.0
10.0
12.0
Distance (ao)

Figure 2.1

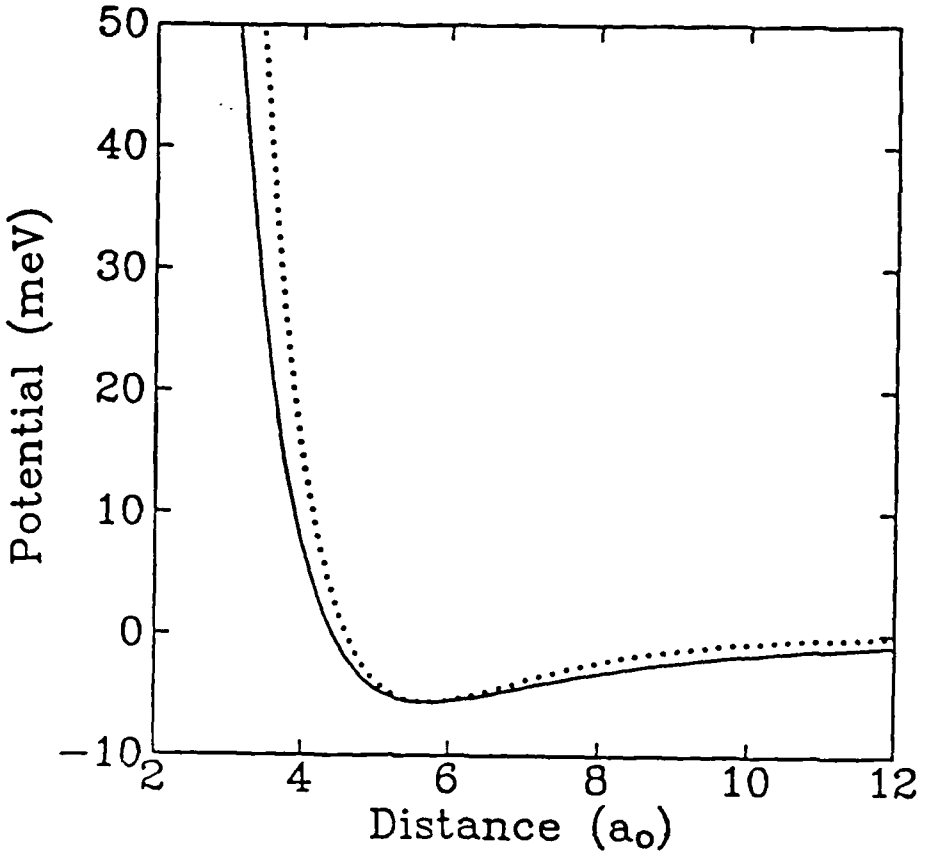

Figure 2.2

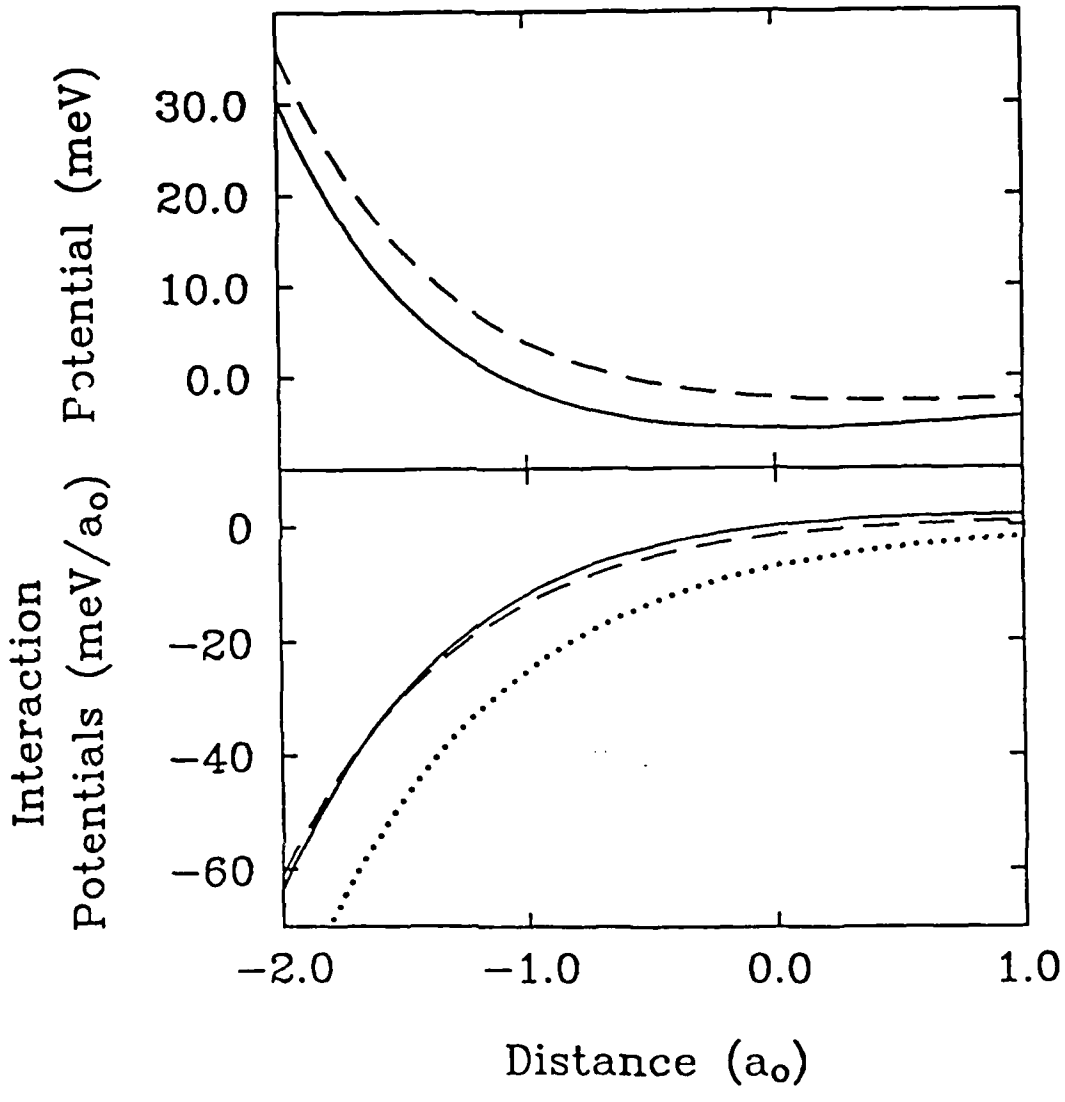
Potential (meV)
30.0
20.0
10.0
0.0
Interaction
Potentials (meV/a_o)
0
-20
-40
-60
-2.0
-1.0
0.0
1.0
Distance (a_o)

Figure 2.3

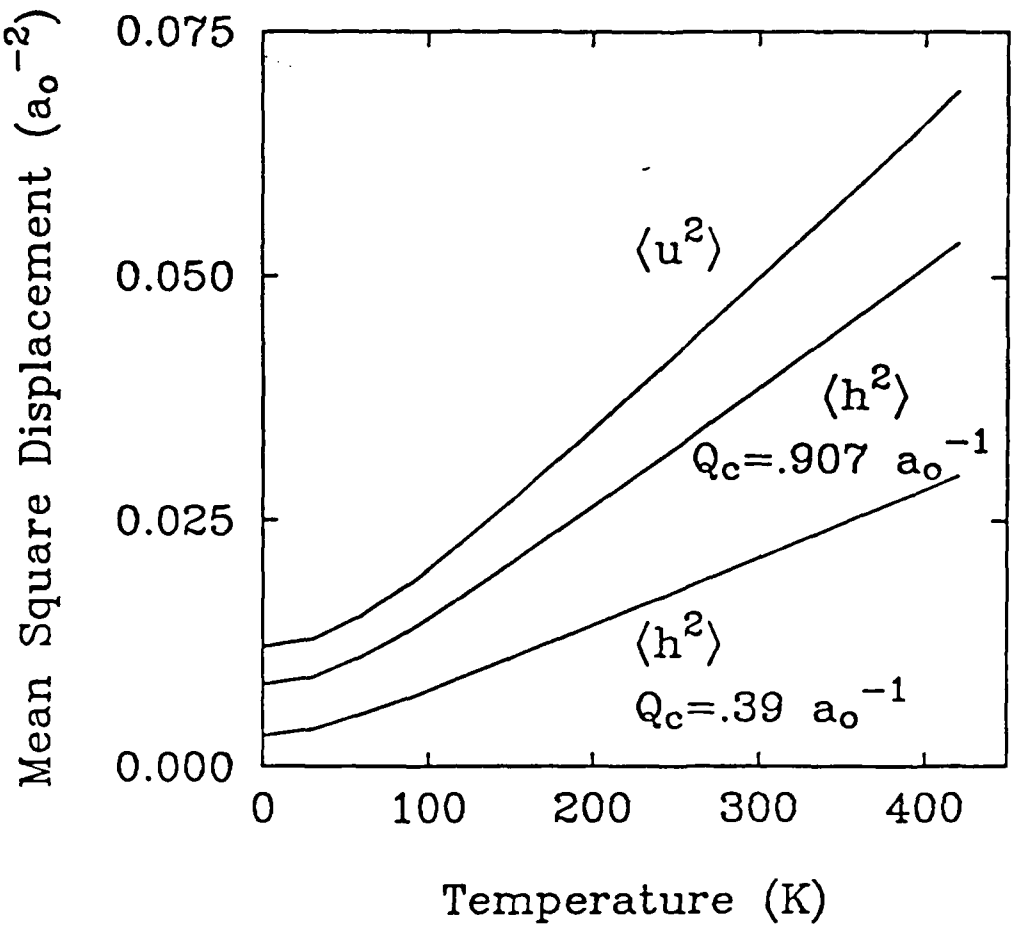
Mean Square Displacement (a_o^{-2})
0.075
0.050
0.025
0.000
0
100
200
300
400
Temperature (K)
$\langle u^2 \rangle$
$\langle h^2 \rangle$
Q_c=.907 a_o^{-1}
$\langle h^2 \rangle$
Q_c=.39 a_o^{-1}

Figure 2.4

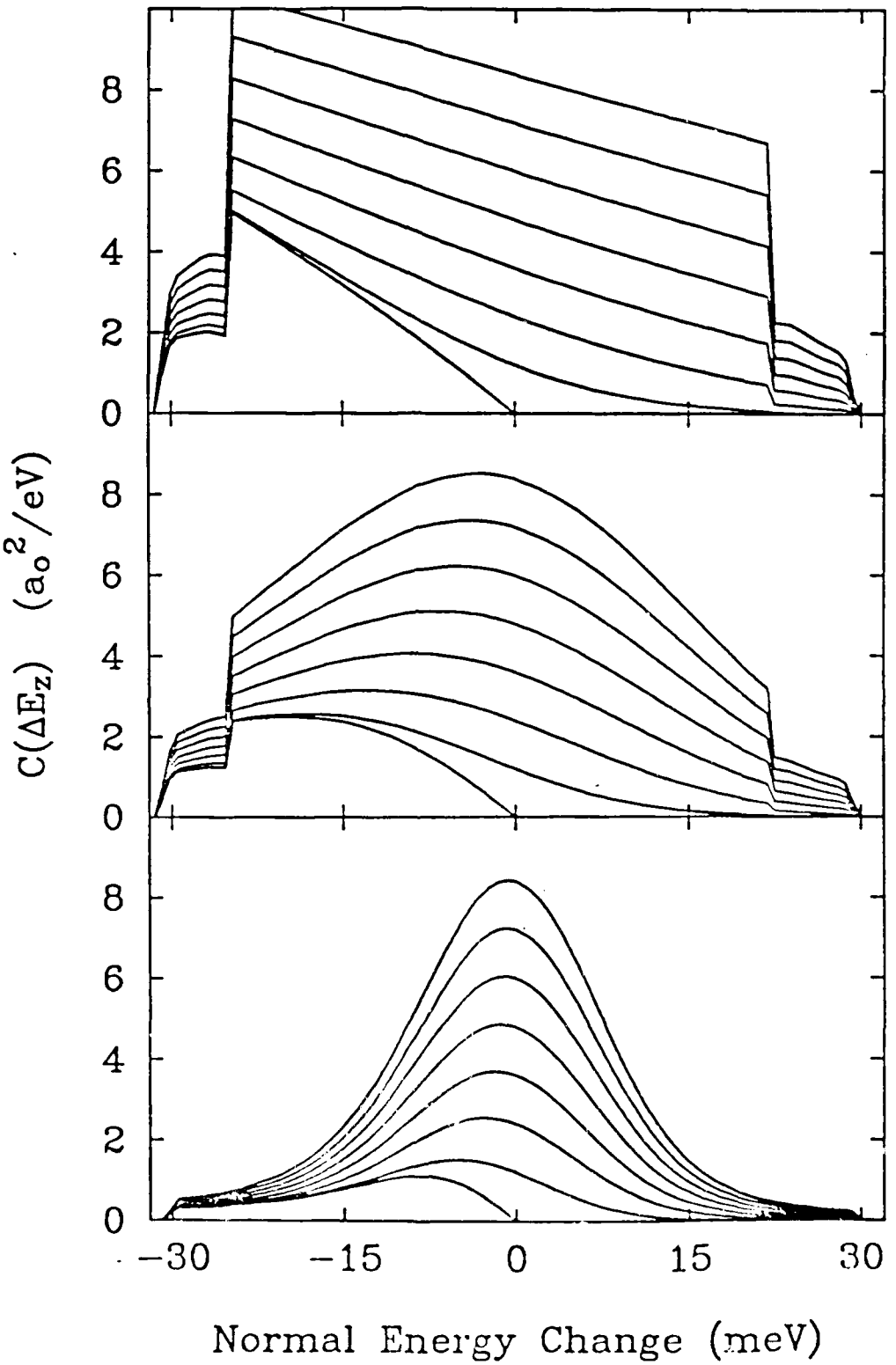
8
6
4
2
0
8
6
4
2
0
8
6
4
2
0
C(ΔEz) (ao2/eV)
−30
−15
0
15
30
Normal Energy Change (meV)

Figure 2.5

AD-A171 507 INELASTIC GAS-SURFACE SCATTERING II RESULTS(U) CORNELL 2/2
UNIV ITHACA NY LAB OF ATOMIC AND SOLID STATE PHYSICS
M D STILES ET AL. 25 AUG 86 TR-27 N00014-82-K-0576
UNCLASSIFIED F/G 20/10 NL

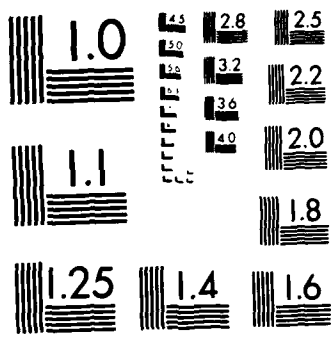

MICROCOPY RESOLUTION TEST CHART

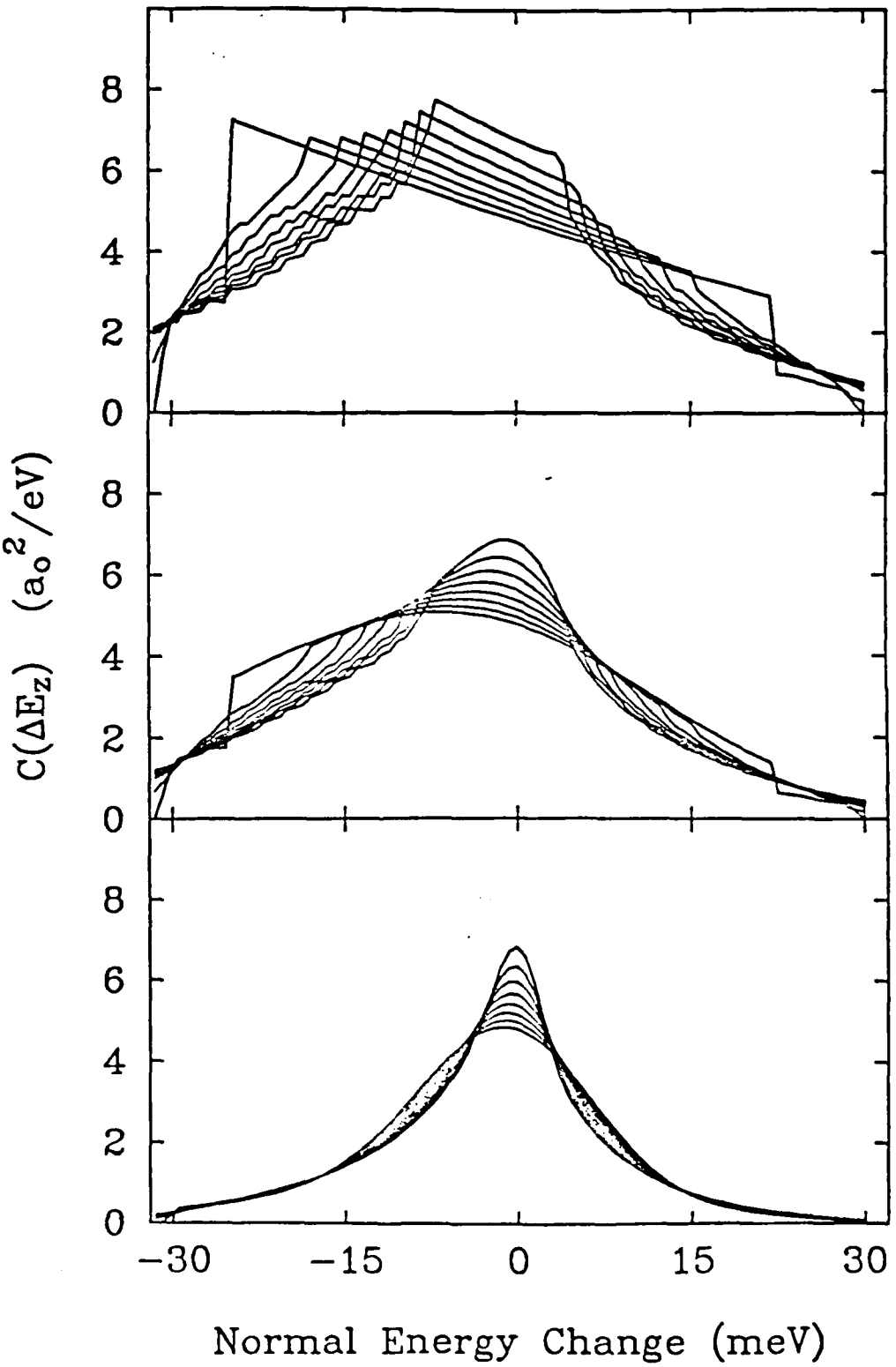

Figure 2.6

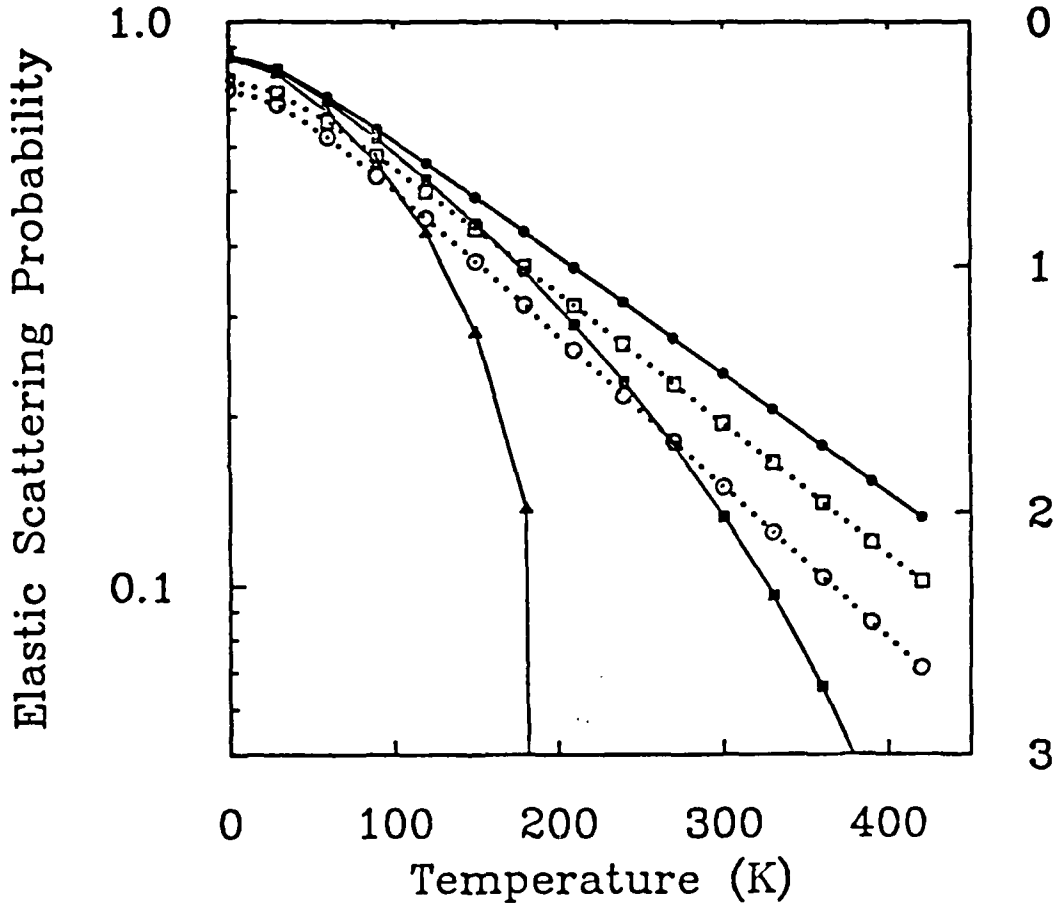
Elastic Scattering Probability
1.0
0.1
0
100
200
300
400
Temperature (K)
0
1
2
3

Figure 3.1

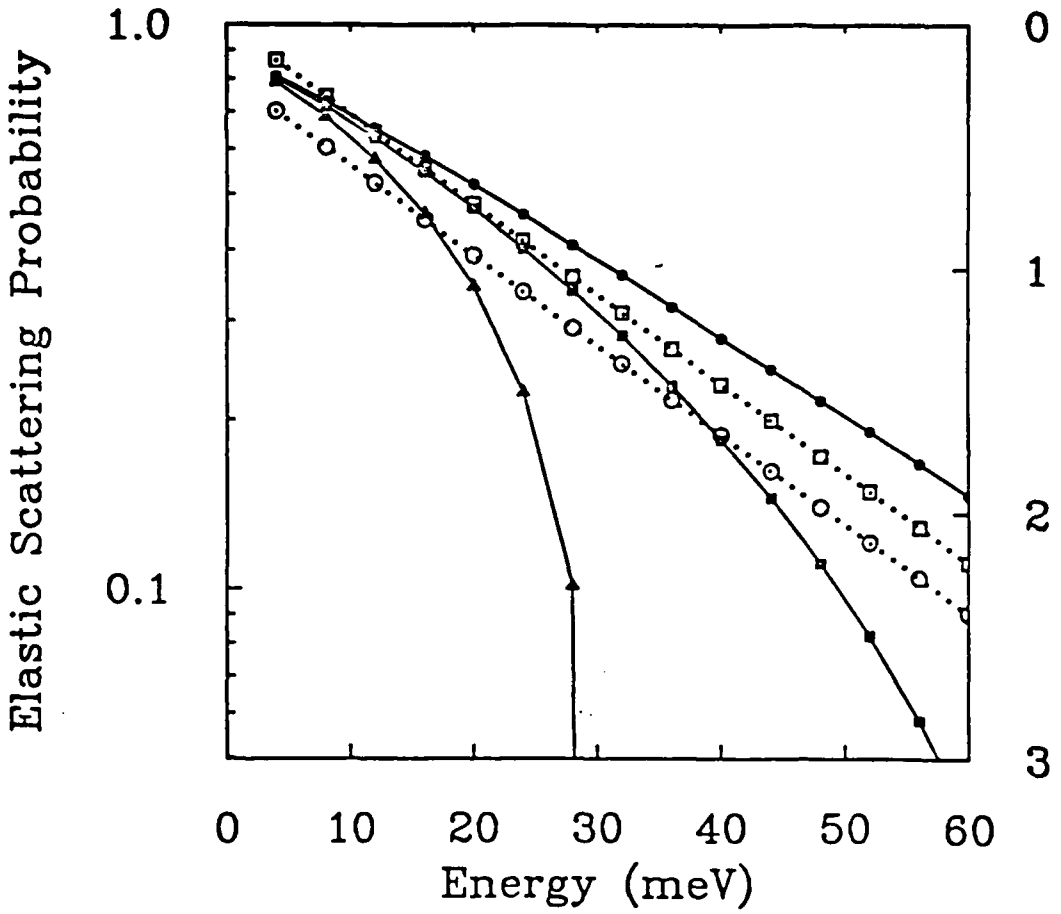
Elastic Scattering Probability
1.0
0.1
0
1
2
3
0
10
20
30
40
50
60
Energy (meV)

Figure 3.2

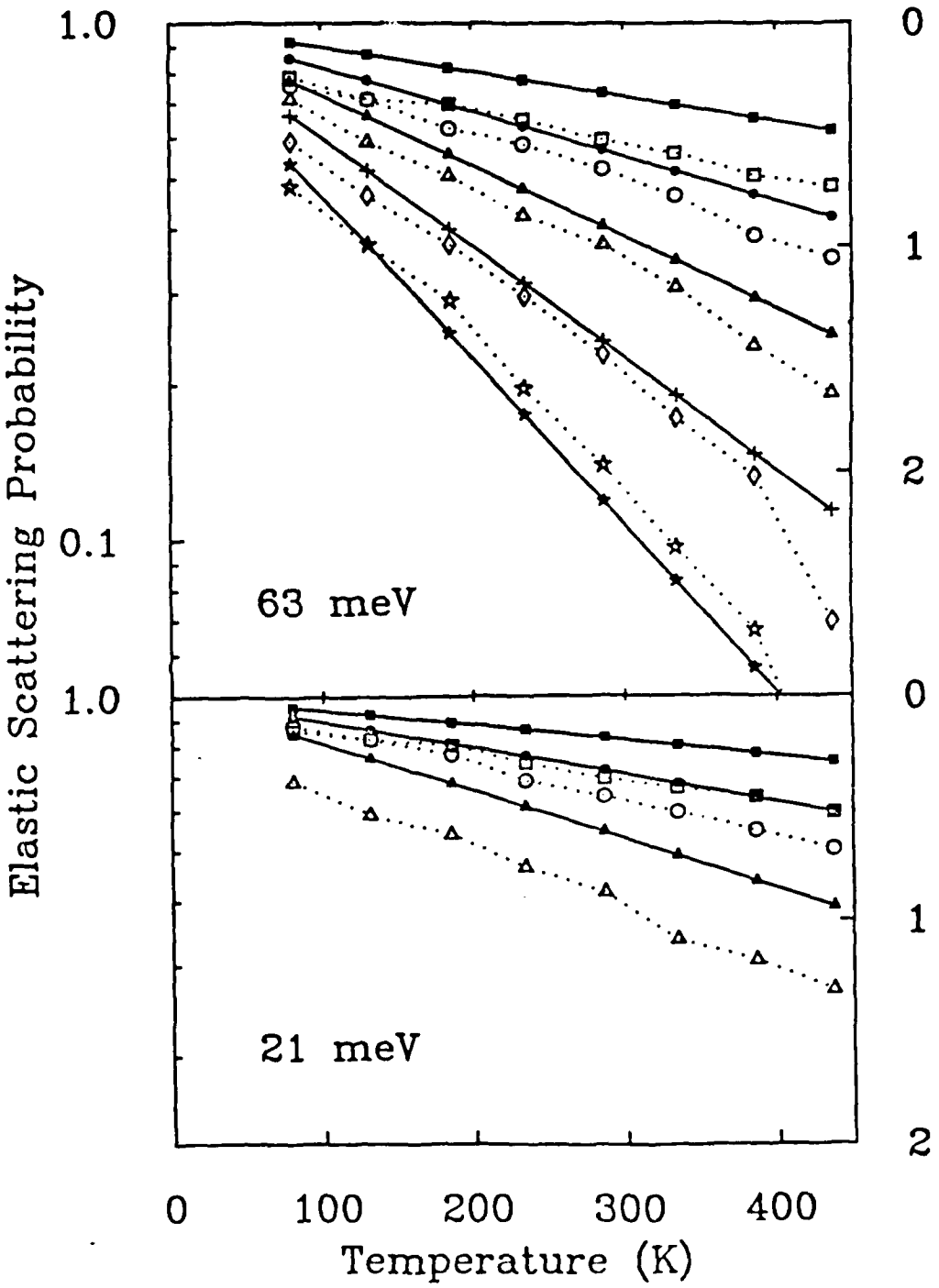
1.0
0.1
1.0
0
1
2
0
1
2
63 meV
21 meV
Elastic Scattering Probability
0
100
200
300
400
Temperature (K)

Figure 3.3

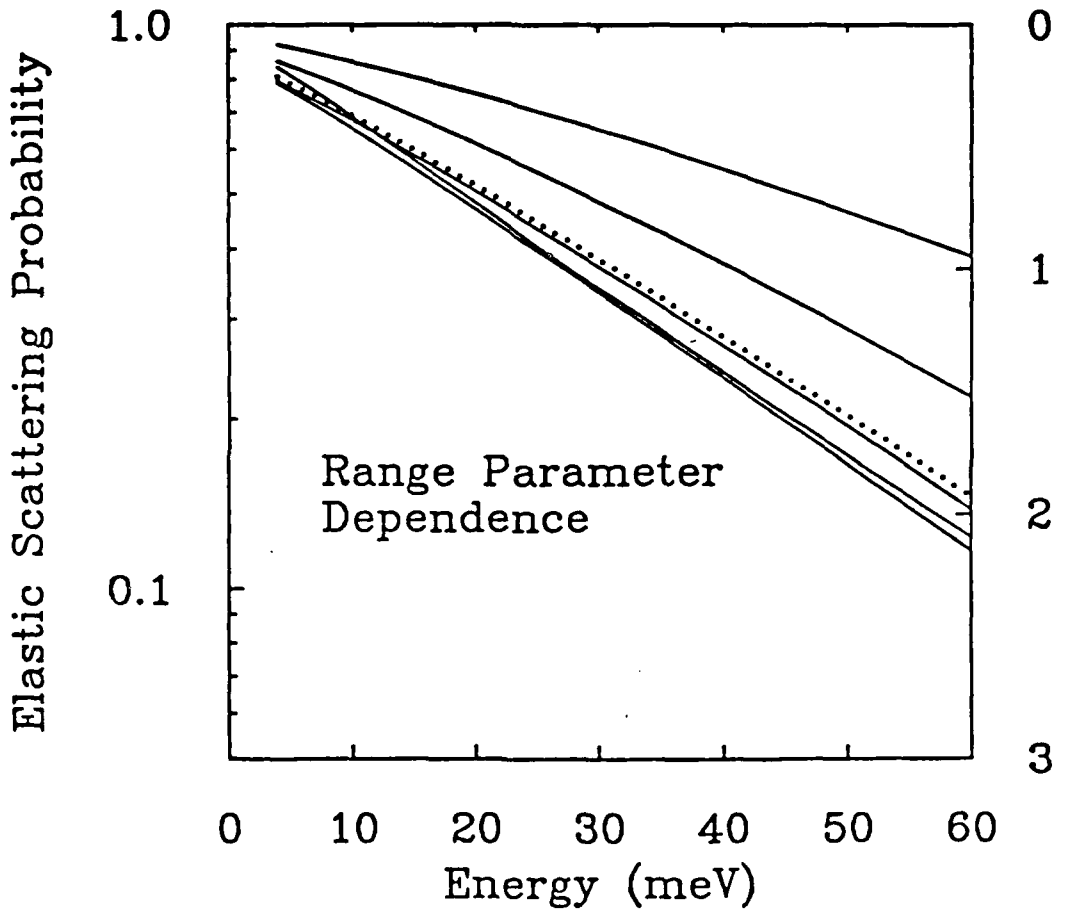
Elastic Scattering Probability
1.0
0.1
0
10
20
30
40
50
60
Energy (meV)
0
1
2
3
Range Parameter
Dependence

Figure 3.4

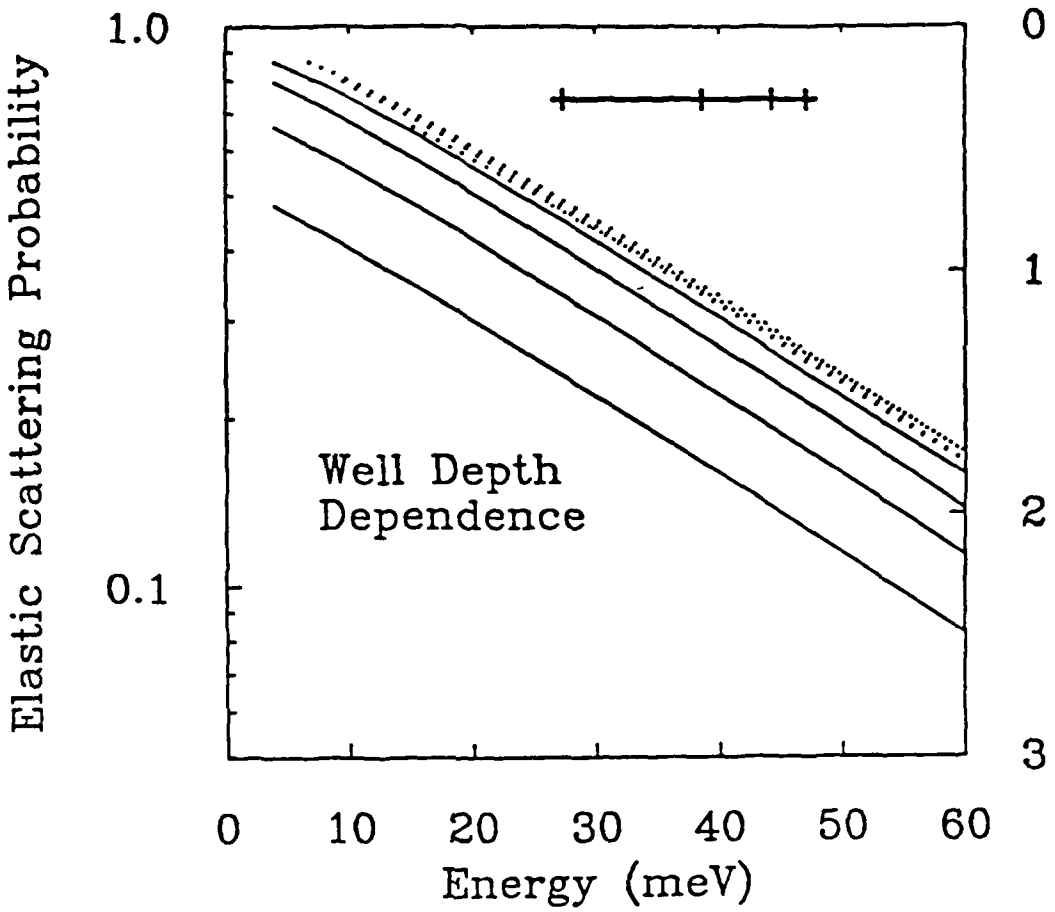
Elastic Scattering Probability
1.0
0.1
0
1
2
3
Well Depth
Dependence
0
10
20
30
40
50
60
Energy (meV)

Figure 3.5

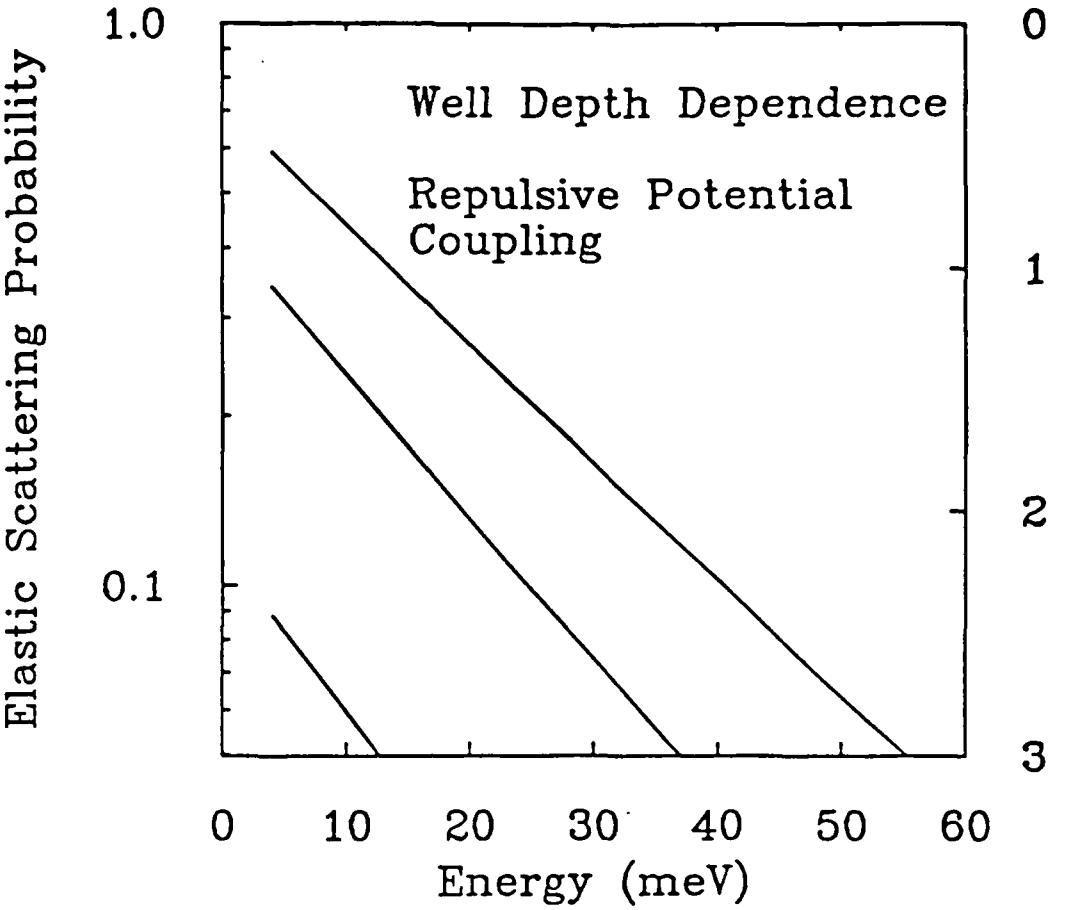
Elastic Scattering Probability
1.0
0.1
Well Depth Dependence
Repulsive Potential
Coupling
0
1
2
3
0
10
20
30
40
50
60
Energy (meV)

Figure 3.6

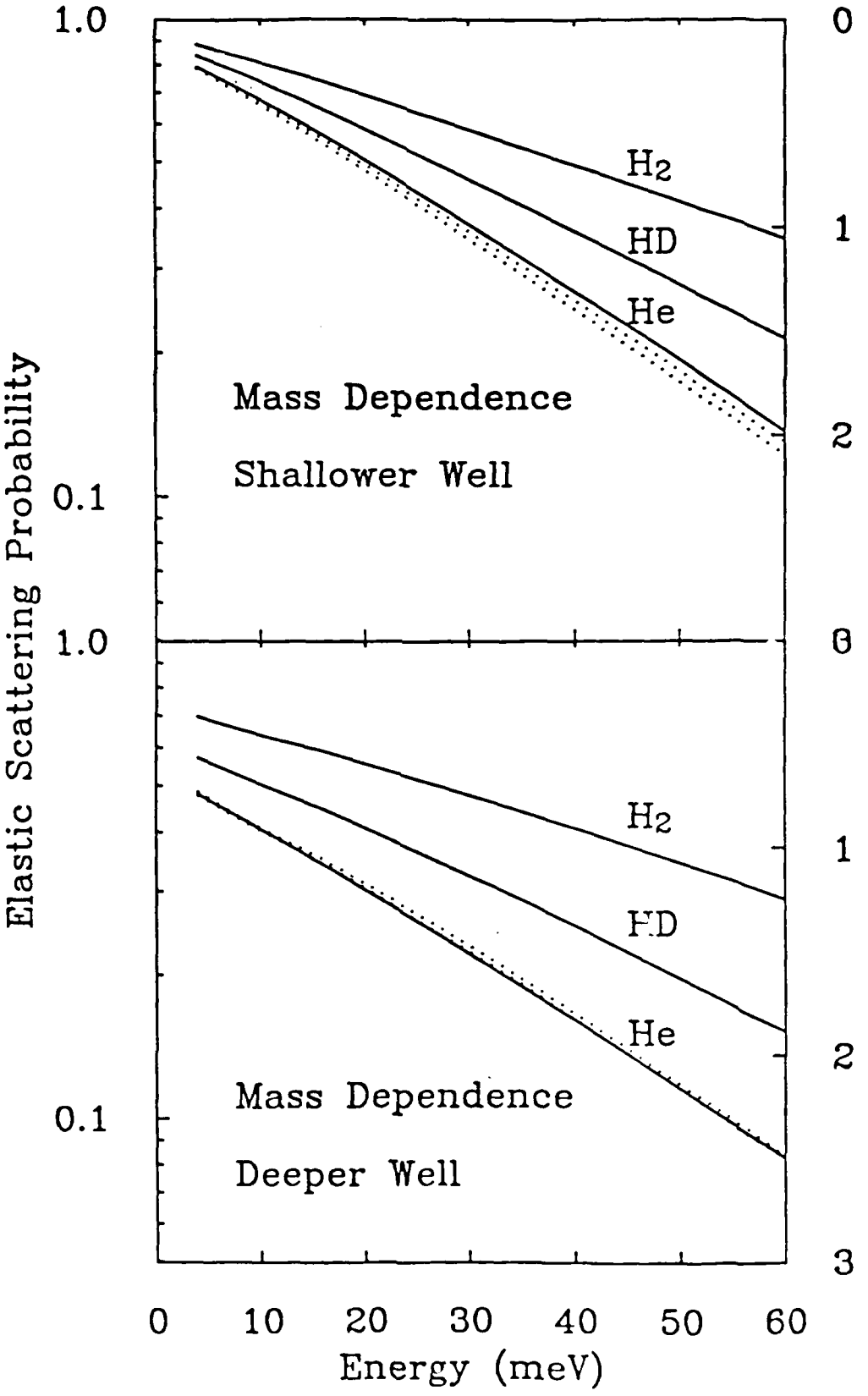
1.0
0.1
1.0
0.1
Elastic Scattering Probability
H2
HD
He
Mass Dependence
Shallower Well
H2
HD
He
Mass Dependence
Deeper Well
0
1
2
0
1
2
3
0
10
20
30
40
50
60
Energy (meV)

Figure 3.7

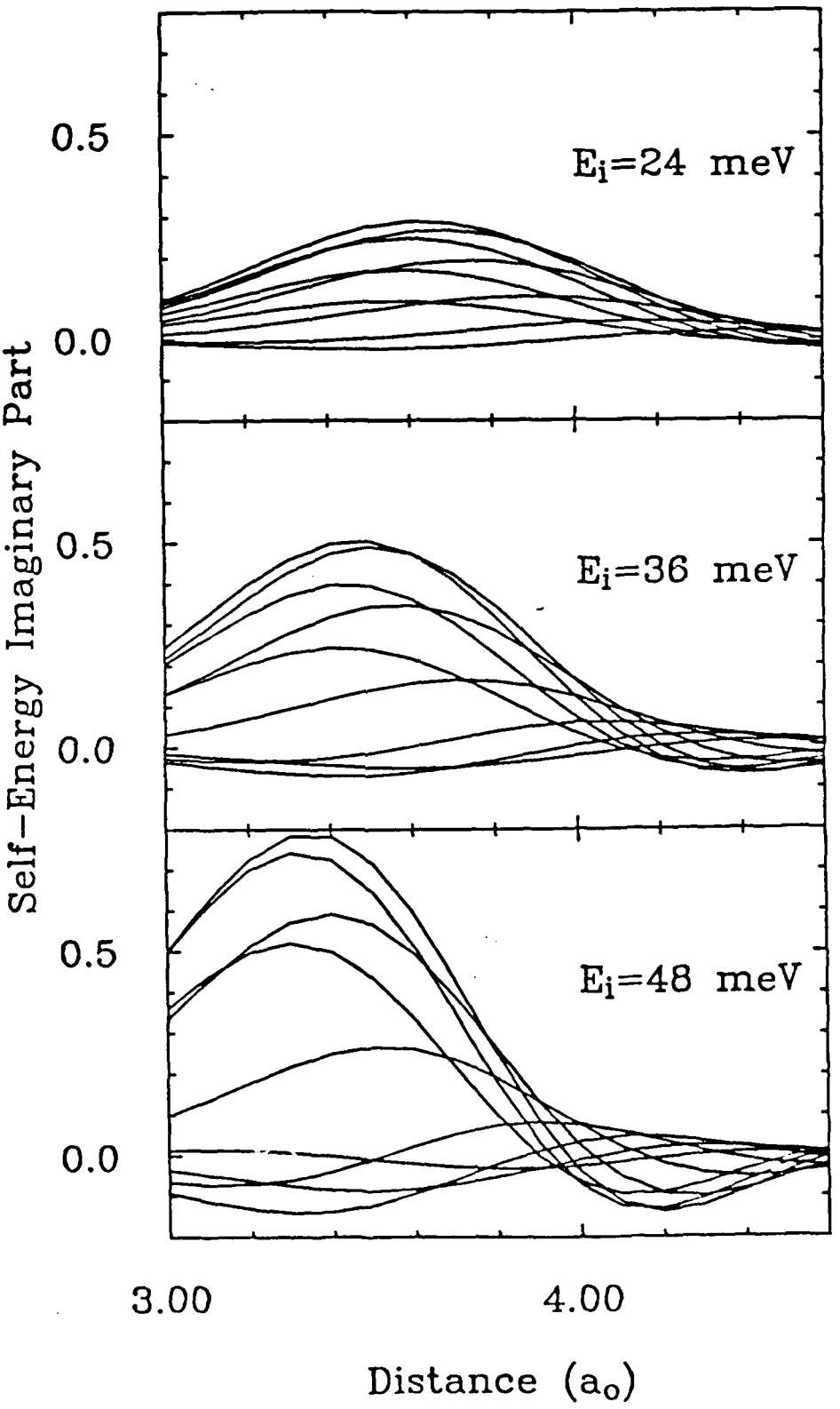
0.5
0.0
E_i=24 meV
0.5
0.0
E_i=36 meV
0.5
0.0
E_i=48 meV
Self-Energy Imaginary Part
3.00
4.00
Distance (a_o)

Fihure 3.8

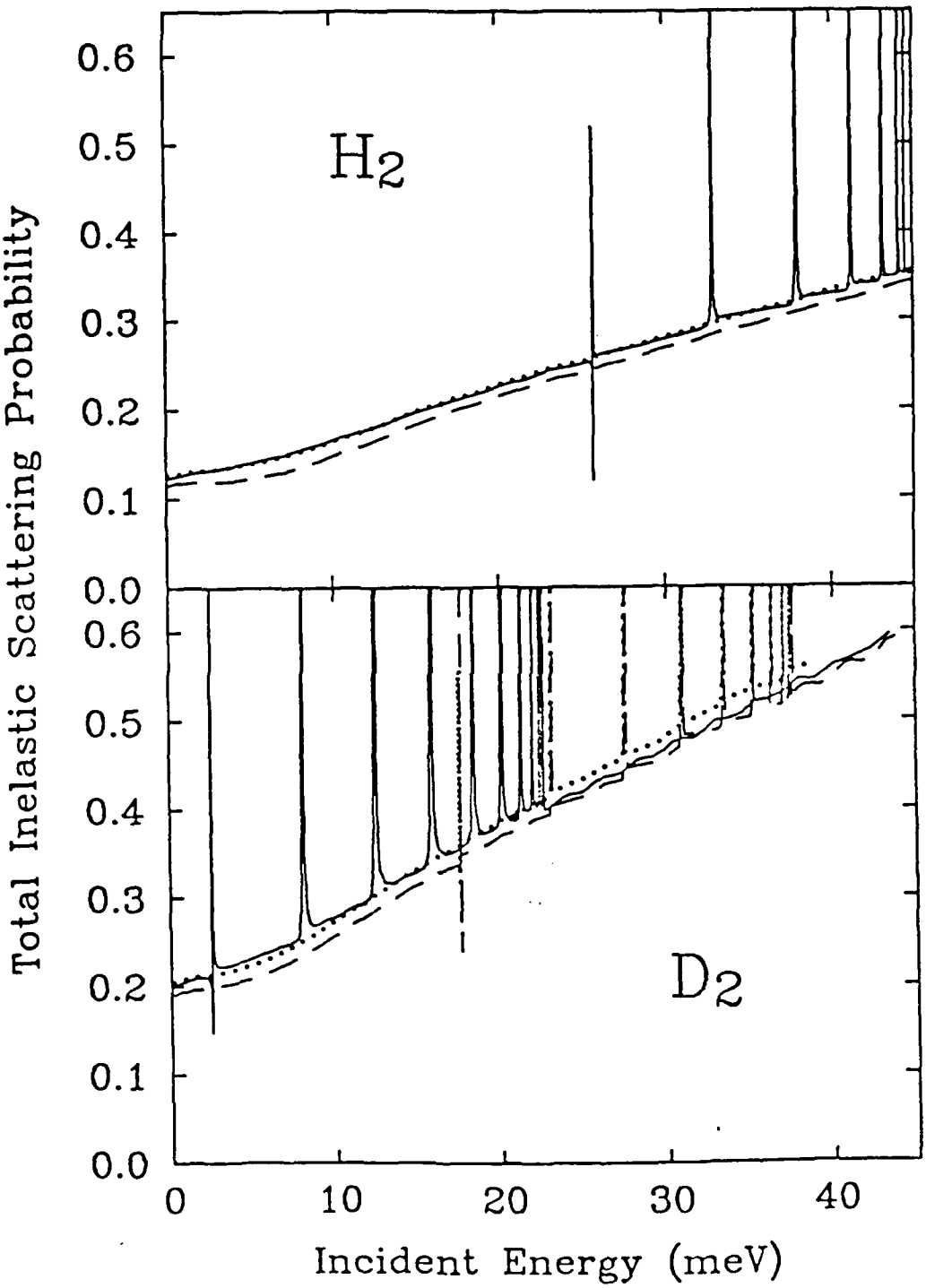
Total Inelastic Scattering Probability
0.6
0.5
0.4
0.3
0.2
0.1
0.0
H2
D2
0
10
20
30
40
Incident Energy (meV)

Figure 3.9

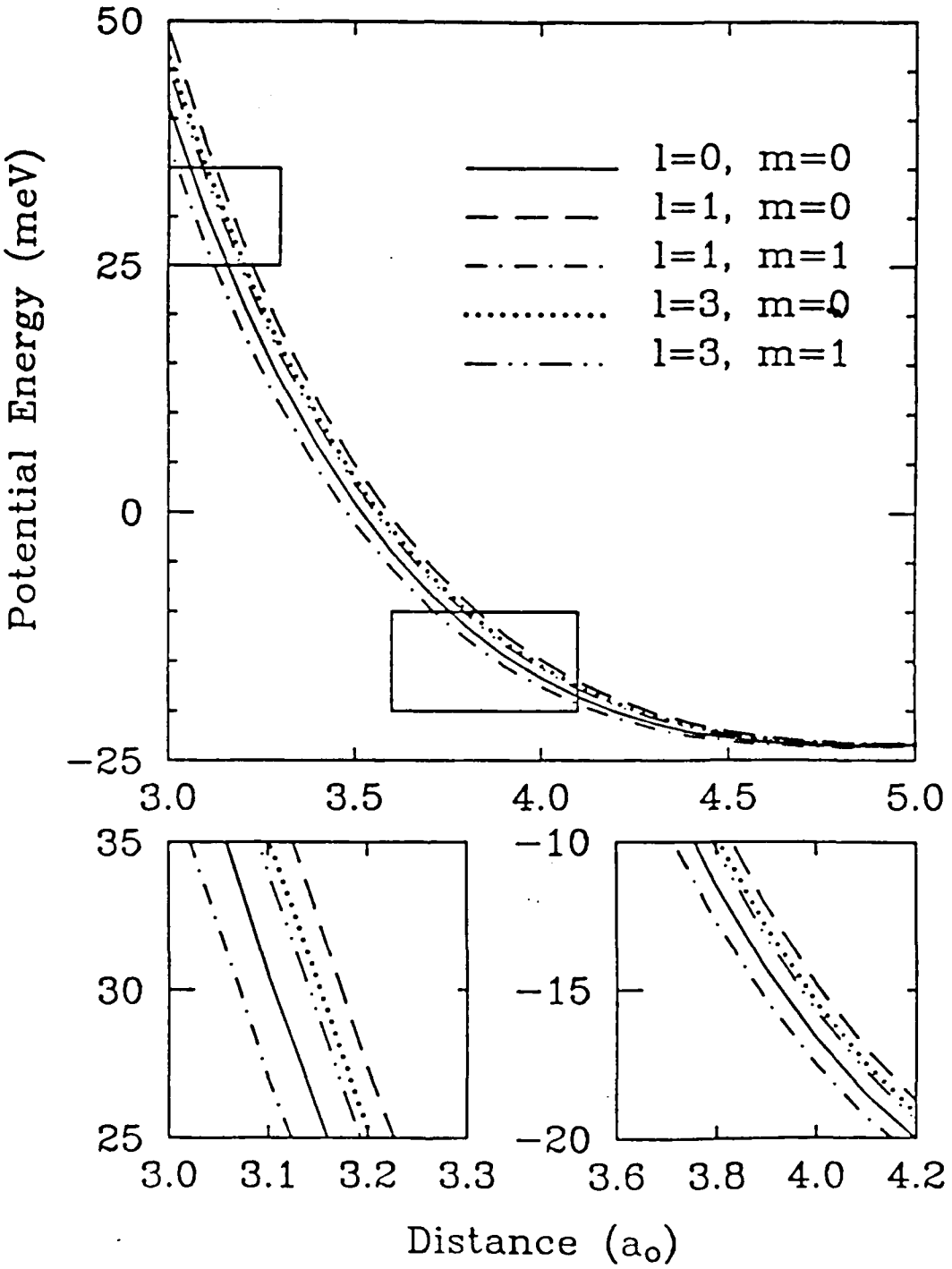
50
25
0
−25
Potential Energy (meV)
l=0, m=0
l=1, m=0
l=1, m=1
l=3, m=0
l=3, m=1
3.0
3.5
4.0
4.5
5.0
35
30
25
3.0
3.1
3.2
3.3
−10
−15
−20
3.6
3.8
4.0
4.2
Distance (a$_o$)

Figure 3.10

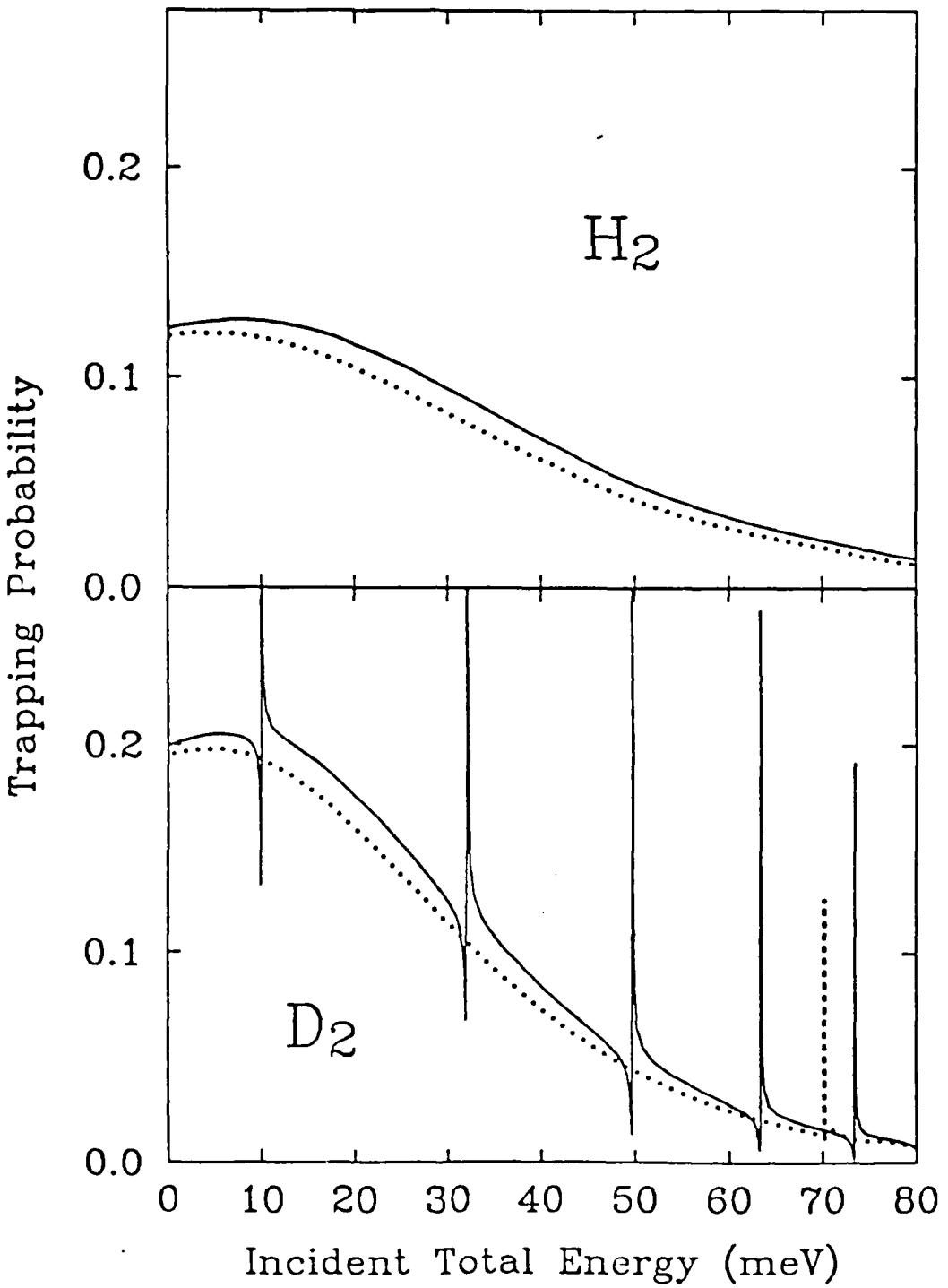
0.2
0.1
0.0
H_2
Trapping Probability
0.0
0.2
0.1
D_2
0.0
0
10
20
30
40
50
60
70
80
Incident Total Energy (meV)

Figure 3.11

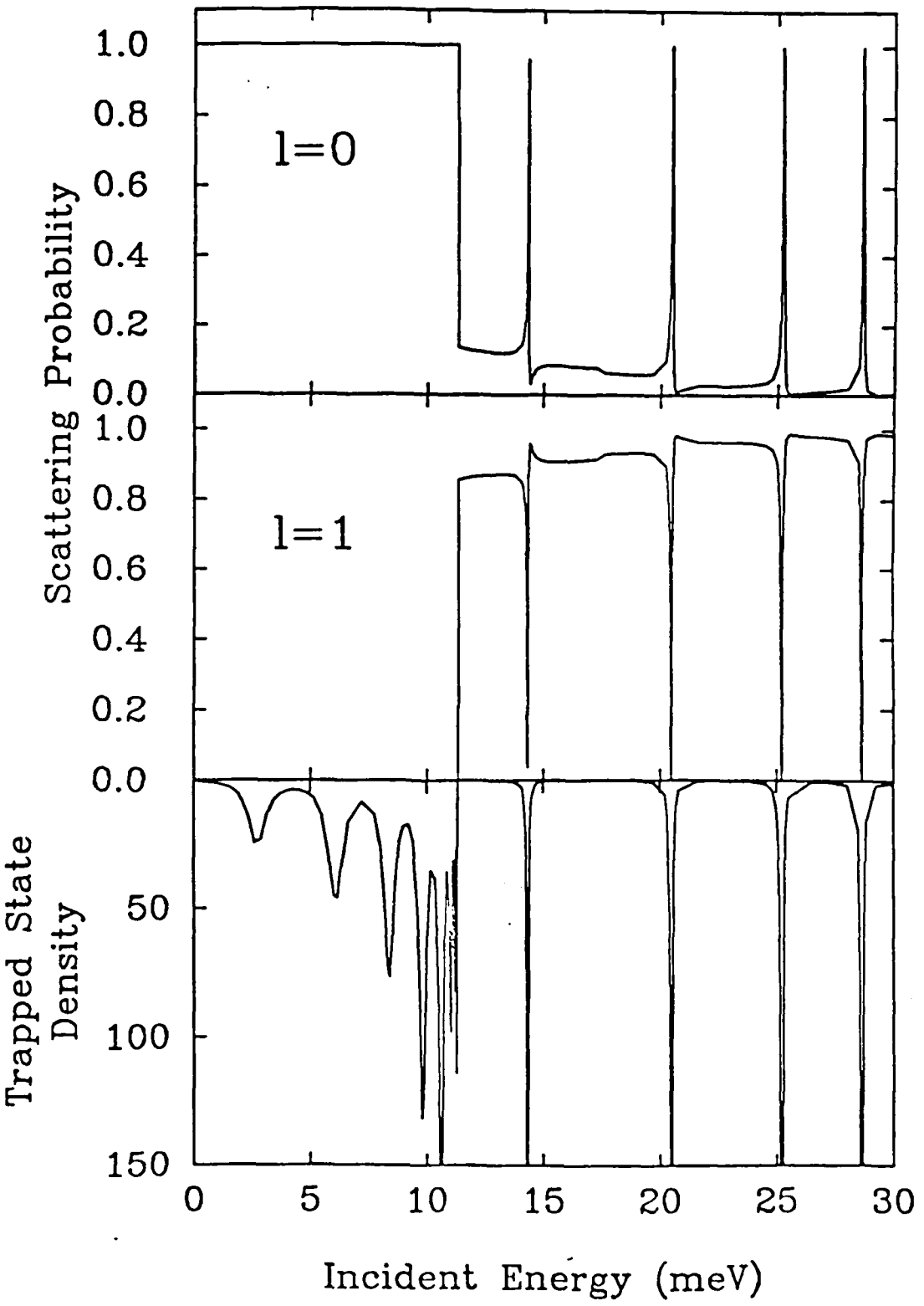
Scattering Probability
1.0
0.8
0.6
0.4
0.2
0.0
l=0
l=1
Trapped State Density
0.0
50
100
150
0
5
10
15
20
25
30
Incident Energy (meV)

Figure 3.12

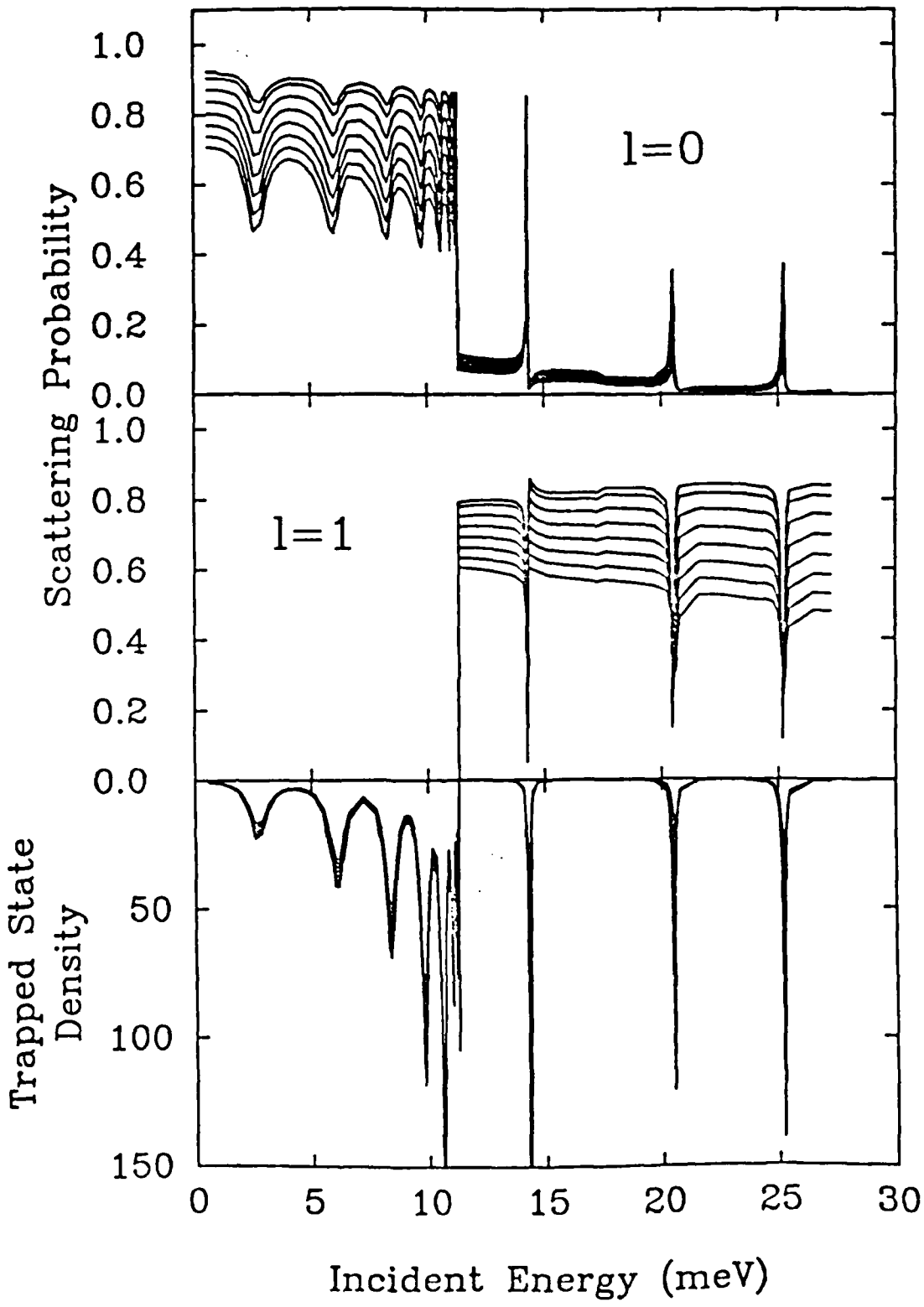
Scattering Probability
1.0
0.8
0.6
0.4
0.2
0.0
l=0
l=1
Trapped State Density
0.0
50
100
150
0
5
10
15
20
25
30
Incident Energy (meV)

Figure 3.13a

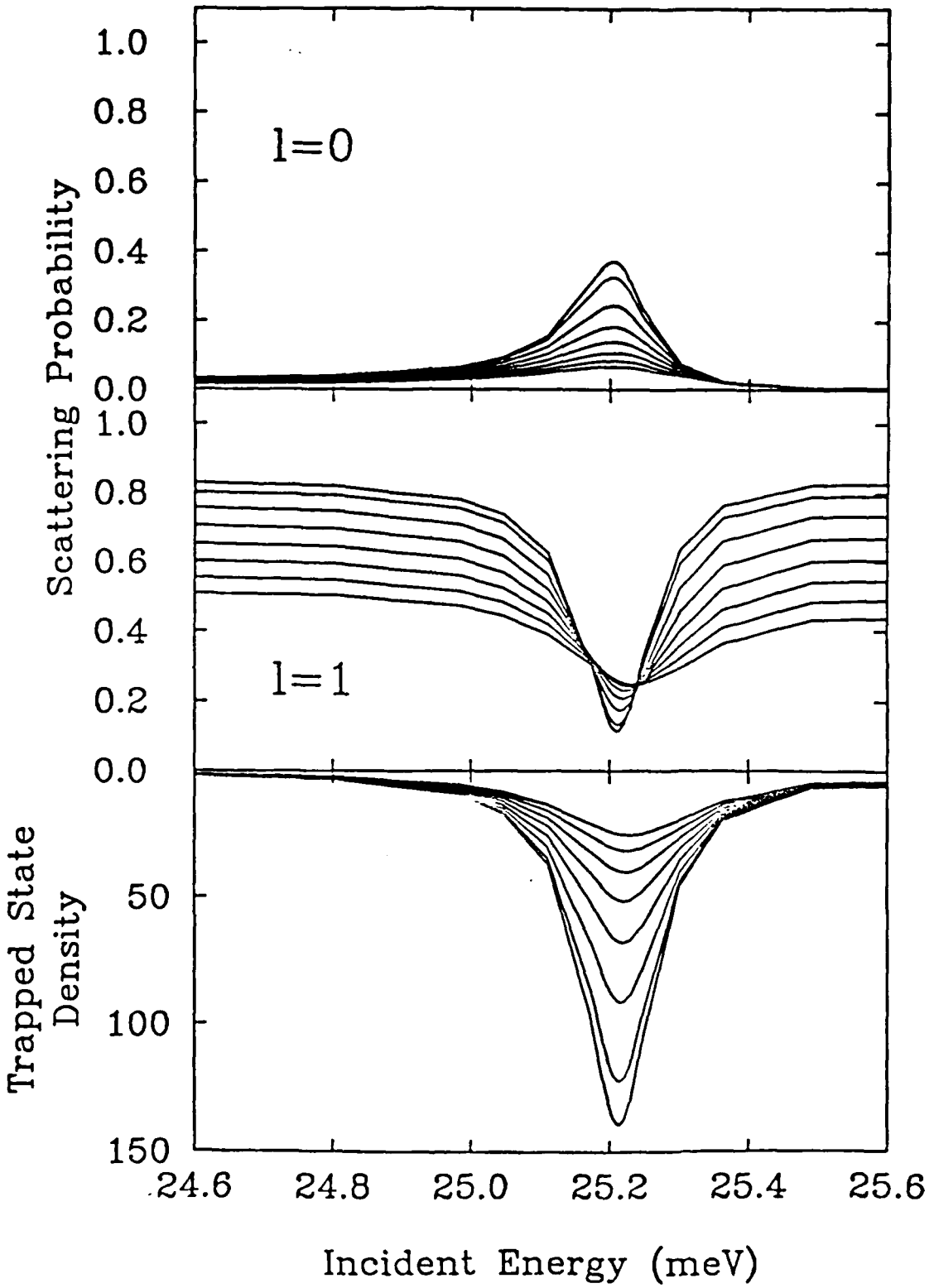
1.0
0.8
0.6
0.4
0.2
0.0
l=0
Scattering Probability
1.0
0.8
0.6
0.4
0.2
0.0
l=1
Trapped State Density
50
100
150
24.6
24.8
25.0
25.2
25.4
25.6
Incident Energy (meV)

Figure 3.13b

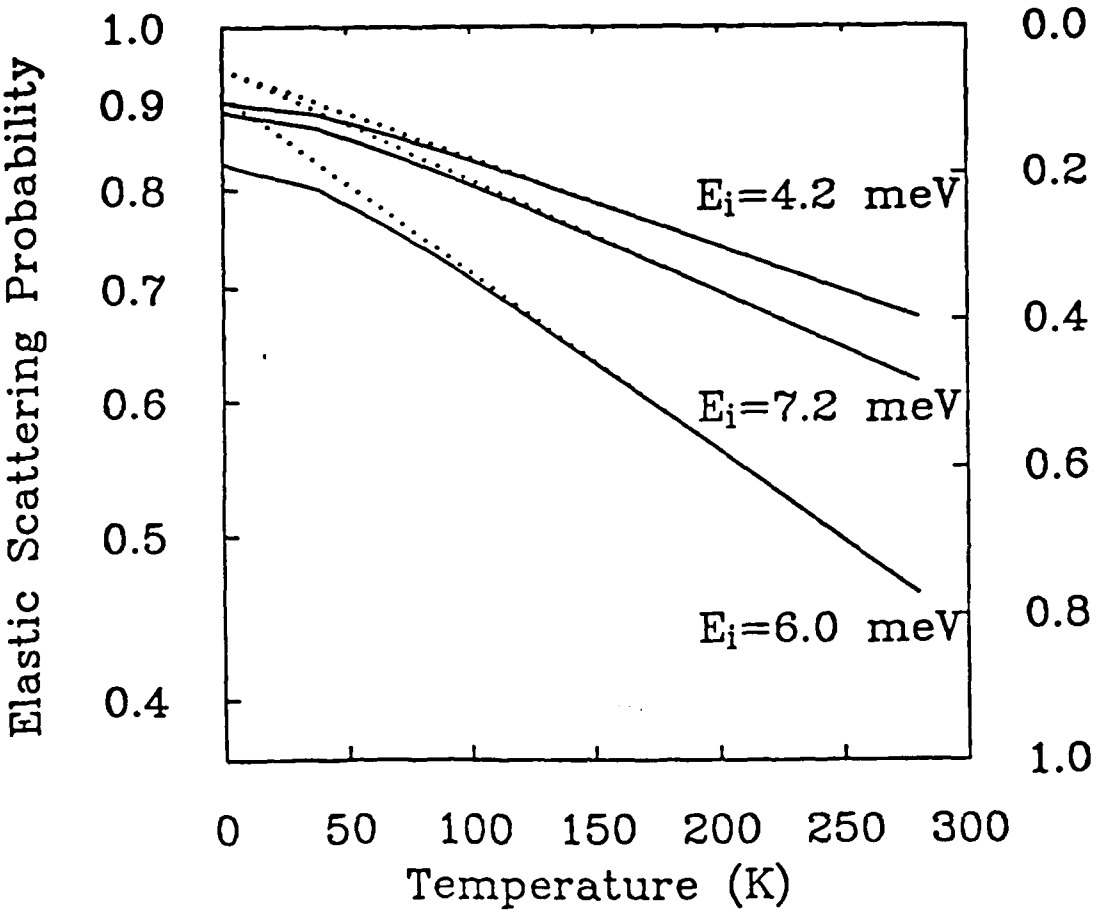
Elastic Scattering Probability
1.0
0.9
0.8
0.7
0.6
0.5
0.4
0.0
0.2
0.4
0.6
0.8
1.0
E_i=4.2 meV
E_i=7.2 meV
E_i=6.0 meV
0
50
100
150
200
250
300
Temperature (K)

Figure 3.14a

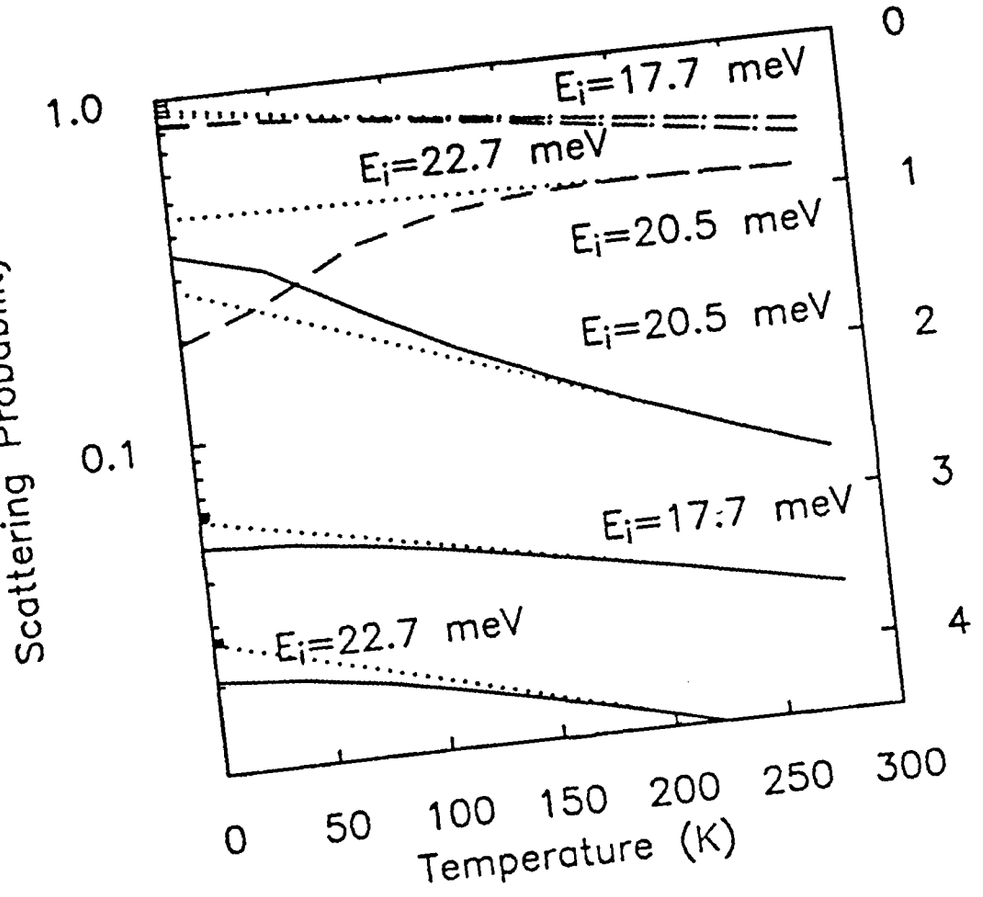
Scattering Probability
1.0
0.1
0
1
2
3
4
E_i=17.7 meV
E_i=22.7 meV
E_i=20.5 meV
E_i=20.5 meV
E_i=17.7 meV
E_i=22.7 meV
0
50
100
150
200
250
300
Temperature (K)

Figure 3.14b

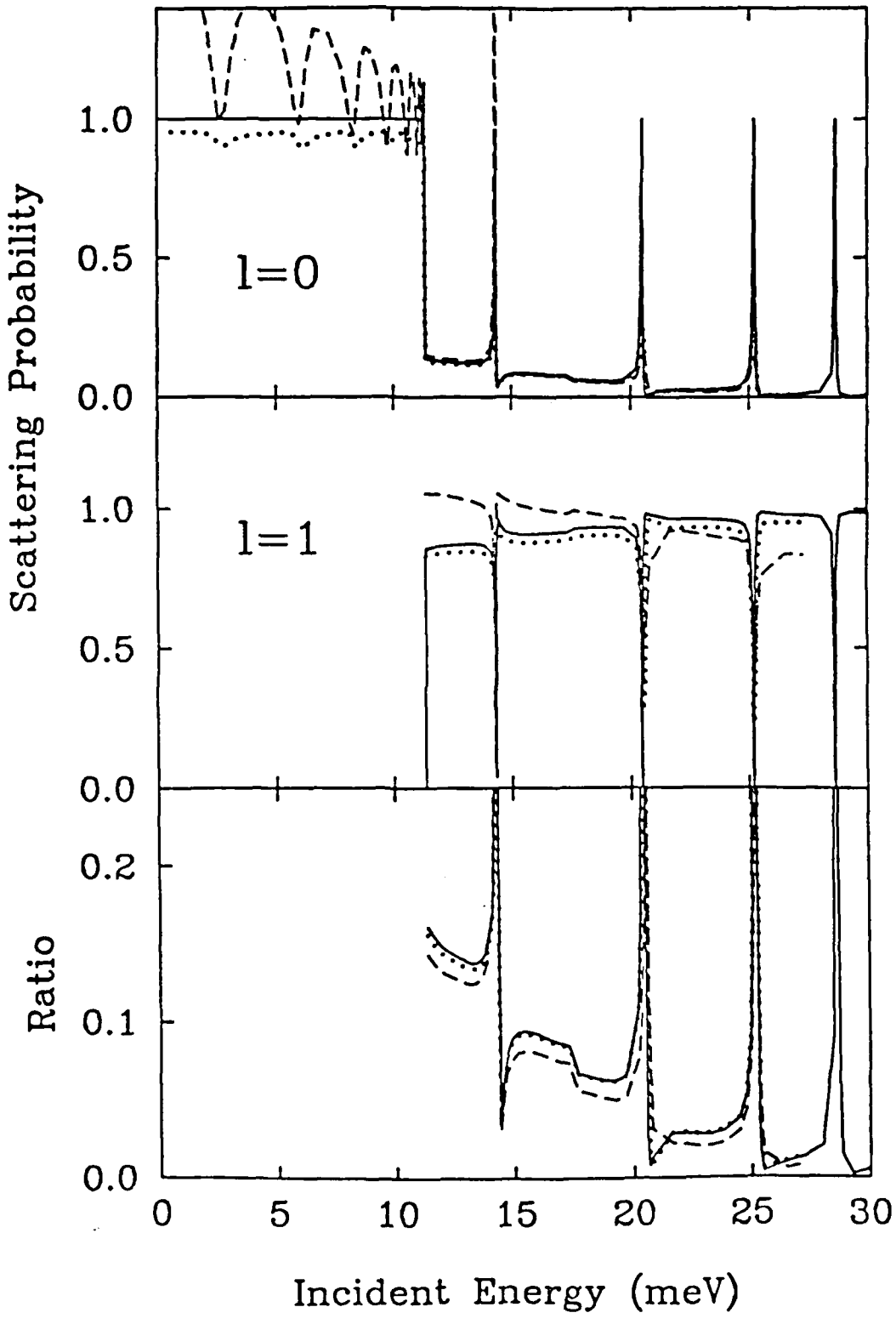
Scattering Probability
1.0
0.5
0.0
l=0
1.0
0.5
0.0
l=1
Ratio
0.2
0.1
0.0
0
5
10
15
20
25
30
Incident Energy (meV)

Figure 3.15

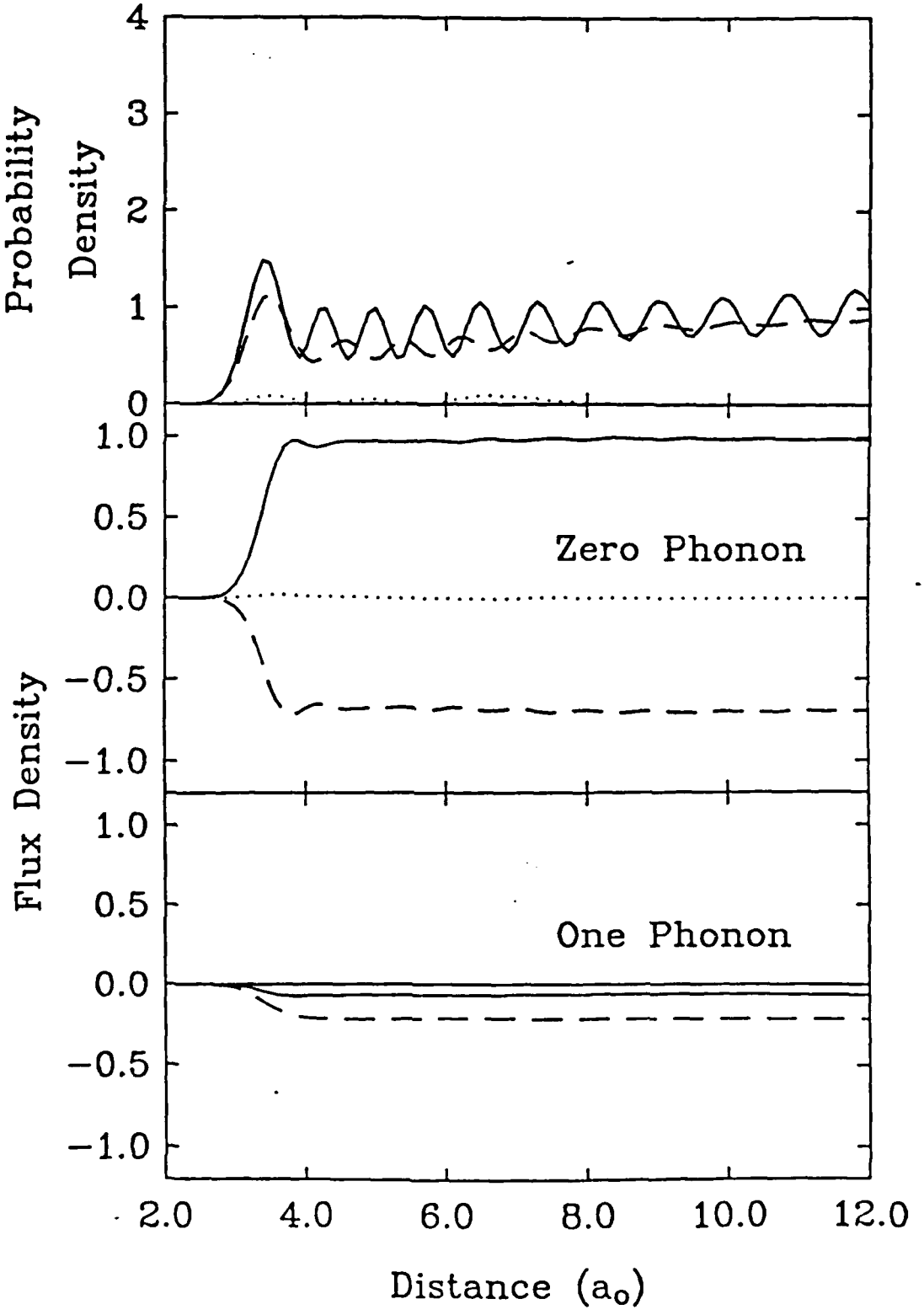
Probability Density
4
3
2
1
0
1.0
0.5
0.0
−0.5
−1.0
Zero Phonon
Flux Density
1.0
0.5
0.0
−0.5
−1.0
One Phonon
2.0
4.0
6.0
8.0
10.0
12.0
Distance (a_o)

Figure 3.16a

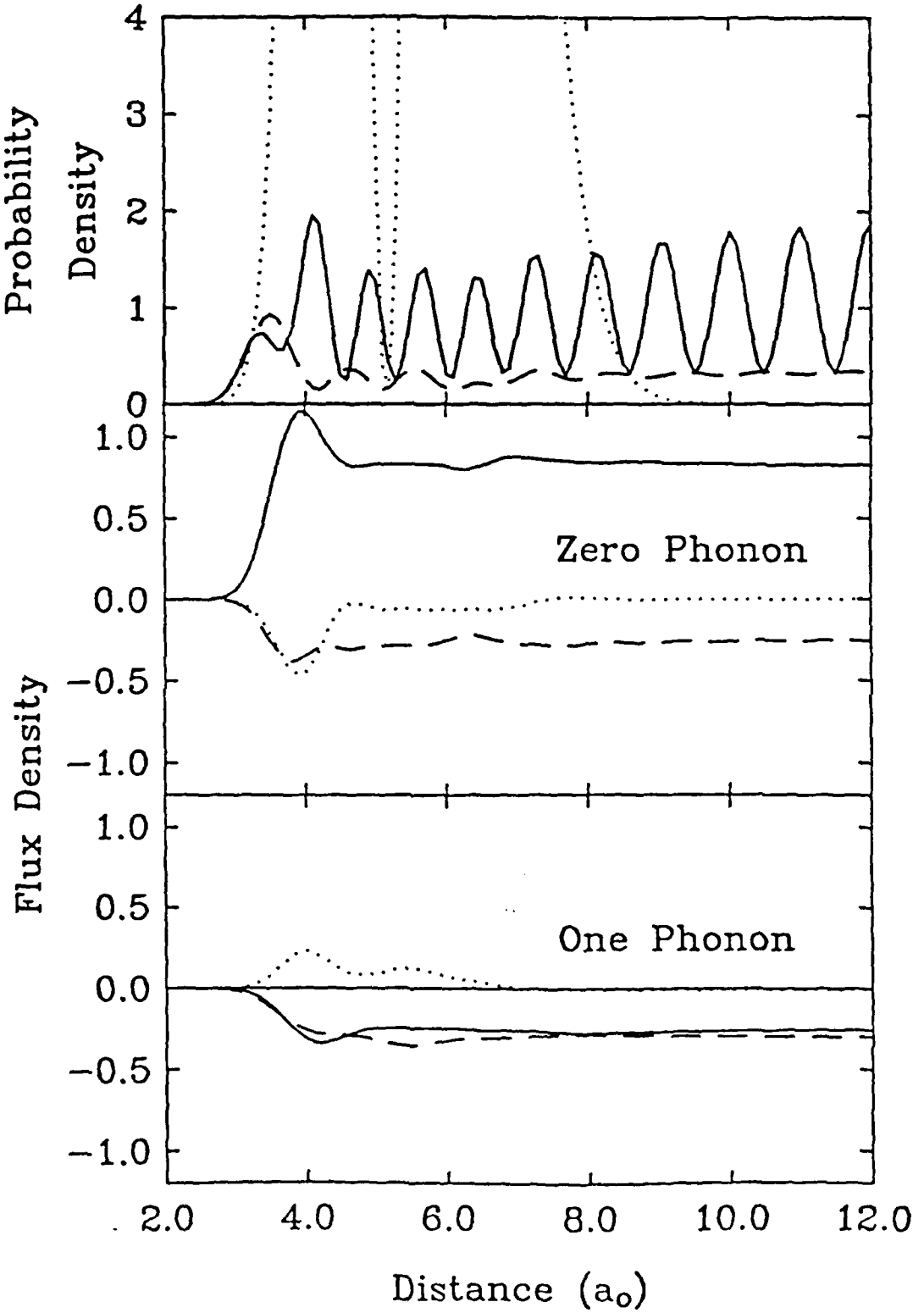
Probability Density
4
3
2
1
0
1.0
0.5
0.0
−0.5
−1.0
Zero Phonon
Flux Density
1.0
0.5
0.0
−0.5
−1.0
One Phonon
2.0
4.0
6.0
8.0
10.0
12.0
Distance (a_o)

Figure 3.16b

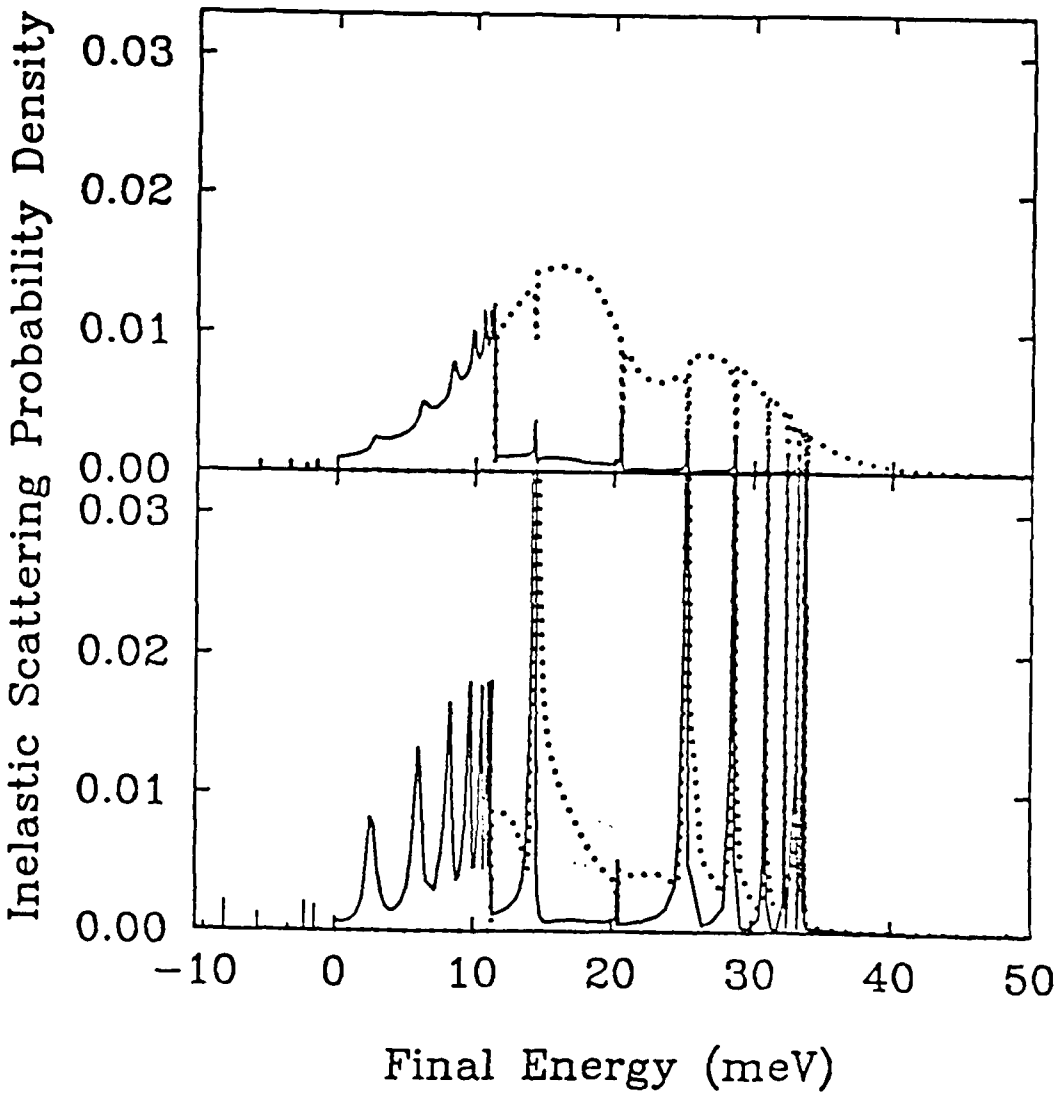
Inelastic Scattering Probability Density
0.03
0.02
0.01
0.00
0.03
0.02
0.01
0.00
−10
0
10
20
30
40
50
Final Energy (meV)

Figure 3.17

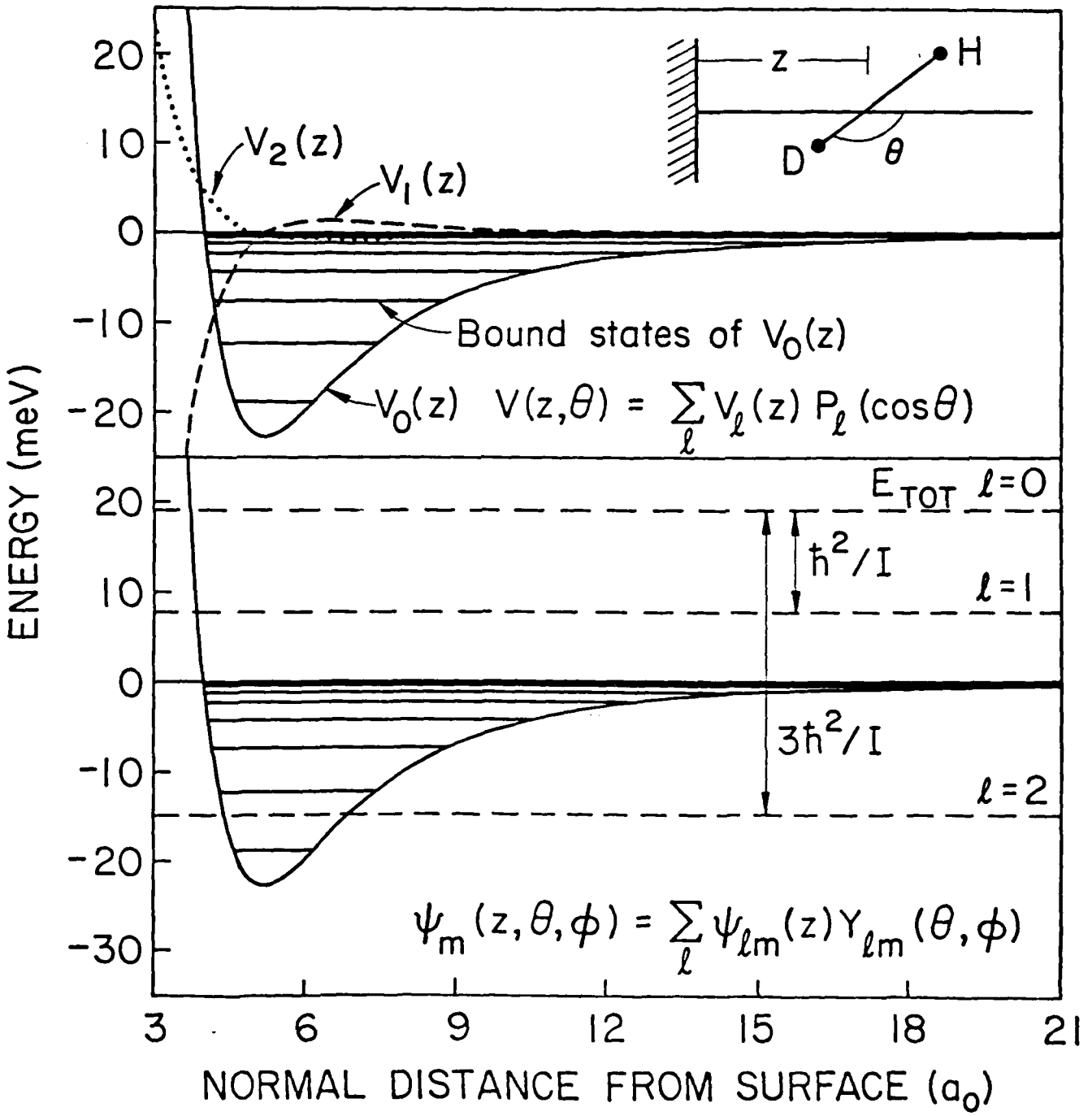
20
10
0
-10
-20
-30
ENERGY (meV)
$V_2(z)$
$V_1(z)$
z
H
D
θ
Bound states of $V_0(z)$
$V_0(z)$ $V(z,\theta) = \sum_\ell V_\ell(z)\, P_\ell(\cos\theta)$
E_{TOT} $\ell=0$
$\hbar^2/I$
$\ell=1$
$3\hbar^2/I$
$\ell=2$
$\psi_m(z,\theta,\phi) = \sum_\ell \psi_{\ell m}(z) Y_{\ell m}(\theta,\phi)$
3
6
9
12
15
18
21
NORMAL DISTANCE FROM SURFACE (a_0)

Figure A1

END

10-86

DTIC